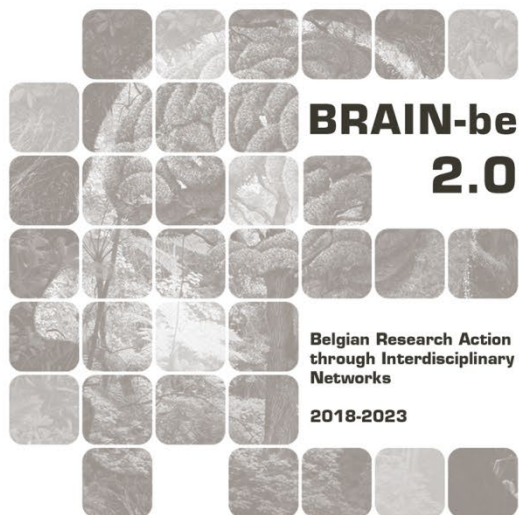


REGE+

Forest regeneration under climate and environmental changes

ANDRE Frédéric (UCLouvain), CANDAELE Romain (ULg - Gembloux Agro-Bio Tech),
GOOSSE Hugues (UCLouvain), HOSSEINZADEHTALAEI Parisa (RMI),
LIGOT Gauthier (ULg - Gembloux Agro-Bio Tech), MARCHI Sylvain (RMI),
PAU Mathilde (ULg - Gembloux Agro-Bio Tech), VAN SCHAEYBROECK Bert (RMI),
JONARD Mathieu (UCLouvain)

Pillar 1: Challenges and knowledge of the living and non-living world



NETWORK PROJECT

REGE+

Forest regeneration under climate and environmental changes

Contract - B2/212/P1/REGE+

FINAL REPORT

PROMOTORS: JONARD Mathieu (UCLouvain)
LIGOT Gauthier (ULg - Gembloux Agro-Bio Tech)
VAN SCHAEYBROECK Bert (RMI)
GOOSSE Hugues (UCLouvain)

AUTHORS: ANDRE Frédéric (UCLouvain)
CANDAELE Romain (ULg - Gembloux Agro-Bio Tech)
PAU Mathilde (ULg - Gembloux Agro-Bio Tech)
MARCHI Sylvain (RMI)
HOSSEINZADEHTALAEI Parisa (RMI)



Published in 2025 by the Belgian Science Policy Office

WTCIII

Simon Bolivarlaan 30 bus 7

Boulevard Simon Bolivar 30 bte 7

B-1000 Brussels

Belgium

Tel: +32 (0)2 238 34 11

<http://www.belspo.be>

<http://www.belspo.be/brain-be>

Contact person: VAN DER WERF Aline

Tel: +32 (0)2 238 36 71

Neither the Belgian Science Policy Office nor any person acting on behalf of the Belgian Science Policy Office is responsible for the use which might be made of the following information. The authors are responsible for the content.

No part of this publication may be reproduced, stored in a retrieval system, or transmitted in any form or by any means, electronic, mechanical, photocopying, recording, or otherwise, without indicating the reference:

ANDRE Frédéric, CANDAELE Romain, GOOSSE Hugues, HOSSEINZADEHTALAEI Parisa, LIGOT Gauthier, MARCHI Sylvain, PAU Mathilde, VAN SCHAEYBROECK Bert, JONARD Mathieu. ***Forest regeneration under climate and environmental changes***. Final Report. Brussels: Belgian Science Policy Office 2025 – 106 p. (BRAIN-be 2.0 - (Belgian Research Action through Interdisciplinary Networks))

TABLE OF CONTENTS

ABSTRACT	5
1. INTRODUCTION	6
2. STATE OF THE ART AND OBJECTIVES	6
3. METHODOLOGY	9
4. SCIENTIFIC RESULTS AND RECOMMENDATIONS	40
5. DISSEMINATION AND VALORISATION	93
6. PUBLICATIONS	94
7. ACKNOWLEDGEMENTS	95
REFERENCES	96
ANNEXES	103

ABSTRACT

The REG+ project investigated how forests, particularly in Belgium, can adapt to climate change while facing growing threats like drought and high densities of browsing ungulates such as deer. Forests provide critical ecosystem services like carbon storage, biodiversity, and climate regulation, but their resilience depends heavily on successful regeneration. However, climate-induced stress and overabundant herbivores hamper regeneration, particularly that of climate-resilient species. The project used HETEROFOR, a highly integrated forest model that was improved during this research, to simulate three forest management strategies: Business as Usual (BAU), Oak Regeneration (OAK) and Diversification (DIV). These strategies were simulated across several climate change scenarios, for which the data series were corrected for climate model biases. Results showed that the DIV strategy offered the greatest biodiversity, resilience, and economic gains but was most vulnerable to ungulate pressure. BAU was most effective for carbon storage and wind resistance but underperformed in regeneration and diversity. OAK ranked in between. Local site conditions significantly influenced outcomes, reinforcing the need for site-specific strategies. Simulations showed that ungulate impacts can rival or exceed those of climate change, reducing regeneration and increasing economic losses—especially for species like birch, hornbeam, and oak. In other respects, it was found that bark peeling by red deer reduce revenue by 19% on average. The study emphasises the importance of integrating wildlife management and site-specific silviculture into adaptive forestry policies to ensure the resilience and functionality of forests in the face of threats associated with climate change.

1. INTRODUCTION

Forests are essential to the Earth's habitability and play a critical role in mitigating climate change through carbon sequestration and local cooling effect. They also serve as biodiversity hotspots and provide a wide array of ecosystem services, such as wood production, recreation, soil and water protection, flood control, and water and air purification. To sustain these multiple functions, including their climate services, forests must be continually regenerated. However, European and, more specifically, Belgian forests face numerous threats. Warm and dry summers weaken trees and seedlings by causing water stresses (carbon starvation, hydraulic failure), which in turn can trigger outbreaks of pests and pathogens. In addition, the management of wildlife populations—particularly ungulates like roe deer and red deer—can significantly impact forest dynamics. High populations of these herbivores can affect regeneration development through browsing, preferentially affecting certain tree species and ultimately changing forest composition over time. In this uncertain and rapidly changing environment, forest managers must focus on enhancing forest resistance and resilience. One potential solution is the establishment of uneven-aged and mixed stands. Mixing tree species with contrasting functional traits offers a broad range of responses to various stresses, thus improving a forest's ability to recover after disturbances.

The diversification of forests—both in terms of age and species composition—fundamentally depends on regeneration. It is through regeneration that tree species composition and forest structure can be changed. Yet, regeneration is complex; it results from an interplay of factors, including forest characteristics, silvicultural practices, natural disturbances, pressure from ungulate populations, and climatic conditions. Promoting regeneration is therefore essential—it is the cornerstone of any meaningful effort toward forest diversification.

2. STATE OF THE ART AND OBJECTIVES

Regenerating forests is vital for maintaining the ecosystem services they provide. In Belgium, forest regeneration has always been a priority for foresters, but it has become even more pressing considering ongoing ecological and climate changes.

Today, Norway spruce accounts for a quarter of the Walloon forest (Filière Bois Wallonie, 2024). The numerous and large spruce stands planted after the Second World War (1950-1970) are currently being regenerated. Given the risks of storms, bark beetle infestation and climate change, it is no longer wise to plant such large areas with a single species. Initially, Douglas fir was seen as a promising species to partially replace spruce. Yet young Douglas fir trees are currently facing significant attacks from various pests and pathogens, such as *Contarinia pseudotsugae*, Swiss needle cast, and *Sirococcus conigenus* (Stemmelen *et al.*, 2023). Given the need for more drastic diversification of the Walloon forest, a grant promoting replantation of mixed tree species (called *Forêt Résilience*) was awarded to public and private forest owners between 2021 and 2024. Traditionally, coniferous stands have been regenerated through plantation after clearcutting and, even if this even-aged approach is gradually being replaced with uneven-aged silviculture, massive recourse to planting was again necessary to

regenerate stands damaged by the bark beetle. For healthy stands that are still in place and not at risk of windfall, the application of continuous-cover forestry principles is an interesting option to enhance forest resistance and resilience by creating structurally complex and species-diverse stands (Hanewinkel *et al.*, 2014; Hilmers *et al.*, 2020; Lafond *et al.*, 2014). Such forests are generally believed to be better equipped to resist and recover from various disturbances. In the current ecological and climatic context, this strategy is considered more economically viable than clear-cutting silviculture. However, it remains uncertain whether it maximizes profits (Knoke, 2012; Vítková and Ní Dhubháin, 2013).

In addition to regenerating spruce stands, regenerating broadleaf stands is equally important. Oak is the dominant broadleaf species in Belgium and is primarily found in stands originating from coppices or coppices with standards. Over time, these oak stands have aged, and the lack of regeneration has become increasingly apparent (Alderweireld *et al.*, 2015). Several factors contribute to this regeneration failure, including irregular fructification (masting), insufficient light conditions, competition with ground vegetation, mildew attacks, and ungulate browsing (Kohler *et al.*, 2020). Notably, increasing ungulate pressure (wild boar, roe deer, and red deer) in Europe is hindering regeneration and could severely impact forest dynamics (Churski *et al.*, 2017). Since ungulates preferentially browse certain species over others, they alter forest composition over time (Champagne *et al.*, 2021; Dobor *et al.*, 2024). For example, beech tends to develop at the expense of oak because it is more competitive, has a higher shade tolerance and a lower palatability (Candaele *et al.*, 2023). Unfortunately, beech is more sensitive to climate change (especially drought events) and has less associated biodiversity than oak (Martinez del Castillo *et al.*, 2022).

Forest managers face complex decisions regarding the optimal choices for (i) tree species selection in the face of pest and pathogen threats and climate change, (ii) regeneration methods (artificial vs. natural), and (iii) silvicultural treatments (even-aged vs. uneven-aged stands). Given this complexity, foresters need clear guidelines with a solid scientific basis derived from field studies. Monitoring field trials is however time consuming and costly. It is therefore worth making an initial selection based on modelling to identify the most promising silvicultural routes to be tested *in situ*.

Simulations can be done with a wide variety of forest dynamics models, but only a few can simultaneously account for the effects of forest management and climate change. Climate change models, such as process-based models, generally operate at the stand scale and do not consider within-stand spatial heterogeneity (Dufrêne *et al.*, 2005). As a result, they are not well-suited for testing silvicultural strategies in structurally complex and species-diverse stands. To simulate the effects of various management strategies in heterogeneous forests, spatially explicit tree models are required, where the position and characteristics of each tree are modelled (Berger *et al.*, 2008; Bravo *et al.*, 2019). Few models combine detailed spatial descriptions with process-based approaches, and only HETEROFOR is specifically calibrated for Belgian conditions. HETEROFOR is an individual-based and spatially explicit model of stand dynamics based on resource use (light, water, and nutrients) and able to simulate the effects of a wide variety of silvicultural routes (de Wergifosse *et al.*, 2020; Jonard *et al.*, 2020). HETEROFOR has been implemented in the CAPSIS simulator, a tool dedicated to tree growth and stand dynamics modelling and is particularly suited for simulating the evolution of

structurally complex stands. As HETEROFOR is part of CAPSIS, it is readily accessible to all users and modelers of this platform.

Given that climate conditions influence most of the processes regulating tree growth, simulating stand dynamics over decades requires considering potential future climate scenarios. For this project, we utilized the most recent climate model simulations available. These simulations originated from a large ensemble of general circulation models (GCMs) as part of the Coupled Model Intercomparison Project Phase 6 (CMIP6). These projections were bias-corrected (BC) to address systematic errors.

The objective of this project was to develop a highly integrated tool that allows testing various forest regeneration strategies while accounting for local climate evolution and varying levels of ungulate density. To achieve this, HETEROFOR was adapted to include the effects of ungulate browsing on seedling development and mortality. Additionally, the model was improved to evaluate forest climate services (e.g., carbon sequestration, evapotranspiration) and provide economic indicators. Simulation experiments were conducted across multiple climate scenarios and case studies (5 representative broadleaved stands to be regenerated over the next 40 years) to test various regeneration and wildlife management strategies. After discussion with stakeholders (private and public forest owners, managers, and hunters), three silvicultural routes were retained:

- (i) Business As Usual (BAU) which consisted in maintaining an even-aged stand and to regenerate it based on the shelterwood method while limiting interventions in the regeneration cohorts,
- (ii) Oak Regeneration (OAK) was like BAU but promoting the regeneration of sessile oak by targeted clearings,
- (iii) Diversification (DIV) aimed to enhance both stand composition and structural diversification by relying on natural regeneration and enrichment plantations.

These simulation experiments enabled us to evaluate tree regeneration success, stand resilience to disturbances, and ecosystem service provision. Our findings offer valuable insights for foresters seeking to understand how climate change and ungulate pressure may influence management strategies aimed at promoting oak regeneration and enhancing functional biodiversity. Additionally, the results can support the development of forest policies at both regional and national levels, helping policymakers and managers assess the potential impacts of different forest and wildlife management scenarios in the face of climate change.

3. METHODOLOGY

3.1 Methodological approach

The REG+ project is structured into eight work packages (Figure 1), each of which is detailed in this section. The primary goal of these work packages was to produce simulations that assessed the impact of climate change, ungulate pressure, and silvicultural strategies on the dynamics of broadleaved stands.

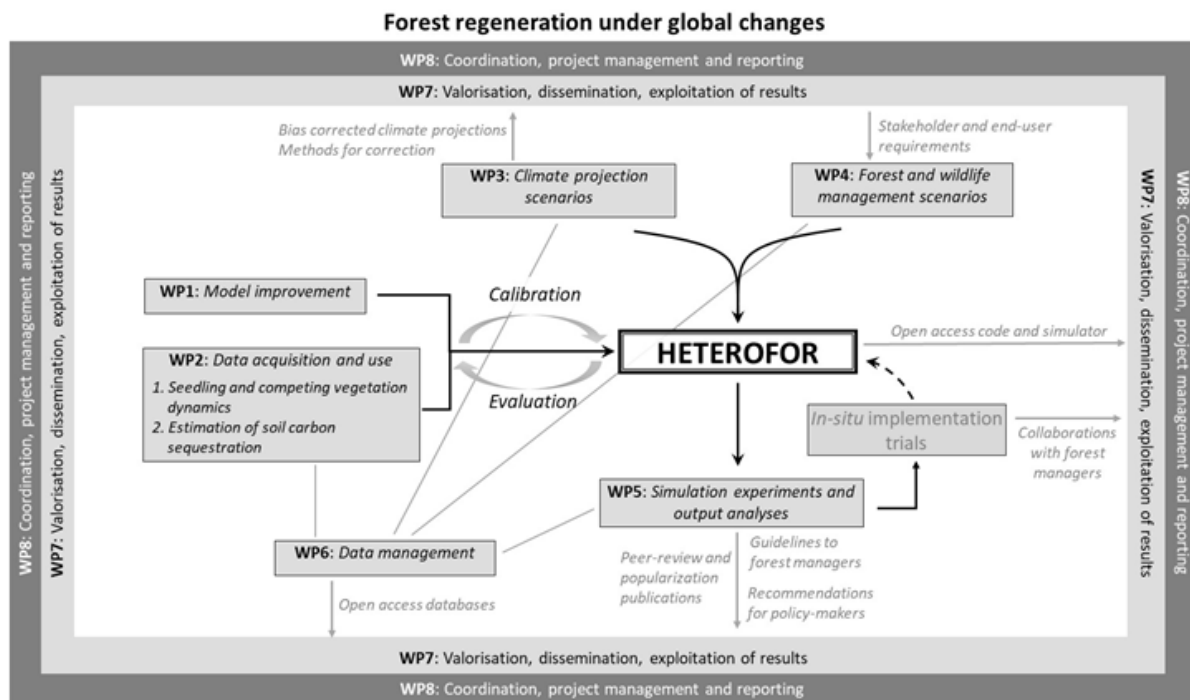


Figure 1. Conceptual scheme of the project

To conduct these simulations, the original version of HETEROFOR was enhanced to incorporate processes such as hydraulic failure, ungulate impacts, carbon sequestration in both soil and forest products, and to provide users with a range of model outputs, including indicators of wood production, profitability, biodiversity, and carbon balance and storage (WP1). Additionally, a disaggregation procedure was developed to enable the model to convert daily meteorological data into hourly data.

Data were collected or utilized to provide some information needed for model initialization, parameterization, and evaluation (WP2). Regeneration dynamics were monitored in situ in both broadleaved and coniferous forests. Browsing damage by ungulates was tracked across an extensive network of paired fenced and unfenced plots. Additionally, a rainfall limitation experiment was conducted to assess the effects of reduced soil water content on seedling growth. Existing data on soil carbon content (from ICP Forests Level II plots in France) were used to evaluate the new soil carbon dynamics module.

In WP3, we bias-corrected the CMIP6 climate model projections before using them in HETEROFOR simulations. In WP4, we defined the silvicultural strategies and ungulate population densities to be used in the simulation experiment itself (WP5).

Data management for the project was handled in WP6. WP7 focused on the optimal valorisation, dissemination, and exploitation of project outcomes, as well as fostering interactions with stakeholders. Lastly, the strategy for ensuring efficient coordination and project management was implemented in WP8.

WP1. Model improvements

Task 1.1 Soil water availability effect on regeneration

A new routine, described below, was implemented to account for the impact of hydraulic failure during droughts and heat waves.

The default version of HETEROFOR simulates tree transpiration using the Penman-Monteith equation and a tree-level adaptation of the Ball *et al.* (1987) approach to calculate the stomatal conductance from carbon assimilation, vapour pressure deficit and soil water potential (de Wergifosse *et al.*, 2020). Tree transpiration and photosynthesis are described in such a way that their response to water stress is fully reversible. Only stomatal regulation is considered: conductivity is reduced when the evaporative demand is high (low relative humidity) and when the soil is dry (low soil water potential) but can fully recover when the soil and atmospheric conditions become less dry (during the night or after a rain event). Such an approach is not sufficient to adequately describe the long-lasting effects of extreme events on the tree hydraulic system. To account for the stress memory of extreme events (heat waves combined with droughts), a new routine was implemented in HETEROFOR to describe tree hydraulics by considering hydraulic failure due to embolism and its consequences on tree vitality (premature leaf shedding and branch mortality).

The new routine is based on the approach of Couvreur *et al.* (2018) which consists in solving a differential equation to predict xylem water potential and conductivity at any tree height considering that conductivity depends on water potential. To solve this equation, the transpiration flux is first fixed at a plausible value (obtained based on the default approach) and the water potential at the trunk base is estimated from soil water potential, tree transpiration and root conductivity. Based on these boundary conditions, the vertical profile of the xylem potential is derived and its value at the top of the tree is used to estimate a new value for the stomatal conductance and tree transpiration. These steps are repeated iteratively until the xylem potential at the top of the tree converges towards a unique value (considering a certain tolerance).

The estimated loss of conductivity at the top of the tree and at the crown base height is then used to predict temporary defoliation and crown dieback, respectively. The temporary defoliation has an effect only during the current vegetation period while the crown dieback affects the defoliation level of the following year. A recovery process is however considered: each year, the tree recovers a proportion of its foliage equivalent to its relative increment in basal area (compared to its sapwood area). For the regeneration cohorts, only the temporary defoliation is considered.

By conducting an in-depth review of the literature, we have collected all the parameters necessary to run the tree hydraulics routine:

- stem saturated hydraulic conductivity,
- xylem hydraulic vulnerability (slope and P50),
- Huber ratio at tree top,
- stomatal conductance reduction function,
- relationship between conductivity loss and defoliation or crown dieback.

The model's ability to predict the xylem water potential was evaluated by comparing these predictions with water potential measurements made in the Lauzelle wood. Similarly, defoliation data collected in the forest monitoring plots were used to validate the relationships between conductivity loss and defoliation or crown dieback.

Task 1.2 Ungulate impact on regeneration

Among others, the REG+ project aimed at testing the ungulate impacts on tree regeneration and long-term forest dynamics through a simulation approach. Ungulates affect stand development by browsing tree seedlings and peeling the bark of coniferous tree species. At the beginning of the project, our forest growth model (HETEROFOR) contained a regeneration module but no routine to account for ungulate browsing and bark peeling.

Two options were considered for modelling ungulate browsing:

- (i) a descriptive approach reducing seedling density and seedling height growth based on a fixed proportion provided by model user. These ungulate effects are applied only on regeneration cohorts below a given height. The seedlings taller than this threshold are no longer browsed.
- (ii) a more process-based approach based on the browsed biomass which is estimated from:
 - the red deer, roe deer and boar population densities,
 - their body mass,
 - their energy requirement,
 - their diet composition,
 - the energy content of seedlings, seeds and external food supply.

The browsed biomass is first distributed among tree species or ground vegetation (e.g. bramble) according to their browsable biomass and palatability. Then, the browsing is applied by randomly selecting regeneration cohorts and by reducing their browsable biomass by a given small quantity (bite). For each tree or ground vegetation species, the process is repeated and the biomass to be browsed is progressively decremented. When the biomass of a regeneration cohort (or ground vegetation layer) is reduced, all its characteristics are adapted accordingly (e.g., seedling height, cohort or vegetation cover or LAI).

The modelling of bark peeling damages (including the progressive development of stem decay on the affected trees) has been integrated in HETEROFOR based on the approach implemented by G. Ligot in [GYMNOS](#), a model of the CAPSIS simulator dedicated to even-aged coniferous stands. These model

developments were achieved for Antoine Crochet's master thesis which aimed at simulating the long-term ecological and economical consequences of ungulate overabundance on coniferous stands. This study was carried out in the communal forest of Stoumont based on well-documented case studies.

The bark peeling algorithm requires the annual bark peeling rate (%) as input parameter, which reflects the ungulate pressure level, especially red deer (*Cervus elaphus*) in this case, and has been found to not only depend on population density but also on other factors such as the environmental carrying capacity, the landscape structure and the severity of winter conditions (Ligot *et al.*, 2013b). In a first step, bark peeling occurring in the current year is shared between individuals already peeled previously and those still unaffected using a model proposed by T. Gheysen (unpublished) expressing the percentage of bark peeling on healthy individuals as a function of annual bark peeling rate and the percentage of already peeled individuals. A set of healthy individuals to be peeled in the current year are then selected to reach the estimated percentage. These healthy individuals to be peeled are chosen considering a probabilistic model describing the sensitivity of individuals to bark peeling as a function of trunk circumference at breast height. Bark peeling damage is then applied on these selected individuals by drawing the damage height, width and length from probability distributions fitted using bark peeling monitoring data (Gheysen *et al.*, 2011). Finally, for each bark-peeled individual, the development of stem decay is described using a model relating total decay length to social status, damage width and length, time since damage occurred and the average annual girth increment (Löffler, 1975). In the evaluation of financial profitability using the ECONOMICS2 library (see below), the market value of the stem part containing decay (leftover part) is considered to be zero, and the value of the healthy part is determined as that of a tree whose circumference at breast height is equal to the circumference of the trunk at 1.3 m above the leftover part. In this way, the value of the healthy part is somewhat overestimated as the increase in taper and relative importance of knots with height is not accounted for, which compensates for the fact that the leftover part could, at least partly, be valued as trituration. This overcomes the difficulty in estimating the price discount to be applied for the healthy part.

Task 1.3 Implementation of a soil carbon module

During the first follow-up committee held in October 2021, the implementation of a soil carbon module was deemed not to be a priority. The opportunity to work on this did arise, however, with the arrival of a Chinese post-doctoral fellow (Huizhou Gao) at UCLouvain. In the framework of the five-year forest research plan in Wallonia (plan quinquennal de recherche forestière), Mathieu Jonard developed a first version of the soil organic carbon module of HETEROFOR which was parameterized and evaluated by Huizhou Gao. For describing the soil organic carbon dynamics in HETEROFOR, various carbon compartments are considered (Figure 2):

- aboveground standing deadwood (snags),
- aboveground deadwood lying on the ground,
- belowground deadwood,
- aboveground decaying litter,
- belowground decaying litter,

- active carbon pools (one per mineral soil horizon),
- stable carbon pools (one per mineral soil horizon).

The deadwood and decaying litter compartments each consist of a series of cohorts at various stages of decay. Each year, new litter and deadwood cohorts are created based on the fresh litter production and on the fresh deadwood resulting from tree mortality and harvesting. A deadwood cohort is characterised by the tree death year, the year of his downfall, its tree species, position (above- or below-ground), size class (diameter < 7 cm or > 7 cm), initial chemical composition (lignin and cellulose contents), current lignin, cellulose and other compound masses (Edelmann *et al.*, 2023). A litter cohort is characterised by its production year, tree species, litter type (leaves, branches, fruits, fine roots), position (above- or below-ground), initial chemical composition (lignin and cellulose contents), current lignin, cellulose and other compound masses (Adair *et al.*, 2008).

From one year to the next, the current biomass (considered as a whole or in different fractions) is updated to take account of decomposition. This can be assessed using simple models (exponential or linear) with species-specific parameters. For most of the species considered in HETEROFOR, the decomposition rate of the exponential model (k) was adjusted based on data collected in the literature (e.g. incubation experiments with litter bags). For deadwood, a linear decomposition model was initially selected and parameterized based on the results of Edelmann *et al.* (2023). When no information was available or specified for a species, decomposition was estimated using the three-pool model of Adair *et al.* (2008). A pool of lignin and cellulose was considered as well as a pool of other organic compounds. In this approach, each pool decomposes at its own rate according to an exponential model and this rate is modulated by a litter quality effect and by a coefficient that accounts for meteorological conditions (Climate Decomposition Index, CDI).

Decomposition of litter and deadwood releases carbon dioxide and produces decaying organic matter transferred to other pools. The part of decomposed deadwood not released as carbon dioxide is transferred to the litter compartment by the creation of a new litter cohort (whose production year corresponds to the date of transfer). The decomposed litter not released as carbon dioxide joins the active carbon pool of the upper mineral horizon (aboveground litter) or of the mineral horizon in which the root litter was produced. The organic matter in the active carbon pool is released as carbon dioxide (active carbon respiration), leached as dissolved organic carbon (DOC) or transferred to the stable pool. For a given mineral horizon, active carbon respiration is obtained by multiplying the active carbon stock by the basal respiration or mineralisation rate and by two modulators accounting for soil climate (soil water content and temperature). The Yan *et al.* (2018) function is used to account for the soil water content effect on active carbon respiration while the Lloyd and Taylor (1994) equation is employed to describe the soil temperature effect. The DOC production is supposed to be proportional to the active carbon respiration and the annual transfer to the stable pool corresponds to a fixed fraction of the active carbon pool.

Aboveground standing deadwood is converted into lying deadwood when the remaining mass of the former reaches 50% of its initial biomass. When the fraction of remaining mass reaches a given threshold depending on the tree species and on the litter type (see the concept of maximum

decomposition of Berg *et al.* (1996)), the remaining mass is transferred to an active carbon pool and the cohort litter disappears.

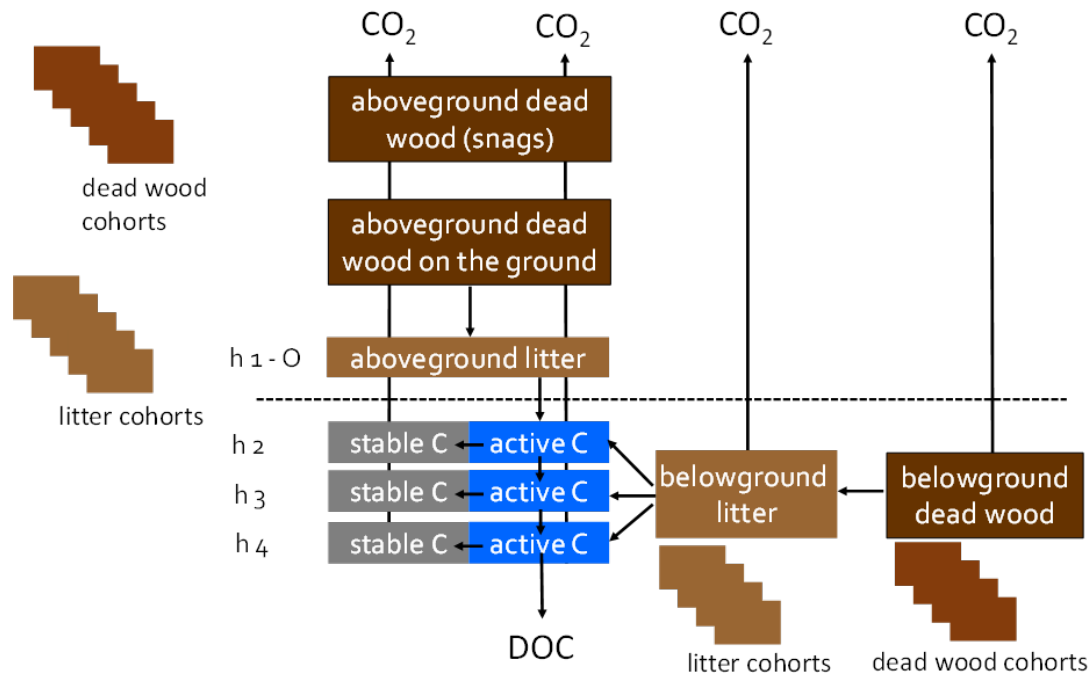


Figure 2. Conceptual diagram of the HETEROFOR module describing soil organic carbon dynamics

Task 1.4 Assessment of forest production and diversity

At the beginning of this project, HETEROFOR provided reliable estimates of tree growth but did not provide outputs, such as economic indicators, that were needed to compare management scenarios. As we aimed to develop a highly integrated decision-support tool, new functionalities had to be added in HETEROFOR to better assess forest diversity, timber production and financial profitability.

As planned, we connected the model HETEROFOR to the ECONOMICS2 library developed by G. Ligot, both tools being implemented in the CAPSIS simulation platform. Thanks to this work, it is easy to assess the profitability of forest management scenarios simulated with HETEROFOR by defining the economical operations associated with each silvicultural intervention carried out during the simulation. Initially, the required economical parameters (e.g., discount rate, silvicultural operation costs, timber price lists) were set by the user using a graphical user interface (Figure 3) once a simulation was completed. In this 'manual' economic setting mode, the dates of each silvicultural operation and the associated expenses and/or incomes had to be specified by the user. A new functionality was implemented in HETEROFOR enabling automatic specification of the economical operations as silvicultural interventions occur during the simulation. In this automatic procedure, the economical operations are defined by combining characteristics of each silvicultural intervention (e.g., type of operation, treated area, number of planted seedlings, type and number of protections against ungulates installed, volume of harvested trees for each species) with the economic settings provided in a text file loaded at model initialization. At the end of the simulation, the economic settings and the automatically generated economical operations may still be adapted manually if necessary. Then, the

user can obtain various economic indicators such as the net present value, forest value at different times, the annuity, the internal rate of return, etc.

The ECONOMICS2 library has moreover been improved to provide reliable economic indicators for uneven-aged and mixed forests. In particular, the computation of annuity indicators has been corrected, and new features have been added such as plots to show the variability of stumpage prices through time et across diameter classes. Moreover, a detailed user guide has been written (<https://orbi.uliege.be/handle/2268/263994>). This document not only provides step-by-step instructions on how to use ECONOMICS2, but also presents the essential theoretical concepts to be able to repeat and interpret the calculations.

1) Define the period
INFINITY_CYCLE_WITH_LAND_OBSERVATION_AT_FIRST_AND_LAST_DATE
First year of the economic scenario : 2012 End of transitory period : 2012 Last year of the economic scenario : 2112

2) Define and load parameters from a file
D:\workspace\capsis4\data\samsara2\economics2\economicOperations2.txt

3) Define discount rate and/or land to compute forest value
Discount rate [0,1] : 0.02 Land value : -1.0

4) check, modify the list of user-defined operation

date	1st date	last date	frequency	label	type	trigger	expense	income
0	0	0	0	gestion	FIXED	YEARLY	50	0

5) check and remove the list of model-defined operation

date	label	type	trigger	expense	income
2022	Uneven-aged thinning	DBH_CLASS	ON_INTERVENTION	0	0
2032	Uneven-aged thinning	DBH_CLASS	ON_INTERVENTION	0	0
2042	Uneven-aged thinning	DBH_CLASS	ON_INTERVENTION	0	0
2052	Uneven-aged thinning	DBH_CLASS	ON_INTERVENTION	0	0
2062	Uneven-aged thinning	DBH_CLASS	ON_INTERVENTION	0	0
2072	Uneven-aged thinning	DBH_CLASS	ON_INTERVENTION	0	0
2082	Uneven-aged thinning	DBH_CLASS	ON_INTERVENTION	0	0
2092	Uneven-aged thinning	DBH_CLASS	ON_INTERVENTION	0	0

6) check, modify the price list

species	upper bound of dbh class	price
Epicea	25	35
Epicea	35	50
Epicea	45	70
Epicea	55	80
Epicea	65	80
Epicea	80	90
Epicea	500	90
Hetre	20	0

Figure 3. Graphical user interface that can be used to define the economical parameters

The computation of several forest diversity indicators has been implemented in HETEROFOR. A first set of indicators are the widely used species richness, Shannon (Margalef, 1958; Shannon and Weaver, 1949) and Simpson (Simpson, 1949) indices, which quantify the number of species, community entropy (combining information on species richness and evenness) and species dominance, respectively. The species proportions used to compute the Shannon and Simpson indices are expressed in terms of basal area. Another set of diversity indicators accounts for the spatial arrangement of trees. Among them, the Clark and Evans index (Clark and Evans, 1954) describes the positioning of trees based on density and on distances among neighbours. It expresses the extent to which the spatial arrangement of trees deviates from that of a completely randomised positioning following a Poisson distribution, in which case it equals to 1. It takes values lower than 1 if clumping of trees occurs in the stand, while it presents

values larger than 1 for stands with regular tree spacing and shows the maximum value of 2.1491 in the case of hexagonal arrangement of trees. A modified version of the original Clark and Evans index, minimising edge effects (Füldner, 1995), has also been implemented in HETEROFOR. Besides, the Von Gadow mixture index (Von Gadow, 1993) describes the spatial association among species within a stand. It can take values between 0 and 1, with low values indicating dominance of one or few species arranged in clusters and high values revealing intimate mixtures of species in the stand. Finally, two other implemented spatial diversity indicators are the horizontal and vertical differentiation indices of Von Gadow (Füldner, 1995; Von Gadow, 1993) which characterise the heterogeneity of the stand structure in terms of trunk circumference at breast height and total height of the trees, respectively. Aside from tree attributes and spatial organisation, tree-related microhabitats (TreMs) are also used as surrogate biodiversity indicators. TreMs are “distinct, well-delineated structures occurring on living or standing dead trees, that constitute a particular habitat for species or species communities, during at least a part of their life cycle, to develop, feed, shelter or breed” (Larrieu *et al.*, 2018). They constitute an important tool for forest managers, notably to guide the selection of habitat trees for the conservation of biodiversity (Asbeck *et al.*, 2021). The emergence and development of TreMs were implemented in the model based on the works of Courbaud *et al.* (2017) and Courbaud *et al.* (2022). The occurrence of TreMs is then used to compute biodiversity indicators integrating the size, the frequency, the degree or rarity and the replacement rate of TreMs appearing on trees during simulations (Larrieu and Amberger, Unpublished). The values of all these indicators can be exported for each year of the simulations allowing to analyse their temporal evolution over the simulated period and to provide averages for the entire period or for sub-periods.

Task 1.5. Assessment of climate services

Forests interact with the atmosphere through exchanges of energy, carbon dioxide and water and influence thereby the climate, either amplifying or mitigating change resulting from human activities. In addition to carbon sequestration in tree biomass, evapotranspiration from forest canopies promotes cooling of the atmosphere. These climate services of forests are expected to be affected by changing climate conditions. Notably, the rise of temperature and modifications in the precipitation pattern may induce severe water stress leading to loss of tree growth, thereby reducing carbon sequestration, and limiting evapotranspiration due to drier soil conditions. On the other hand, studies have shown a gain in tree growth associated with the CO₂ fertilization effect. Therefore, predicting the effects of climate change on forests and, consequently, on their climate service provision is not straightforward. Likewise, forest management will also influence forest climate services either positively or negatively with regard to mitigation of climate change effects. Indeed, changes in forest canopy structure and species composition due to management actions affect exchanges with the atmosphere and, thereby, forest climate services.

These forest climate services are assessed in HETEROFOR. Carbon sequestration in biomass and evapotranspiration were already among the outputs of the version model in effect at the start of the project. During the project, HETEROFOR has been connected to [CAT](#), a carbon accounting tool software dedicated to the assessment of the carbon balance of managed forests following the guidelines of the International Panel on Climate Change (IPCC) for national greenhouse gas inventories in the Land use,

land-use change and forestry (LULUCF) and Waste sectors (Pichancourt *et al.*, 2018). Beyond the evolution of the aboveground and belowground living biomass and of the dead organic matter compartments already simulated in the newly implemented carbon module of HETEROFOR (see Task 1.3), CAT also considers the harvested wood product (HWP) carbon pool in use or deposited at landfill sites. Based on a user-customizable flux configuration scheme describing the carbon life cycle of wood products including transformation, recycling and disposal steps, CAT provides estimates (i) of the material and energy substitution, corresponding to the greenhouse gas emissions avoided when a HWP is used in place of an alternative product, (ii) of the fossil fuel carbon emissions during the HWP life cycle, (iii) of the evolution of both degradable and non-degradable HWP at landfill sites and (iv) of emissions due to landfilled HWP degradation (CH_4) and wood combustion (CH_4 , CO , COV). In the framework of the present project, a flux configuration scheme established for the Walloon wood processing sector based on the works of Wohlfrom (2022) and Charles (2023) was used.

Task 1.6. Disaggregation of daily meteorological data

Data from climate-model projections used in REG+ to investigate the impact of climate change on forests consist of multiple projections or an ensemble of projections that is being made available by the international climate community within different projects (e.g. CMIP6 or CORDEX). These are the same datasets that are being used by the Intergovernmental Panel on Climate Change (IPCC) and the *ensemble* approach is necessary in order to estimate the uncertainties of future impacts. Even though some of these datasets and variables are available at the hourly timescales (e.g. within CORDEX) most are provided at the daily timescales. Therefore, in order to allow for a proper quantification of the climate-projection uncertainties, meteorological parameters at the daily timescale are preferred. However, the HETEROFOR model used within REG+ requires hourly data as input. A technique called *disaggregation* or also *temporal downscaling* is therefore used to transform the datasets from daily up to hourly values. For this, empirical relations are fitted on observed hourly meteorological variables as a function of their daily characteristics.

Different approaches have been tested and developed for disaggregating the different variables including incoming solar radiation (R_s), temperature (T), precipitation (P), relative humidity (RH) and wind speed (W). The disaggregation methods used mostly stem from Förster *et al.* (2016) but were partly further developed. A validation effort was performed. It revealed some issues, that have been fixed since then. A systematic bias in relative humidity has been detected. The origin of this bias is likely associated with the use of the minimum temperature in place of the dew point temperature to estimate the saturated vapour pressure. Therefore, a new approach for disaggregating the relative humidity directly was developed to solve this problem.

We made use of ALARO-0 data for calibrating and validating the disaggregation procedure. ALARO-0 is a high-resolution atmospheric model developed within the scope of the CORDEX.be project (Termonia *et al.*, 2018). It was developed at a spatial resolution of 4 km by the Royal Meteorological Institute of Belgium (RMI) based on the numerical weather prediction model called Aire Limitée Adaptation Dynamique Développement International (ALADIN). At the RMI, the physics parameterization package of the ALARO model was specifically designed for running at convection-permitting resolutions, with

the modular multiscale microphysics and transport (3MT) precipitation and cloud scheme. The ALARO model was forced by the CMIP5 CNRM-CM5 model developed at Météo-France (Termonia *et al.*, 2018). The precipitation, average temperature, u and v directions of wind speed, solar radiation, and specific humidity data from the ALARO model for the historical period (1976-2005) are used. In the following we describe the temporal disaggregation methods that do not need further investigations.

Air temperature

The following cosine function was proposed by de Wit (1978) for disaggregating daily temperature to hourly temperature:

$$T_{hr} = \frac{T_{max}-T_{min}}{2} \times \cos\left(\frac{\pi(hr-15)}{12}\right) + T_{avg} \quad (3.1)$$

where T_{hr} is temperature (°C) at time hr varying in the range 1–24; T_{max} , T_{min} , and T_{avg} are the maximum, minimum and average daily temperatures, respectively, (°C). The equation was calibrated for Wallonia as follows:

$$T_{hr} = \frac{T_{max}-T_{min}}{2} \times \left[\alpha \times \cos\left(\frac{\pi(hr-hr_{Tmax})}{12}\right) \right] + T_{avg} \quad (3.2)$$

where α is a calibration coefficient, and hr_{Tmax} is the hour at which daily maximum temperature is observed on average, expressed in [1-24] for GMT0. For the REG+ case study sites, $\alpha = 0.8$ and $hr_{Tmax} = 15$. The calibration was performed using hourly data of six stations (Baileux, Eupen, Gedinne, Louvain-la-Neuve, Ukkel, Virton) following the statistical fitting procedure.

So as to avoid the presence of discontinuities in temperature values at the transition between consecutive days, trends for the temperature average and the amplitude were accounted for with the following equations. Average temperature and average temperature amplitude at the transition between the preceding day ($d-1$) and the current day (d) are determined as:

$$T_{avg_start,d} = \frac{T_{avg,d-1} + T_{avg,d}}{2} \quad (3.3)$$

$$T_{ampl,d-1} = \frac{T_{max,d-1} - T_{min,d-1}}{2} \quad (3.4)$$

$$T_{ampl,d} = \frac{T_{max,d} - T_{min,d}}{2} \quad (3.5)$$

$$\overline{T_{ampl_start,d}} = \frac{T_{ampl,d-1} + T_{ampl,d}}{2} \quad (3.6)$$

where $T_{avg_start,d}$ (°C) is the temperature average at the start of the current day, $T_{ampl,d-1}$ (°C) and $T_{ampl,d}$ (°C) are the temperature amplitude for the preceding and the current days, respectively, and $\overline{T_{ampl_start,d}}$ (°C) is the average temperature amplitude at the start of the current day. These quantities are similarly calculated for the transition between the current day and the next ($d+1$) day. Temperature at time hr (in [1-24] format) is then computed as follows:

If ($hr \leq 12$)

$$T_{avg_diff} = T_{avg,d} - T_{avg_start,d} \quad (3.7)$$

$$T_{ampl_diff} = T_{ampl,d} - \overline{T_{ampl_start,d}} \quad (3.8)$$

$$T_{hr} = \overline{T_{ampl_{start,d}}} + (hr - 1)/12 \cdot T_{ampl_{diff}} \cdot \alpha \cdot \cos\left(\frac{\pi(hr - hr_{Tmax})}{12}\right) + T_{avg_{start,d}} + (hr - 1)/12 \cdot T_{avg_{diff}} \quad (3.9)$$

else

$$T_{avg_{diff}} = T_{avg_{end,d}} - T_{avg,d} \quad (3.10)$$

$$T_{ampl_{diff}} = \overline{T_{ampl_{end,d}}} - T_{ampl,d} \quad (3.11)$$

$$T_{hr} = T_{ampl,d} + (hr - 13)/12 \cdot T_{ampl_{diff}} \cdot \alpha \cdot \cos\left(\frac{\pi(hr - hr_{Tmax})}{12}\right) + T_{avg,d} + (hr - 13)/12 \cdot T_{avg_{diff}} \quad (3.12)$$

Rainfall and wind speed

To perform temporal disaggregation, the subdaily distribution of analog days is employed to distribute daily precipitation totals into hourly intervals (Carreau *et al.*, 2019; Mehrotra *et al.*, 2012). Here, analog days are defined as days that are similar in terms of daily cumulative precipitation at the location of interest. For the projections to be disaggregated, the most similar day in the historical period (considering only the corresponding month) is selected and its hourly precipitation distribution is used to define the hourly evolution of rain for this day. Compared to the method of fragments initially tested, this approach does not generate weak rainfall for all hours of the day. The pronounced evapotranspiration detected in HETEROFOR is no more simulated. The same approach was also used for wind speed.

Solar radiation

The method of fragments (MOF) is used to disaggregate daily solar radiation. The main idea behind the MOF is to disaggregate the day of interest using the long-term diurnal pattern and impose the relative distribution (i.e., fragments) on the day of interest (Sharma and Srikanthan, 2006; Westra *et al.*, 2012). In our case where the disaggregation is conducted from daily to hourly values, the number of fragments is 24. The relative distribution of hourly values, therefore, consists of 24 relative weights that sum up to 1. The hourly data of the stations are first aggregated to daily values. The weights (factors) for a given hour in the entire time series are then calculated as the ratio of the value in that hour to the respective total daily value. The weights are averaged per hour to determine the relative distribution of hourly to daily values, which are subsequently averaged over the stations to find the regional pattern. The regional, hourly weights are finally applied to daily model simulations to disaggregate them to hourly values. We calculated the hourly fragments separately for each month of the year, which led to a slight enhancement in the results compared to not distinguishing between months.

Task 1.7. Exports of indicators for simulation result analysis and comparison

To ease exportation and analysis of the simulation results, exports of pre-processed indicators were implemented considering three integration formats: (i) ecosystem level over the simulation period, distinguishing the species for some of the indicators, (ii) yearly at the ecosystem level and (iii) yearly at species level (see Table I). For the latter format, the following ‘status’ were also distinguished for each species: living trees, dead trees, cut trees, trees recruited on the current year, wind damaged trees, all seedlings and new seedlings (germinated or planted during the current year). To evaluate stand resistance to wind, a storm is generated at regular time interval (default is 10 years) when executing the exports for formats (i) and (iii) and the basal area proportions of overturned, broken, impacted (i.e., damaged by the fall of a neighbouring tree) and undamaged trees are calculated.

Table I. Exports of pre-processed indicators implemented in HETEROFOR

Indicators	Integration levels		
	Ecosystem level over the simulation period ¹	Yearly at ecosystem level	Yearly at species level ²
Stand dendrometry & density			
Number of individuals /ha	Avg; Dead, recruited (/species)		
Trunk circumference (cm)			
Total height (m)			
Dominant height (m)			
Basal area (m ² /ha)	Avg; Trees, seedlings (/species)		
Leaf area index (m ² /m ²)	Avg; Trees, seedlings (/species)		
Volume (m ³ /ha)			Trunks, branches, harvestable branches, total
Biomass (kgC/ha)			Trunks, branches, harvestable branches, leaves, fruits, roots, total
Productivity			
GPP (kgC/ha)	Avg; Trees, seedlings (/species)	Total, trees, seedlings	
NPP (kgC/ha)	Avg; Trees, seedlings (/species)	Total, trees, seedlings	
Water balance			
Rainfall (mm)			
Transpiration (mm)		Total, trees, seedlings	
Potential transpiration (mm)		Trees, seedlings	
Transpiration deficit (mm)		Trees, seedlings	
Evaporation (mm)			
Evapotranspiration (mm)	Avg (/species)		
Deep drainage (mm)			
Financial profitability			
Land market value (eur/ha)	Set as economic parameter		
Land expected value (eur/ha)	Net present value at perpetuity, for infinite cycle with land observation		
Total net present value (eur/ha)	Net present value for land and trees		
Net present value of trees (eur/ha)	Total net present value minus land market value		

Table I. Exports of pre-processed indicators implemented in HETEROFOR (continued)

Indicators		Integration levels
Fixed discount rate (%)	Set as economic parameter	
Optimized internal rate of return (%)	Internal rate or return evaluated based on land market value, for infinite cycle with land observation	
Calculated internal rate of return (%)	Ratio between average profit and average stand market value	
Stand market value (eur/ha)	Avg, initial, final (/species)	
Commercial volume (m ³ /ha)	Initial, final	
Harvested volume (m ³ /ha/year)	Avg	
Income (eur/ha/year)	Avg	
Expenses (eur/ha/year)		
Profit (eur/ha/year)	Avg	
Carbon module		
Living biomass (MgC/ha)	Avg, initial, final, variation	
Dead wood (MgC/ha) Standing, lying, belowground	Avg, initial, final, variation	
Decaying litter (MgC/ha) Aboveground, belowground	Avg, initial, final, variation	
Stable C (MgC/ha)	Avg, initial, final, variation	
Active C (MgC/ha)	Avg, initial, final, variation	
Soil heterotrophic respiration (MgC/ha)		
DOC production (MgC/ha)		
CAT		
Living biomass (MgC/ha) Woody aboveground, belowground	Avg, initial, final, variation	
Dead biomass (MgC/ha)	Avg, initial, final, variation	
Products in use (MgC/ha)	Avg, initial, final, variation	
Fossil fuel carbon emissions (MgC/ha)	Cumulated	
Material and energy substitution (MgC/ha)	Cumulated	
Landfill degradable pool (MgC/ha)	Avg, initial, final, variation	
Landfill non-degradable pool (MgC/ha)	Avg, initial, final, variation	
Landfill methane emissions (MgC/ha)	Cumulated	
Wood combustion emissions (MgC/ha)	Cumulated	

Table I. Exports of pre-processed indicators implemented in HETEROFOR (continued)

Indicators		Integration levels
Diversity		
Simpson index	Avg	
Diversity score based on dendro microhabitats	Avg	
Wind resistance³		
Overturned proportion	Avg (/species)	
Broken proportion	Avg (/species)	
Impacted proportion	Avg (/species)	
Undamaged proportion	Avg (/species)	

¹Avg: average value over the simulation period, Initial: value on initial year, Final; value on final year, Variation: final – initial; /species: indicator is provided both for all species together and separately for each species. ²For each species, the following status are considered: living trees, dead trees, cut trees, trees recruited on the current year, wind damaged trees, all seedlings and new seedlings (germinated or planted during the current year). ³Determined from storms generated at regular time intervals (default is 10 years) when executing the export.

WP2. Data acquisition and use

The calibration and validation of newly implemented features in the HETEROFOR model (see WP1) require targeted observations and measurements. While most of the necessary data were already available, additional complementary data were needed. To address these gaps, we collected field data to calibrate key forest ecosystem processes, including sapling and pole height growth dynamics, the impact of ungulate browsing on sapling growth, and the effects of reduced rainfall on sapling development.

Task 2.1 Regeneration dynamics

In situ monitoring of advanced regeneration dynamics in broadleaved forests

In broadleaved forests, the growth of juvenile trees in the understory has already been well described by Ligot *et al.* (2013a) but this work was limited to juvenile trees of less than 3-4 meters in height. To be able to accurately model the growth of small and tall juvenile trees, we collected new data about the growth, mortality, and density of taller trees (3-10 meters in height, hereafter called poles).

Initially, we planned to monitor pole growth and mortality in a selection of 7 plots out of the 27 fenced plots studied by Ligot *et al.* (2013a). Finally, we collected data in 10 sites. In all sites, most poles were taller than 3 meters and smaller than 8 meters. 5 sites were established in beech-dominated pole clumps and 5 sites were established in oak-dominated pole clumps. In each site, 10-30 poles were selected and identified among the dominant poles without important defect (forks, wounds, ...). The diameter at breast height (dbh) and the height were recorded for each pole. The selected trees were at least 4 meters apart. Additionally, a circular plot of about 50 poles (plot radius of 3-3.5 meters) was established in the middle of each studied clump (Figure 4). These measurements were conducted during the winters of 2012-2013, 2014-2015, 2016-2017, 2021-2022 and 2023-2024.

As planned, additional measurements were performed during the winter of 2022-2023. The trees around the studied pole clumps were measured. These trees were last mapped and measured in 2013

(Figure 5). Since then, the trees have grown and, more importantly, some of them have been harvested. Therefore, the competitive environments around the pole clumps have changed. As we aim to use this dataset to model pole growth and mortality in response to the competitive environment (e.g. as function of the amount of intercepted light, Figure 5), it was important to update the measurements. Every tree with a girth larger than 40 cm and within less than 20 meters from the studied pole clumps (or from the fence) were mapped and measured. The studied identified poles as well as plot centres were also mapped.



Figure 4. Monitored oak-dominated clumps. The poles with a blue mark are located within the circular plots and the poles with a yellow mark and a plastic tag are the dominant selected poles

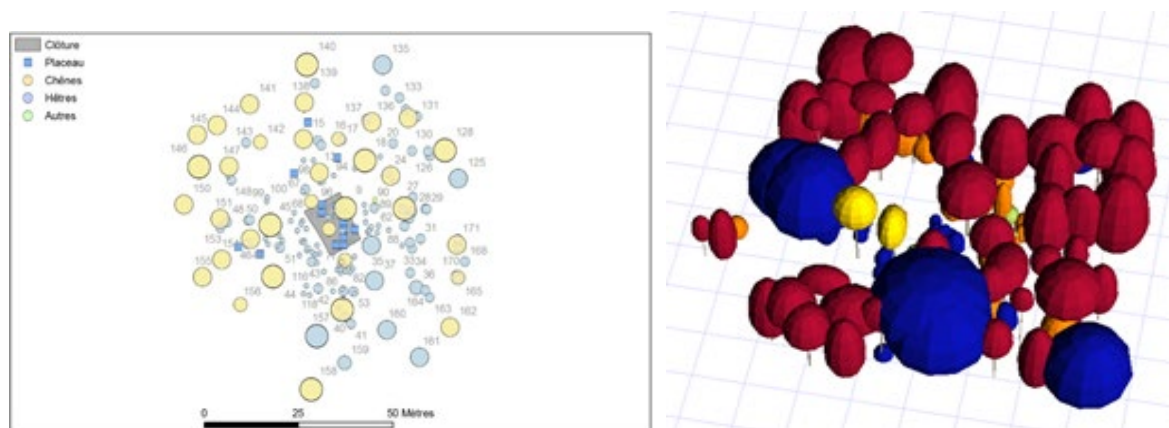


Figure 5. The trees around studied regeneration were mapped and measured. These measurements are used to build 3D mock-ups of the stand to compute the amount of light that is available for each tree, pole and seedling

***In situ* monitoring of regeneration dynamics in coniferous forests**

In coniferous forests, the natural regeneration has been monitored since 2015 in the Belgian Ardennes within 108 plots installed at 9 sites. Though the monitoring of this network of plots is funded by another project, the collected data was used by the REG+ project. During the winter of 2021-2022

and 2023-2024, all the plots of this network were monitored as planned. With this data, it is therefore now possible to compute regeneration dynamics parameters in the understory of coniferous stands over a valuable 8-year period.

***In situ* monitoring of ungulate damage on regeneration**

Species-specific browsing damage by ungulates have been monitored in a vast network of pairs of fenced and unfenced plots. 971 pairs of plots were installed in 2016, 734 pairs of plots were measured until 2021 by the “Département de la Nature et des Forêts” (DNF, SPW) and supervised by the “Département de l’Etude du Milieu Naturel et Agricole” (DEMNA, SPW) and Gembloux Agro-bio Tech (ULiège). Pairs of fenced/unfenced plots have been mostly settled in broadleaved forests managed with continuous cover forestry system (493 pairs of plots). Some plots were also installed in coniferous and mixed stands (190 pairs of plots), and in clearcuts (26). All plots were installed where the conditions were assumed (by the field operators) favourable for a good development of the natural regeneration.

In the 6-m² plots, the operators measured the height of the 5 tallest saplings of one or two main target species, the height of the 10 tallest saplings of the other species, the height of the 4 tallest individuals of *Vaccinium myrtillus* or *Rubus ideaus*, sapling density, the number of saplings of each species, and ground vegetation cover. For each plot, the abundance of ungulates was estimated with culling statistics and red deer population estimates (carried out by the DEMNA).

In addition, it appeared important to collect additional and more detailed observations of browsing effects on individual seedlings. These measurements aimed to model the probability of a seedling to be browsed as a function of seedlings size, species, and environmental conditions and to estimate the annual amount of biomass consumed by ungulate per browsed seedling. The additional measurements were carried out in more than 100 unfenced plots scattered across 3 forests with contrasted ungulate densities, in 2022. In each plot, 4 seedlings were sampled per height class ([10-60],]60-120] and]120-180] cm) of each present species. The height and collar diameter were measured for all these sampled seedlings. For each seedling, the apical shoots and 5 lateral shoots were also measured. We measured their length, the diameter at shoot lower part, the height at shoot lower part. We also recorded whether each of these shoots had been browsed. Additionally, the surrounding environmental conditions were assessed. We measured the basal area of the surrounding trees as well as the vegetation cover of bramble, the proportion of browsed bramble stems (Boulangier, 2010) and the density of ungulate faeces as a proxy of local ungulate density. This work was mainly performed by Mérielie Diacre during her Master thesis (Diacre, 2022).

These datasets were used to:

1. Quantify the effect of browsing on regeneration height and biomass with descriptive statistics.
2. Model the effect of browsing on regeneration height and biomass with statistical models.
3. Quantify the effect of browsing on seedling architecture and biomass.

The results of these analyses are presented below in Section 4.

Rainfall limitation experiment

To investigate and quantify the effects of climate changes and, in particular, of drought on seedling development, an *in situ* rainfall limitation experiment was conducted in regeneration patches of the Lauzelle wood (Louvain-la-Neuve, Belgium). This forest presented patches with well-established oak and beech regeneration in which experimental zones (blocks) were set up. Each experimental zone consisted into (i) a 'treatment unit' subject to artificial drought and (ii) a 'control unit' receiving natural throughfall (i.e., no artificial interception). In the treatment unit, drought was induced through the installation of a partially covered roof (4 x 4 m horizontal area) consisting of 25 cm wide transparent plastic strips spaced 12.5 cm apart (i.e., 2/3 covered area). The roof was around 1.5 m and 2.5 m high at its lowest and highest sides, respectively, and was adjusted depending on the height of the seedlings underneath it. Besides, a plastic sheet was inserted vertically in the ground to a depth of 40 cm at the periphery of the roof to avoid lateral transfers of water between the soil subject to natural throughfall and the soil under the roof (Figure 6). The control unit (2 x 2 m area) was delimited in the proximity of the roof: not too close to avoid an influence of the roof on the throughfall reaching the control unit area neither too far to stay in the same environmental conditions, especially with regards to light, soil and water supply. Such experimental zones were replicated three times for each considered species (sessile oak and European beech), resulting in a total of six experimental zones (blocks).



Figure 6. Partially covered roof installed above seedlings to induce artificial drought

Measurements were carried out on seedlings over the complete area of the 'control' units (2 x 2 m) and over the central 2 x 2 m area of the 'treatment' units, considering thereby a 1 m wide peripheral buffer zone in this latter case. A set of 32 seedlings was selected in each of the 12 experimental units, covering the encountered height range and evenly distributed over the 0-25 cm, 25-50 cm, 50-100 cm, 100-150 cm and >150 cm height classes. These seedlings were labelled with a unique identifier and seedling height and collar diameter were measured on each of these selected individuals. Besides, complete counting of the alive and dead seedlings is carried out in each experimental unit. These

observations were performed at setup installation (March 2021) as well as in March 2022, January 2023 and February 2024. Furthermore, since summer 2022, shoot increment, corresponding to the elongation of the apical shoot during the vegetation period, was also measured for each of the 32 selected seedlings in the experimental units. Indeed, shoot increment appeared to be a more relevant measure than total height and collar diameter to quantify seedling growth given the larger inaccuracies associated with the latter measurements. Moreover, so as to gain information on the variation of the growth dynamics during the vegetation period, shoot increment measurements were carried out in July and December in 2022 and 2023 and in May and December in 2024. Finally, shoot increment could also be determined for the year 2021 given the presence of scarfs on the seedling stems delimiting the growth periods and allowing thereby to go back in time. Shoot increment was found to be highly correlated with both total height and collar diameter increments (see Section 4.2) and, for the sake of efficiency, total height and collar diameter were not measured during winter 2024-2025.

Besides, soil water content within the upper 30 cm soil layers and temperature at soil surface were continuously monitored in each experimental unit using, respectively, frequency domain reflectometry (FDR) and thermistor sensors.

During the summer of 2022, these measurements were completed by the acquisition of physiological data to monitor the hydrodynamics of the seedlings and to study its dependence on the soil water status. Leaf water potential and stomatal conductance of seedlings were regularly measured using a Scholander bomb and a porometer, respectively. Moreover, one of the beech experimental zones has been equipped with psychrometers and tensiometers for more intensive monitoring of the stem and soil water potentials. Photosynthetically active radiation (PAR) sensors have also been installed in this zone. Both PAR and soil water potential were monitored continuously from June 2022, while stem water potential measurements were not repeated after 2022.

In addition, all trees with trunk circumference larger than 15 cm within a radius of 30 m of each experimental zone were measured (trunk circumference, total height, crown base height, height of largest crown extension, crown radii in the four cardinal directions) and mapped. These data enabled the initialization of the HETEROFOR model. This was notably useful to characterize the light environment of each experimental zone based on the outputs of the radiative balance module of the model, but it also allowed to validate the parametrization of the regeneration module by comparing seedling growth and mortality measurements to corresponding values predicted by the model. In other respects, hemispherical photographs were taken above each experimental unit during the vegetation period to further characterize their light environment. Finally, seedling biomass measurements were carried out on individuals sampled in the surroundings of each experimental zone.

Task 2.1 Estimation of soil carbon sequestration

The soil carbon module of HETEROFOR was parameterised based on an in-depth analysis of the scientific literature. For the deadwood decomposition rates of the different tree species, we relied on those obtained by Edelmann *et al.* (2023). The litter decomposition parameters were directly taken from Adair *et al.* (2008). Their three-pool decomposition model requires information on the initial

organic chemistry of the litter. A literature review was therefore carried out to collect data on the lignin and cellulose content of the different litter types for the tree species parameterised in HETEROFOR. Data on litter decomposition rate was also collected in order to better estimate the litter decomposition parameters (fitting of species-specific exponential decomposition models, improvement and regional adaptation of the approach of Adair *et al.* (2008) and determination of the remaining litter mass fraction when the maximum decomposition limit is reached (Berg *et al.*, 1996)). We used the same values as Kurz *et al.* (2009) for the fraction of decomposed deadwood transferred annually to litter (0.25) and for the fraction of decomposed litter transferred annually to the active carbon pools (0.17).

Literature searches were also carried out to estimate the basal respiration rate of the active carbon pools of the mineral soil. The transfer from the active to the stable pool as well as the DOC production was not considered.

The soil organic carbon data collected in the plots of the forest monitoring network in France (RENECOFOR) during two surveys carried out 15 years apart were used to evaluate the ability of the soil carbon module to reproduce the soil organic carbon (SOC) stock changes in the different soil horizons (Jonard *et al.*, 2017). These data were useful to initialise the model (total organic carbon content, fraction of stable carbon for each mineral soil horizon) and to evaluate it by comparing observed and predicted SOC stock changes. They were also used to fit some parameters (e.g., basal respiration rate of the active carbon pools).

By way of illustration, Figure 7 shows the temporal change of soil carbon pools in a beech stand of the Pyrénées atlantiques (HET64 of RENECOFOR) as predicted by the soil carbon module of HETEROFOR.

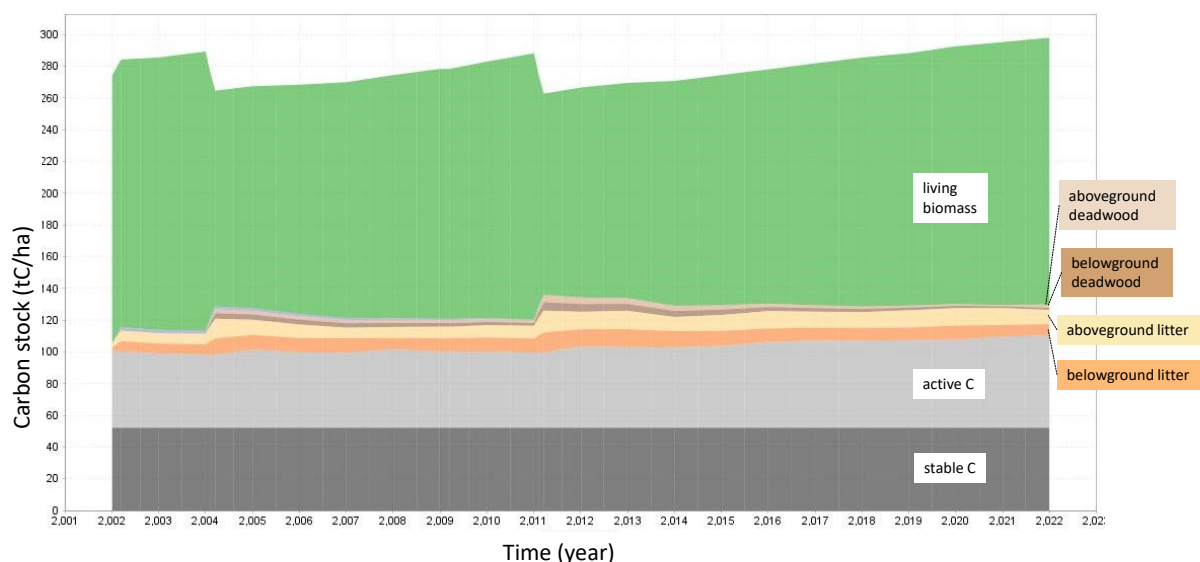


Figure 7. Illustration of the temporal evolution of carbon pools in a beech stand in the RENECOFOR network (HET64)

WP3. Establishment of climate projection scenarios

Task 3.1 Downscaled and bias-corrected multi-variable projections

For this work, we utilized the most recent climate model simulations available. These simulations originate from a large ensemble of general circulation models (GCMs) as part of the Coupled Model Intercomparison Project Phase 6 (CMIP6). We focus on seven variables: near-surface relative humidity, precipitation, near-surface minimum temperature, near-surface average temperature, near-surface u and v directions of wind speed, and solar radiation. They correspond to the variables available to force HETEROFOR. The simulations cover the period from 1976 to 2100, encompassing both historical data and future projections. For the CMIP6, the concept of representative concentration pathways (RCP) was integrated with the Scenario Model Intercomparison Project (ScenarioMIP) (O'Neill *et al.*, 2016) and was combined with Shared Socioeconomic Pathways (SSPs). While the RCPs represent pathways towards different levels of greenhouse gas concentrations and their corresponding radiative forcing in the year 2100 (van Vuuren *et al.*, 2011), the different SSPs describe changes in demographics, human development, economy and lifestyle, policies and institutions, technology, environment and natural resources (O'Neill *et al.*, 2016). For this study, the four Tier 1 scenarios in the CMIP6 (SSP1-2.6, SSP2-4.5, SSP3-7.0, and SSP5-8.5) are chosen, describing different challenges related to climate change adaptation and mitigation. In other words, these four scenarios envision different future worlds, respectively referring to the low-forcing sustainability pathway, medium-forcing middle-of-the-road pathway, medium- to high-end forcing pathway, and high-end forcing pathway. The complete archive of CMIP6 output is accessible from the multiple Earth System Grid Federation portals.

Eleven GCMs (listed in Figure 8) provide data for all variables required in this study for the historical period and the four future scenarios. For a given model and scenario, model centres generally provide multiple simulations to test the impact of the initialization procedure, different parametrization schemes or the sensitivity to the initial conditions. To give an equal weight to the GCMs in the ensemble mean, only one run per model (member r1i1p1f1) is used (Tabari *et al.*, 2019). As not all the CMIP6 models selected in this study simulate leap years (365-days calendar for four of them), time series were linearly interpolated in time to fill the missing days (29th of February). Finally, the data of each GCM are extracted for the grid cells covering the locations of the selected case study sites (see Task 4.1 and Table II).

Table II. The study locations in Belgium

No.	Location	Latitude [°]	Longitude [°]
1	Baileux	50.02	4.4
2	Buchholz	50.36	6.31
3	Eupen	50.59	6.10
4	Gedinne	49.96	4.83
5	Les-Fossés	49.78	5.46
6	Louvain-la-Neuve (LLN)	50.68	4.60
7	Petit-Thier	50.31	5.98
8	Séviscourt	49.94	5.39
9	Ukkel	50.8	4.4
10	Virton	49.53	5.57
11	Wellin	50.05	5.22

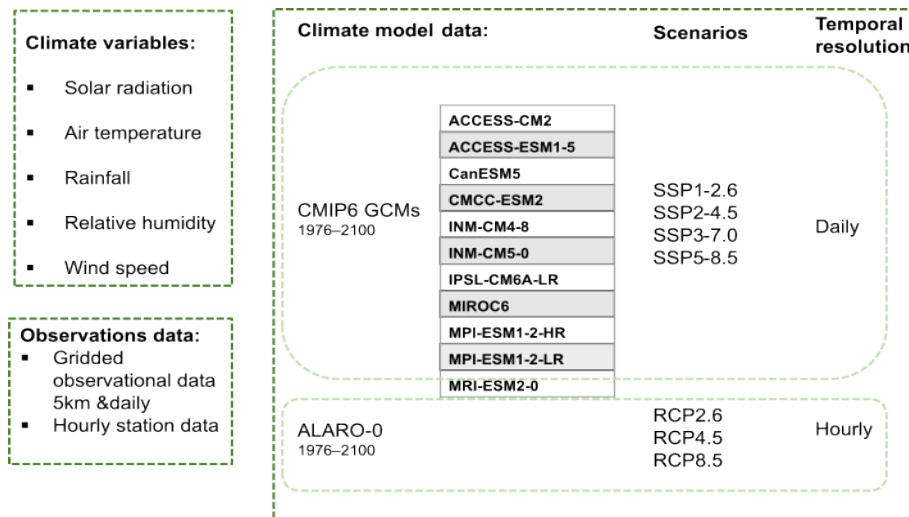


Figure 8. Schematic overview of the climatic variables, the observations and GCM data used to generate the input data for HETEROFOR

CMIP6 offers a comprehensive framework for effectively quantifying climate projection uncertainties. This framework enables the proper assessment of two key sources of uncertainty: 1) model uncertainty arising from various modelling choices and physical assumptions within climate models, and 2) scenario uncertainty linked to different emission pathways of greenhouse gases. However, to utilize the HETEROFOR model effectively, meteorological data input must be unbiased, ensuring an accurate representation of current-day climate conditions. Recent research has identified systematic biases in CMIP6 models, particularly in surface temperature, precipitation, and soil moisture over Europe (Carvalho *et al.*, 2021; Ossó *et al.*, 2023). These errors are partly attributed to variations in atmospheric circulation patterns over Western Europe and, consequently, Belgium. To address these biases, we have implemented two bias correction techniques, elaborated in a dedicated section below. Another major obstacle to the direct use of CMIP6 data is that meteorological data input must be at an hourly resolution. As raw CMIP6 model data are available at daily frequency, data necessitated temporal downscaling for compatibility with HETEROFOR's hourly input requirements (refer to Task 1.6). To complement CMIP6 GCM data, we also used climate projections and scenarios RCP2.6, RCP4.5 and RCP8.5 from the RMI model ALARO for which hourly data is available and that cover the period 1976-2100. ALARO data were mostly used for developing and validating the disaggregation procedure (Task 1.6). The entire data processing chain, encompassing both bias correction and temporal disaggregation, is illustrated in Figure 9.

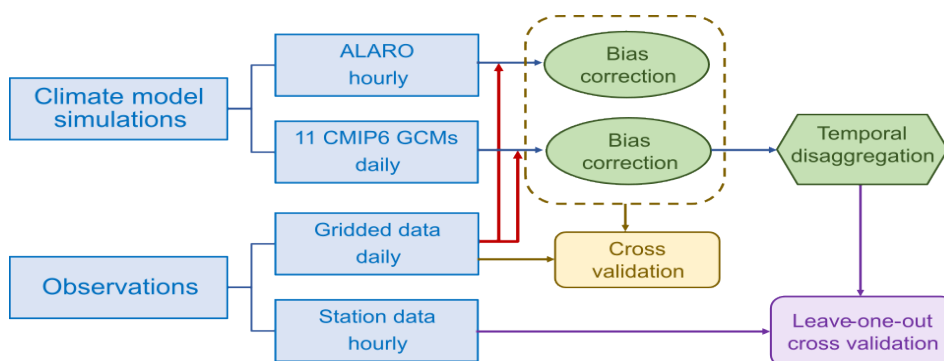


Figure 9. Data processing chain used to establish and validate the meteorological input data for HETEROFOR

Validation of the bias correction methods was conducted using cross-validation (holdout technique) spanning 60 years, with the first 30 years used for calibration and the subsequent 30 years for validation on independent data. The leave-one-out method is employed to validate the temporal downscaling approach. For the bias-correction of climate projections, we used a gridded observational product at a spatial resolution of 5 km covering the entire Belgium which is developed at the Royal Meteorological Institute of Belgium (RMI, 2022). The gridded observational dataset provides data for all the variables required for this study. Solar radiation, relative humidity and wind speed data are available from 1961 onwards, while precipitation and air temperature data are available since 1951 and 1954, respectively. The gridded observational data was selected for the bias correction because of 1) the unavailability of station observations for some of the study locations and 2) a spatial scale mismatch between the station observations and climate model outputs. For the latter, model outputs represent area averages rather than point values which is the case for stations (Tabari *et al.*, 2016). Specifically, extreme precipitation values obtained from station observations are expected to be more intense compared with the ones from gridded model output (Chen and Knutson, 2008), because of the smoothing associated with the spatial averaging of precipitation characteristics over the model grid cells (Sivapalan and Blöschl, 1998). In addition to the daily gridded observational data, hourly data were available for six stations (Baileux, Eupen, Gedinne, Louvain-la-Neuve, Ukkel, Virton) which were employed for the validation of the disaggregation methods for all variables (see Task 1.6).

Figure 8 outlines the observations and modelled data used to obtain the raw meteorological input data for the five considered meteorological variables.

Bias-correction methods

Historical simulations by climate models can show systematic deviations from observations due for instance to incorrect model initialization, imperfect representations of the atmospheric physics in the model, or errors in the parameterization chain (Ehret *et al.*, 2012). This thus calls for a bias correction of climate model outputs before using for quantitative impact studies for applications that are sensitive to input climate data as REG+ (Hosseinzadehtalaei *et al.*, 2021). We implemented two statistical corrections.

1) Additive and scaling corrections

Two easy-to-implement methods for bias correcting model outputs are the additive and scaling corrections. The additive approach generates a future time series by subtracting the present-day model bias from the simulated future time series. Mathematically,

$$M_{i,\text{corr}}^f = M_{i,\text{raw}}^f - (\bar{M}_{\text{raw}}^p - \bar{O}^p) \quad (3.13)$$

where $M_{i,\text{raw}}^f$ is the raw model future time series at time i , \bar{M}_{raw}^p is the model present-day mean and \bar{O}^p the corresponding observed mean.

For bounded variables (rainfall, wind speed, relative humidity, and solar radiation), an additive correction is not applicable as it can result in values outside of the physically-allowed bounds (e.g., negative rainfall or relative humidity of >100%) (Hempel *et al.*, 2013). For example, a positive additive

correction of rainfall would amount to all days becoming wet. For such variables one would typically consider relative changes, i.e.

$$M_{i,\text{corr}}^f = M_{i,\text{raw}}^f \times \frac{\bar{O}^p}{\bar{M}_{\text{raw}}^p}. \quad (3.14)$$

This formulation is known as linear scaling. It assumes a constant coefficient ($\frac{\bar{O}^p}{\bar{M}_{\text{raw}}^p}$) of variation, leading to a mean and variance rescaled by the same factor.

We did not correct relative humidity directly. We made corrections to the quantity (1-relative humidity) and then inferred the relative humidity in a subsequent step. This is because relative humidity in Belgium usually fluctuates between 50% and 100%. There is, therefore, a significant risk of surpassing the saturation point (100%).

We use these two methods to modify hourly (ALARO) and daily (CMIP6) simulated data by a constant offset or multiplicative correction factor that corrects long-term monthly mean deviations of the model simulated data from observed monthly mean data in the historical period. In such a manner, the long-term trend of the simulated data (Hempel *et al.*, 2013) and the seasonality of climate change signals (Hosseinzadehtalaei *et al.*, 2019) are preserved.

2) Quantile mapping

The additive and scaling corrections only correct the mean difference (variance also for scaling) between the observed and simulated climate signal. They assume that higher-order moments are correctly simulated. Climate model biases often do not only affect the long-term mean, but also higher-order statistical moments such as variance or the tail behavior. Quantile mapping accounts for those corrections by adjusting different quantiles individually. From all modelled and observed values M_i^p and O_i^p over the calibration period, the corresponding cumulative probability functions $F_M(M_i)$ and $F_O(O_i)$ are estimated. In general, statistical transformations attempt to find a function TF which maps a modelled variable M_i such that its new distribution equals the distribution of the observed variable O_i . This transformation can be formulated as

$$O_i = TF(M_i). \quad (3.15)$$

If the distribution of the variable of interest is known, the transformation is defined as

$$O_i = F_o^{-1}(F_m(M_i)) \quad (3.16)$$

where F_m and F_o are the cumulative distribution function of M_i and O_i . F^{-1} denotes the inverse *CDF* (or quantile function). The actual formulation of the transfer function depends on the implementation. The ISIMIP3 algorithm that we used (some details are provided below) employs theoretical parametric distributions for solving F , such as a normal distribution for temperature and a gamma distribution for precipitation (see Table III). Other variables as relative humidity or shortwave radiation make use of estimated cumulative probability functions inferred from data.

Table III. Specification of the ISIMIP3 bias adjustment method for all climate variables considered in this study. Where a lower (upper) bound is specified, no values smaller (greater) than this bound will occur in the bias-adjusted data. For every lower (upper) bound, a lower (upper) threshold is defined, which is only slightly greater (smaller) than the bound. The lower (upper) threshold is used to adjust the relative frequency of values smaller (greater) than the threshold. The lower threshold of pr is equivalent to 0.1 mm/day. If the distribution is not specified, then a non-parametric quantile mapping with 50 quantiles is used. hurs: near-surface (2 m) relative humidity; pr: total precipitation; rsds: surface downwelling shortwave radiation; sfcWind: near-surface (10 m) wind speed; tas: near-surface (2 m) air temperature; tasmin: minimum near-surface (2 m) air temperature

Variable short name	Lower bound	Lower threshold	Upper bound	Upper threshold	Distribution	Trend preservation	Detrending	Other
hurs	0	0.01	100	99.99	–	bounded	no	–
pr	0	0.1/86400	–	–	gamma	mixed	no	–
rsds	0	0.0001	1	0.9999	–	bounded	no	upper bound scaling
sfcWind	0	0.01	–	–	weibull	mixed	no	–
tas	–	–	–	–	normal	additive	yes	event likelihood not adjusted
tasmin	–	–	–	–	normal	additive	yes	event likelihood not adjusted

The implementation of quantile mapping according to Eq. 3.16 assumes a correction (hence model biases) which explicitly depends on the value the variable takes. A value M_i will thereby be transformed according to the transfer function $F_o^{-1}(F_m(.))$ irrespective of its occurrence within the time series. As such, trend in the time series is not guaranteed. This problem is overcome in the variant of quantile mapping that we used, i.e. ISIMIP3, to correct ALARO and CMIP6 simulations. The method is approximately trend-preserving in all quantiles and therefore features a more comprehensive trend preservation than less sophisticated approaches where only trends in the mean are preserved.

In the rest of this section, we present some specificities of the quantile mapping algorithm that we used, namely the “Inter-Sectoral Impact Model Intercomparison Project, version3” algorithm (ISIMIP3) (Lange, 2019; Lange, 2020). The ISIMIP3 bias adjustment method (version 3.0.2) is a parametric quantile mapping method that has been designed to (i) robustly adjust biases in all percentiles of a distribution and (ii) preserve trends in these percentiles. It operates on daily time series. The method is applied to every variable, grid cell and calendar month independently. Table III lists the different options used for the variables that we corrected.

The bias-adjustment of the RCP/SSP scenarios follows the ISIMIP3b protocol described in Lange (2020). The method is calibrated using the historical simulation over the period 1976–2014 (39 years) for CMIP6 GCMs and 1976–2005 (30 years) for ALARO. The estimated correction is then applied to RCP/SSP scenarios. Like the calibration period, all application periods have the same duration. Application periods used for SSP scenarios were 2015–2053 (keeping 2015–2043), 2039–2077 (keeping 2044–2072) and 2062–2100 (keeping 2073–2100). Application periods used for RCP scenarios were 2006–2035 (keeping 2006–2029), 2027–2056 (keeping 2030–2053), 2051–2080 (keeping 2054–2077)

and 2071–2100 (keeping 2078–2100). The calibration period was also used as an application period for bias-adjusting the historical simulation.

The ISIMIP3 method can deal with trends within time series (not only between application periods). Before quantile mapping is applied, linear trends within the time series of historical observations, historical simulation and future scenario are removed. This is to prevent the effect of trend on estimated distributions and, as a result on quantile mapping. By default, only the near-surface temperature (daily mean and minimum) is detrended before applying quantile mapping. Trends are restored after the quantile mapping is applied.

In the ISIMIP3 version we employed, we activated a feature enabling bias adjustment in a running-window mode with a customizable step size. This innovation, in contrast to a month-by-month bias adjustment, effectively mitigates statistical irregularities, particularly in multi-year daily mean values, occurring at each transition between months. For REG+, the running window we utilized has a width of 31 days, and it moved over the annual cycle in steps of 1 day. The final outcome is determined by the results obtained for the central day of each window.

Bounded variables (one lower bound, one upper bound or both) have a supplementary step, which consists in randomizing values beyond defined thresholds in the time series of historical observations, historical simulation and future scenario (see values in Table III). Thresholds located slightly above the lower bound and slightly below the upper bound are used to bias adjust the frequencies of occurrence of values close to the bounds. In particular, the lower threshold of pr is used to bias-adjust the frequency of dry days, that is the frequency of occurrence of $pr < 0.1 \text{ mm day}^{-1}$. This threshold is a minimum value for estimating the uncertainty related to the detection of precipitation (precision of pluviometers; no contribution of the uncertainty associated with the spatial interpolation of station data over Belgium in the RMI dataset).

CMIP6 models are known to simulate too many supersaturated days where the near-surface relative humidity is higher than 100%. As near-surface relative humidity values of 140% can happen (Ruosteenoja *et al.*, 2017), modelling centres participating to CMIP do not generally clip near-surface relative humidity at the suggested upper limit of 100.001 % (Juckes *et al.*, 2020). The ISIMIP3 protocol for *hurs* takes care of the too many supersaturations by fixing the supersaturation probability at the observed level. Trends in relative humidity beyond threshold is, therefore, not preserved.

Subselection of CMIP6 models

CMIP6 provides a large ensemble of simulations for HETEROFOR to run. Given 11 models, 4 scenarios, 2 bias-correction techniques and 11 forest sites, it would lead to 968 distinct input datasets to test. To decrease the number of experiments, we selected six models based on three criteria: model quality, model independency and diversity of responses to climate change. The selection procedure follows the work of Sobolowski *et al.* (2023) to produce the new EURO-CORDEX dataset.

We first discriminated between the eleven models, based on their intrinsic performances. We computed the model performances relative to the model ensemble median over the period 1976-2014 in a similar fashion as Gleckler *et al.* (2008), limiting the analysis to the growing vegetation period (15th

of April to 15th of November). The relative error $E'_{m,f}$ for a given model m and a given field f is defined as:

$$E'_{m,f} = \frac{E_{m,f} - \bar{E}_{m,f}}{\bar{E}_{m,f}} \quad (3.17)$$

where $E_{m,f}$ is the model error and $\bar{E}_{m,f}$ is the typical model error defined as the median of all model errors. Model errors are evaluated from monthly climatological values using the root mean squared differences between the model and the observations. Mathematically,

$$E_{m,f} = \sqrt{\frac{1}{S} \sum_s \frac{1}{12} \sum_{month=1}^{12} (\bar{M}_{month,s} - \bar{O}_{month,s})^2} \quad (3.18)$$

where S is the number of independent sites. It varies from one model to another, but $S \leq 11$. Due to the model coarse horizontal resolution, model values at different sites might be identical. Duplicated sites are discarded before computing $E_{m,f}$ to avoid attributing different weights to the model pixels (biases for each site are not area-weighted, as grid cells have similar areas over Belgium). Results for the relative errors are presented in Figure 10. From this analysis, we selected six models: ACCESS-CM2, CanESM5, IPSL-CM6A-LR, MPI-ESM1-2-LR, MPI-ESM1-2-HR and MRI-ESM2-0.

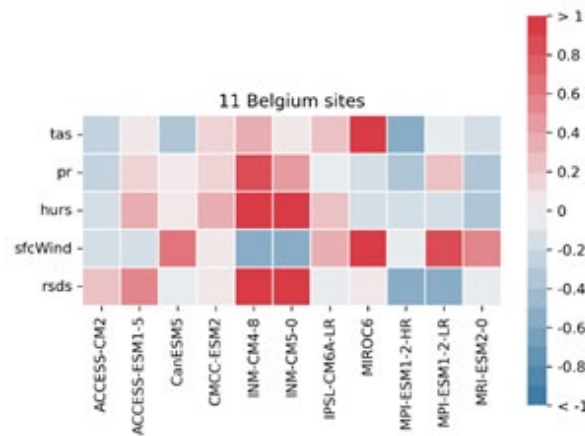


Figure 10. Relative errors in CMIP6 models over the period 1976-2014. Errors are evaluated for the vegetation growing season and for the variables used to force HETEROFOR. The relative performance is displayed, with blue (red) shading indicating better (worse) performance than the median of all models. hurs: near-surface (2 m) relative humidity; pr: total precipitation; rsds: surface downwelling shortwave radiation; sfcWind: near-surface (10 m) wind speed; tas: near-surface (2 m) air temperature

To make an optimal sampling of the model diversity, our decision to keep or reject models relies on Figure 5 of Brunner *et al.* (2020). This study assessed the level of model dependency between CMIP6 models. For instance, CMIP6 models can be similar because they share the same model for one or several components (atmosphere, ocean...), they have approximatively the same spatial resolution or they embed the same model complexity. All selected models at the previous step were found to be rather independent, except for the two MPI models. We did not reject one of these two models, though, as they have different spatial resolutions which might lead to different model behaviours and, as a result, climate change sensitivities (see next criterion).

Finally, we also considered the diversity of model responses to climate change. For the eleven models, we computed the changes in near-surface temperature and precipitation (limited to the vegetation

growing period) simulated for the end of the century compared with the present period. We focused on those two variables, as they have a significant influence on forests. Results are presented in Figure 11, which shows that our selection adequately sample the diversity of responses to climate change of the full ensemble of models. The impact of moderate and severe increases in temperature can be analysed and combined with various levels of reduction in precipitation.



Figure 11. Scatterplot of the projected changes in near-surface temperature and precipitation for the SSP5-8.5 scenario for the end of the century (2071-2100). Changes are relative to the present time (1976-2014) and limited to the vegetation growing season for the precipitation. Changes are averaged over independent forest sites. The eleven points represent the eleven model responses to climate change. Red points indicate our subselection of models

WP4. Definition of silvicultural and wildlife scenarios

Task 4.1 Selection and characterization of case studies

Stands representative of the main forest types to be regenerated within the next 40 years in Belgium were selected as case studies. Several of these stands were selected among plots of the Long-Term Ecosystem Research (LTER) and the International Cooperative Program on Forests (ICP-Forests, level II sites) networks for which data series over more than 20 years are available while others belong to the IRRES network installed to study the conversion of even-aged stands into uneven-aged ones. The selected sites are dominated by the major forest tree species in Belgium and encompass different species compositions and structures. A first set of 13 stands was designated as potentially relevant case studies. Yet, following the meeting with the stakeholders for the definition of the silvicultural scenarios to be tested, this initial selection was revised. Indeed, some of the stands turned out to be too young to consider initiating their regeneration in the relatively near future. In contrast, other stands, especially Norway spruce (*Picea abies*) dominated ones, were too old and the risk of windthrow following a decrease of stand density to initiate natural regeneration was high, which limited the possibilities of regeneration to almost only plantation after clear cutting. As a result, the initially selected oak-dominated plot of Baileux was replaced by a coppice-with-standards stand close to Chimay, which presents a similar species composition but with older trees and then closer to the regeneration phase. The two Norway spruce stands of Buchholz and Les Fossés have been excluded from the selection as being too old. Instead, it was proposed to consider two contrasted ages for the

spruce stand of Gedinne, namely the stands in 1999 and in 2018, to allow considering the effect of the age at which conversion is initiated. In other respects, the two Douglas fir (*Pseudotsuga menziesii*) stands initially chosen were redundant cases as presenting similar development stages and the stand of Séviscourt was replaced by the younger of Blanche Virée, located close to Wellin. Finally, the sustainability of mixture in stands composed of species with contrasting growth dynamics, in particular oak-beech mixtures, is a major concern for forest managers. Therefore, it appeared interesting to consider case studies presenting contrasting degrees of development of the two species, namely (i) a stand dominated by oak presenting oak and beech regeneration (Stoumont C111), (ii) a stand with a balanced mixture of both species with beech regeneration (Baileux mixed plot) and (iii) a stand dominated by beech with a significant proportion of oak in the overstory (Stoumont C114). This gradient in oak-beech mixture will allow to investigate the ability of maintaining oak depending on the context. The initially selected beech stand of Baileux and the oak-beech mixture of Wellin were discarded as being relatively young. This results in a final selection of 11 case studies. Their main characteristics are presented in Table IV and a more detailed description together with the corresponding input data files for the HETEROFOR model are available on the [REG+ website](#). Finally, only the broadleaved sites were considered as initial stages for the simulation experiment (see Task 4.2).

Table IV. Main characteristics of stands selected as case studies for the REG+ project

Site	Ecoregion	Structure	Species	Density (trees/ha)	Basal area (m ² /ha)	Mean girth (cm)	Dominant height (m)
Chimay	Fagne	Even-aged	<i>Quercus petraea</i>	65	16	177	21.3
			<i>Carpinus betulus</i>	583	8	41	17.4
Stoumont C111	Eastern Ardenne	Even-aged in conversion to uneven-aged with oak and beech regeneration	<i>Quercus petraea</i>	194	21.9	119	21.3
			<i>Fagus sylvatica</i>	57	3.6	89	15.7
			<i>Betula pendula</i>	51	1.9	69	15.4
Stoumont C114	Eastern Ardenne	Even-aged with beech regeneration	<i>Fagus sylvatica</i>	118	16.7	133	23
			<i>Quercus petraea</i>	31	6.2	158	26
Baileux mixed plot	Western Ardenne	Even-aged with beech regeneration	<i>Quercus petraea</i>	93	13.6	135	27.2
			<i>Fagus sylvatica</i>	206	14.5	94	27.2
Eupen	Eastern Ardenne	Even-aged with regeneration	<i>Fagus sylvatica</i>	226	24.3	116	28.9
Louvain-la-Neuve	Loam region	Even-aged with regeneration	<i>Fagus sylvatica</i>	60	19.9	205	32.7
			<i>Quercus petraea</i>	16	4.5	188	32.2
Gedinne 1999 2018	Ardenne	Even-aged with regeneration	<i>Picea abies</i>	469	31.6	92	24.7
			<i>Picea abies</i>	220	31.8	135	32.0
Petit-Thier	Eastern Ardenne	Even-aged in conversion to uneven-aged	<i>Pseudotsuga menziesii</i>	162	40.1	176	39.2
Blanche Virée	Ardenne	Even-aged in conversion to uneven-aged	<i>Pseudotsuga menziesii</i>	552	38.5	94	30.7
Louvain-la-Neuve	Loam region	Even-aged	<i>Pinus sylvestris</i>	196	31.4	142	21.1
			Others	119	2.8	54	12.9

Task 4.2 Definition of silvicultural routes

To determine the best management approach for ensuring forest resilience to climate change and increasing wildlife pressure, we defined three distinct silvicultural scenarios. These three silvicultural scenarios offered distinct pathways to managing forests under changing climatic and ecological conditions.

The first scenario, referred to as Business As Usual (BAU), maintained an even-aged stand with at least one existing commercial species while limiting silvicultural interventions. Thinnings from below, preferentially removing smaller trees, were conducted every 12 years to maintain a basal area of about 24 m²/ha. Regeneration cuts were triggered when the mean diameter of the 20 largest trees reached the acceptable exploitation threshold. Over 36 years, four regeneration cuts progressively removed more trees. Bramble clearing took place every 6 years, while regeneration clearing was done every 12 years during regeneration cuts.

The second scenario, called to as Oak Regeneration (OAK), prioritized the preservation of oaks, a species highly valued both economically and ecologically in Western Europe. Like BAU, thinning from below was conducted every 12 years, maintaining a basal area of about 24 m²/ha. Regeneration cuts began once the dominant mean diameter reached the acceptable exploitation threshold. To promote natural oak regeneration, annual clearing reduced competition from species like hornbeam and beech, along with bramble control. These interventions spanned 13 years, starting six years before and ending six years after the second regeneration cut.

The third scenario, referred to as Diversification (DIV), aimed to enhance both stand composition and structural diversification by relying on natural regeneration and enrichment plantations. This scenario began with the creation of 3 enrichment gaps of 400 m², followed by the plantation of 2,500 protected plants, each 4 years old and 0.5 m tall. Twenty-four years later (in 2039), three new enrichment gaps and plantations were established. Three different species were selected for planting based on site suitability and resilience to future climate conditions: oak (*Quercus*), linden (*Tilia*), and birch (*Betula*). After each plantation, regeneration and vegetation clearings were conducted annually for three years to support their establishment. Additionally, thinnings were carried out every 12 years to diversify the stand and transition it into an uneven-aged structure.

WP5. Simulation experiments and output analyses

We aimed to determine which management approach would be best suited to maintain a resilient forest providing multiple ecosystem services while taking climate change and wildlife pressure into account. Simulations were then carried out on 6 of our study cases presented in Task 4.1, those composed of deciduous species. These sites are: Baileux, a stand consisting of a balanced mixture of oak and beech with the presence of beech regeneration; Chimay, an oak and hornbeam coppice-with-standards stand from 1880; Stoumont C114, a mixed stand dominated by beech with a significant proportion of oak in the overstory; Louvain-la-Neuve, an old beech stand from 1884 mixed with old oaks; Stoumont C111, a mixed stand dominated by oak with the presence of oak, beech and birch regeneration; and Eupen, an even-aged beech stand from 1934. A more detailed description of the sites is available on the REG+ website.

The silvicultural routes, described in more depth in Task 4.2, were tested on these sites. As a reminder, the aims of the silvicultural routes are: for BAU (Business As Usual), to maintain an even-aged stand with at least one existing commercial species; for OAK, to maintain an even-aged stand with natural oak regeneration; and for DIV (Diversification), to diversify the stand in terms of age and species to improve its resilience, with plantations.

Two separate sets of simulations were run: one to investigate the climate change impacts and one to analyse the effects of wildlife pressure.

To address the impacts of climate change, 5 different climate scenarios were used in the simulations: Historical, corresponding to climate over the 1976-2005 period; SSP1, called Sustainability ("Taking the Green Road"), with the expected level of radiative forcing of 2.6 W/m² in the year 2100 corresponding to CO₂ emissions cut to net zero around 2075; SSP2, "Middle of the road", considering that current emission levels are maintained until 2050 and then fall but without reaching net zero by 2100 (4.5 W/m² radiative forcing in 2100); SSP3, named Regional Rivalry ("A Rocky Road"), assuming a doubling of CO₂ emissions by 2100 (7.0 W/m² radiative forcing); and SSP5, "Fossil-Fueled Development", for which CO₂ emissions are assumed to triple by 2100 (8.5 W/m² radiative forcing). Simulations were run twice for each SSP scenario: (1) with temporal variations in atmospheric CO₂ concentrations corresponding to the emission scenario and (2) with atmospheric CO₂ fixed at 380 ppm. This allowed to separate the effect of climate change in the strict sense from that of CO₂ fertilization on ecosystem functioning. Only atmospheric CO₂ fixed at 380 ppm was used for the historical scenario. In each case, 6 global climate models were considered: ACCESS-CM2, IPSL-CM6A-LR, MPI-ESM1-2-LR, MPI-ESM1-2-HR, MRI-ESM2-0 and CanESM5. Finally, the simulations were repeated for each of the 6 selected study cases and for the 3 silvicultural routes in each case. This resulted in a set of 972 (6 sites x 3 silvicultural routes x 6 climate models x [4 SSP x 2 CO₂ modalities + historical]) runs.

To assess wildlife pressure, 4 ungulate pressure levels were simulated based on observed levels of ungulate density. The first level (no pressure) corresponded to situations observed in fenced plots where no ungulates were present. The second level (low pressure) was assumed to correspond to what would be recommended for sustainable management. The third level (medium pressure) was assumed to correspond to the average impact observed in Wallonia. The fourth level (high pressure) corresponded to the most problematic situation recorded in Wallonia. We used an empirical approach by applying a reduction in seedling height growth, based on Candaele *et al.* (2023), for each tree species under different ungulate population levels (Table V). For this simulation experiment on ungulate pressure, only the MPI-ESM1-2-HR climate model and the SSP1-2.6, SSP2-4.5 and SSP3-7.0 scenarios were considered. The simulations were repeated for the 6 study sites and the three silvicultural routes and only variable CO₂ concentration was considered, resulting in a total of 216 simulations (6 sites x 3 silvicultural routes x 4 ungulate pressure levels x 1 climate model x 3 SSP x 1 CO₂ modality).

Table V. Reduction in seedling height growth (%) for each species under different ungulate density levels

Ungulate density	Oak	Beech	Birch	Hornbeam	Linden
No pressure	0	0	0	0	0
Low pressure	39	18	35	25	25
Medium pressure	90	40	80	60	60
High pressure	100	80	90	85	85

Simulation execution was automatized using scripts. The simulation period covered 120 years, from 2015 to 2135. As SSP climate scenarios are only established up to 2100, climate data beyond this year were randomly selected from the last 30 years of the corresponding scenario. For the historical scenario, climate data were randomly selected from the 30-year series throughout the simulation period. Various files were required to run the simulations, including species parameters, inventory data, soil horizon descriptions, meteorological data, parameters for discretizing daily meteo records to hourly records, economic parameters, dendro-microhabitat parameters and temporal evolution of atmospheric CO₂ concentrations. The HETEROFOR model provided outputs directly under the form of pre-processed indicators (see Table I). These indicators were analysed and used to compare simulations so as to identify the most appropriate management strategies for ensuring sustainability and resilience of the Walloon forest while favouring the provision of climate services.

The outcomes of the simulations dealing with the impact of climate change were analysed separately from those dealing with the effect of ungulates, but following the same approach. In a first step, indicators were grouped by types reflecting productivity and financial profitability, climate service provision (e.g., evapotranspiration, carbon storage), diversity and resilience. For each of these groups of indicators, a principal component analysis (PCA) was carried out to determine which indicator or combination of indicators explained most of the information in the group. Mixed linear models were then fitted expressing the indicator(s) retained in each PCA as a function of the factors used to define the simulations (i.e., silvicultural route, climate scenario, climate model, ungulate pressure, atmospheric CO₂ variation mode, site). These models allowed statistical comparisons of indicator values among factor levels, as well as quantifying the importance of each factor on indicator variability.

WP7. Valorisation, dissemination, exploitation of results

Task 7.1 Website design and management

A website has been designed for the REG+ project and is available at <https://www.regeplus.be/> and serves as a platform for project overview, for result and model dissemination and for interactive exchanges with stakeholders and end-users. It consists of different sections. A first section gives a general [presentation of the project](#), describing the research context, its objectives and the expected impacts. A second section presents the [HETEROFOR model](#) and its functionalities and provides access to an installer containing a recent version of the model and to the model user manual. It is regularly updated as improvements are made to the model. A third section describes in detail each [case study](#) selected for the project and contains links to the corresponding HETEROFOR input data files enabling to perform simulations. A fourth section is devoted to the presentation of the [project results](#) and is designed as a blog allowing for interactive exchanges with stakeholders and end-users. A fifth section

describes the main [datasets](#) used to initialize, calibrate and evaluate the model as well as outputs from the simulations. Finally, other sections are dedicated (i) to the [news and events](#) (e.g., meetings, field trainings, training courses) related to the project, (ii) to project detailed description, reporting and scientific and popularization [publications](#) associated with the project, (iii) to the presentation of the [project partners and follow-up committee](#) and (iv) to [contact](#) request with the project partners. The website is hosted at UCLouvain.

4. SCIENTIFIC RESULTS AND RECOMMENDATIONS

4.1 Ungulate impacts

Descriptive statistics of ungulate impacts on regeneration

After 5 growing seasons (2016 to 2021), the 734 fenced-undefenced pairs of plots allowed foreseeing an important ungulate impact on the species composition of the recruited trees. Strong growth differences were observed across treatments and species (Figure 12). The growth of some species was only moderately reduced, whereas that of other species was highly suppressed. The fastest growing species is expected to dominate the future stands whereas the others will be progressively suppressed and rarefied. With these observations, we can then predict which species can successfully regenerate across different conditions.

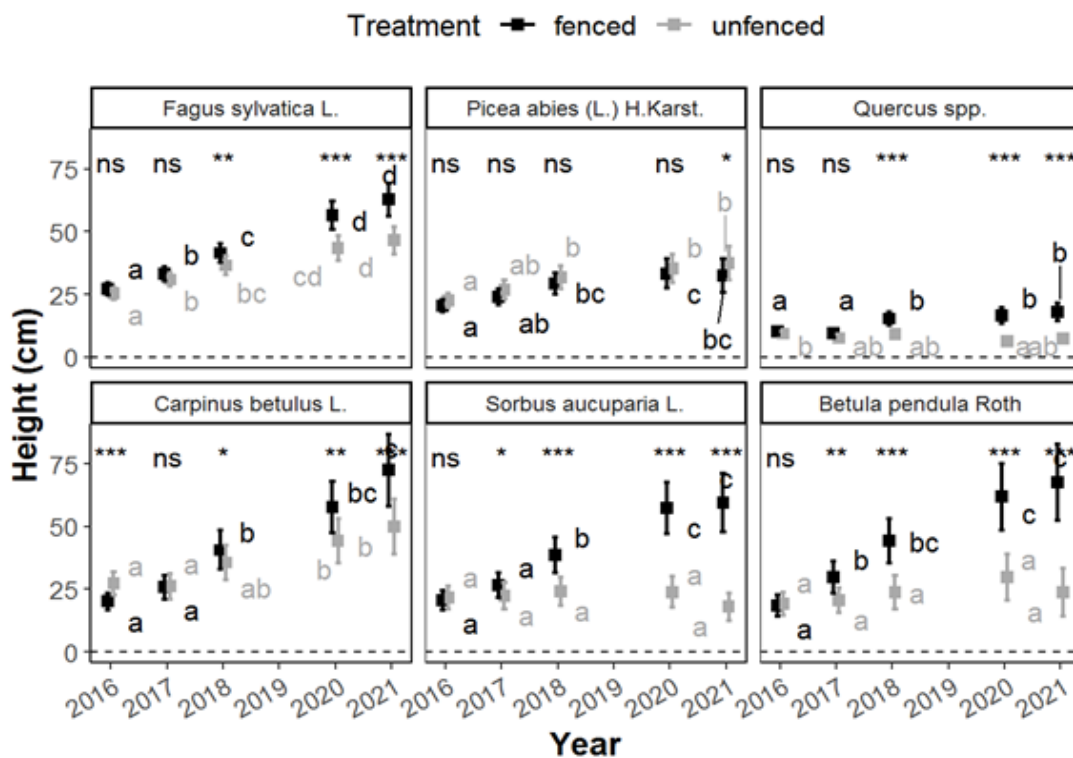


Figure 12. Evolution of seedling height through time in the fenced and undefenced plots. Within a species and a treatment (fenced or undefenced), squared dots without common letters denote significantly different means following the max-t test. Means are displayed with their 95% confidence intervals. The impact of ungulates is particularly strong on oak, rowan and birch seedlings.

Considering seedling growth potential and browsing sensitivity, we classified the 6 most frequent species into 3 groups following the classification of *Walters et al. (2020)*. Beech (*Fagus sylvatica* L.) and spruce (*Picea abies* (L.) H. Karst) belonged to the *broad* group as these species are frequent, shade tolerant and browsing resistant. They can regenerate under the broadest range of light and ungulate pressure. Birch (*Betula pendula* Roth) and rowan (*Sorbus aucuparia* L.) belonged to the *high-light* group. They grow fast in high-light conditions but they are highly browsing sensitive and shade intolerant. Oak (*Quercus* spp.) belonged to the *nowhere* group. Its growth is limited in all the sampled conditions, and it is very browsing sensitive. Oak hardly regenerates naturally in most forests managed with a continuous cover (except maybe where nutrient or humidity constraints the development of other tree species). Finally, hornbeam (*Carpinus betulus* L.) shares the characteristics of *high-light* (high growth potential and palatability) and *broad* groups (high growth under ungulate impact).

Ungulates drastically reduced the recruitment potential of high-light species (birch, rowan) as their growth was clearly limited in the unfenced plots. When these species were present in the fenced plots, they had however the fastest growth (Figure 12). Ungulate impact is also important for oak but other key factors impede its regeneration (mainly the competition with the other species). The growth of oak seedlings was generally lower than that of the admixed species in both fenced and unfenced plots. Finally, the *broad* species (beech, spruce) seemed to regenerate naturally easily in the sampled conditions and can even grow faster in unfenced plots.

Browsing additionally affected regeneration diversity and presumably future forest diversity (Figure 13A). As the broad species in the study area were not very tolerant to drought and warmer conditions, the effect of browsing is also affecting future forest resilience. At the end of the study period, the ecological affinity indexes (EAI, Figure 13) of the seedling assemblage showed that the seedlings were composed of less heat and drought tolerant species (Figure 13B, C) and more shade tolerant species (Figure 13D).

In conclusion, the results evidence that ungulates critically affect the growth of the species that are the most palatable, the less shade tolerant and the best adapted to future climatic conditions.

The complete description of this study has been published in the Open-Access journal “Forest” and is available online (<https://hdl.handle.net/2268/307006>) (Candaele *et al.*, 2023).

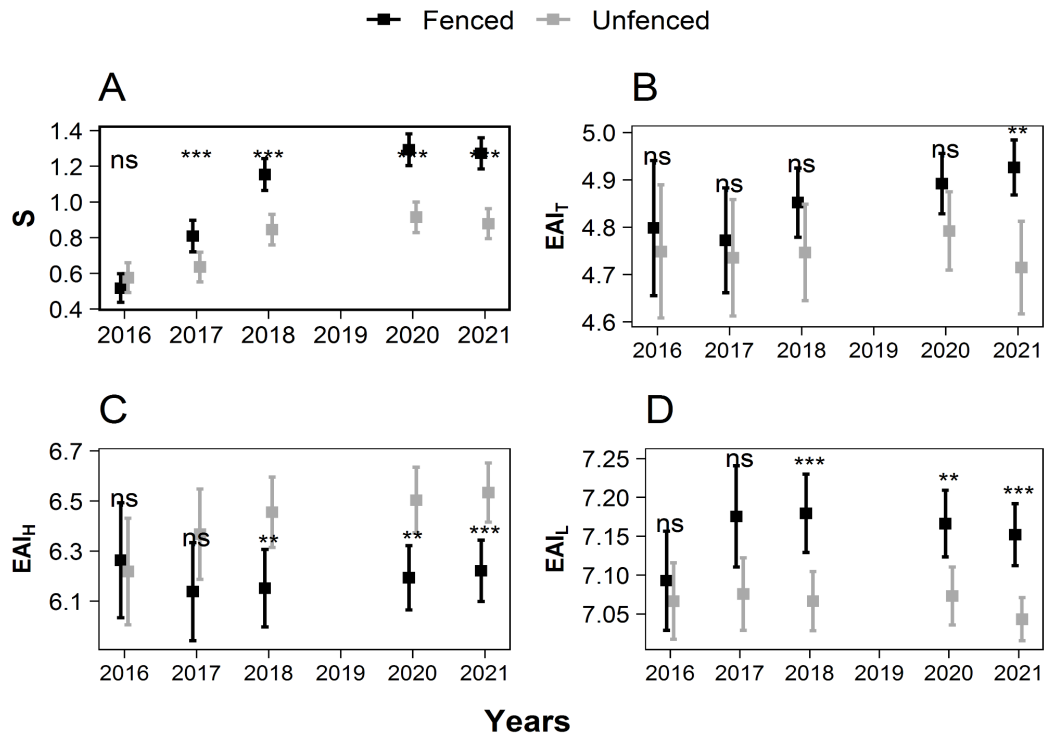


Figure 13. Evolution of the species richness (A), Ecological Aptitude Index for temperature (B), atmospheric humidity (C) and light (D) in the fenced and unfenced plots. The species richness was computed as the number of species with minimum one seedling taller than 50 cm. The EAI are height weighted means of the seedling species aptitude scores from the Baseflora database (Julve, 1998). The means are displayed with their 95% confidence intervals.

Models of ungulate impacts on regeneration

Besides evidencing the effects of ungulate browsing with descriptive statistics, it was expected to model the impact of browsing on regeneration development. It was required to model how browsing affects seedling height and ground vegetation biomass (seedlings and bramble). Using the data collected in 734 fenced-unfenced pairs of plots, we computed a large set of variables describing the impacts of browsing (response variables), local ungulate densities and environmental conditions (explanatory variables, Table VI).

Height increment estimate

For each year and plot, the height of the 5 tallest saplings was measured. For each year and plot, we had thus observations of the maximum height reached by the different study species. In some plots, one species could be monitored during the first censuses but not in the last ones (as the seedlings of that species were no longer among the 5 tallest seedlings). The height increment was computed for each plot and species with the first and last census available such as $iH = (H_f - H_i)/\Delta T$. Where H_i and H_f were the initial and final heights and ΔT is the number of years elapsed between the censuses. ΔT could differ between the paired plots (fenced or unfenced).

For each plot pair, the height increment was estimated for fenced and unfenced conditions. The difference between the paired estimates was also computed. Such differences were only computed for the plot pairs in which iH could be estimated for both fenced and unfenced plots.

Table VI. Description and summary statistics of the tested model explanatory variables. These variables are indicators of ungulate densities and environmental conditions

Variable	Description	mean	s.d.	min.	max.
agri_dist	Distance from the nearest agricultural area (m)	1 010.62	878.71	0	5 719.99
ba	Basal area (m ² /ha)	19.57	8.61	0	52
build_dist	Distance from the nearest building (m)	710.95	381.94	48.05	2 147.93
carrying_capacity	Carrying capacity for red deer. Punctual estimation of the calf weight on November 15 (kg)	38.73	2.23	33.08	44.3
deer_AdultTotalRatio	Ratio of shot adult males red deer to total shot red deer	1.84	2.75	0	22.02
elevation	Elevation a.s.l. (m)	411.79	114.71	163	666
game_shot	Ungulate density index: cumulated ungulate abundance index based on shot statistics at the hunting district (inspired from Kupfershmidt., 2020). Red deer = 1, roe deer = 1/5, fallow deer = 1/4, mouflon = 1/4. (ungulates/km ²)	2.3	1.11	0.4	6.98
palatability	The mean of species palatability weighted by biomass	4.7	2.5	0.03	10
palatability_biomass	Sum of the products of biomass and palatability score by plot	194.35	251.85	0.01	2 265.81
path_dist	Distance from the nearest path (m)	134.93	148.05	0.33	992.51
redDeer_density	Estimated red deer population at the beginning of the monitoring campaign in hunting districts, in 2016-2017 (deer/1000 ha)	51.6	27.05	0	165
redDeer_shot_fd	Number of red deer harvested in forest district (deer/km ²)	1.85	1.42	0	8.27
redDeer_shot_hd	Number of red deer harvested in hunting districts (deer/km ²)	1.75	1.15	0	6.56
redDeer_shot_hd_smooth	Spatially smoothed indicator of the number of shot red deer (deer/km ²)	0.24	0.15	0	1.01
roads_dist	Distance from the nearest road (m)	659.18	535.8	3.43	3 560.07
roeDeer_shot_hd	Number of shot wild boars in hunting districts (boar/km ²)	2.67	1.55	0.62	6.78
slope	Slope (%)	9.53	6.62	0.19	49.05
wildBoar_shot_hd	Number of shot roe deer in hunting districts (deer/km ²)	4.72	3.7	0.73	18.09

Biomass estimates

Allometric relationships were fitted to predict the biomass of seedlings and ground vegetation. The biomass of seedlings was predicted in response to seedling maximum height ($H_{max,sp}$) and seedling density (n_{sp}) (Equation 4.1).

$$B_{sp} = a \cdot H_{max,sp}^b \cdot n_{sp}^c \quad (4.1)$$

where B_{sp} (kg) was the biomass of species sp and a , b and c were the fitted parameters. The biomass of bramble was estimated with the equations proposed by *Balandier et al. (2013)* (Equation 4.2).

$$B_{bramble} = \frac{LAI}{SLA} \quad (4.2)$$

$$LAI = (0.327 \cdot \log(cover))^2 \quad (4.3)$$

where LAI is the leaf area index and SLA (m^2/kg) is the specific leaf area. SLA was set to $26 m^2/kg$. The biomass of the ground vegetation (bramble and seedlings) was estimated for each plot and year.

The biomass increment was computed similarly to the height increment. For each plot, we kept the first and last census available. In the plots without seedlings and bramble, the biomass was $0 g/m^2$. The biomass increment was then computed from the difference between the initial and final biomass: $(B_f - B_i)/\Delta T$.

For each plot pair, the biomass increment was computed in fenced and unfenced conditions. The difference between the two estimates was used as an indicator of browsed biomass.

Statistical analyses

As our dataset contained many explanatory variables (Table VI), with some of them being correlated, we carried out a principal component analysis to reduce the dimensionality and ease the interpretation. The principal component analysis was performed with all numeric variables. The principal component analysis was built on the correlation matrix ensuring that every variable had the same weight in the analysis. For each plot pair, we extracted the score of the two first principal components. These scores were next used as explanatory variables in some models.

To model browsing impact, we fitted different linear mixed models (with lme4 R package) and linear models. At first, we tested whether the initial regeneration height and biomass were similar in the fenced and unfenced plots. It was tested fitting Equation 4.4 and Equation 4.5.

$$H_{sp,j,t,r} = a + b_r + c_{sp} + d_t + e_{sp,t} + \alpha_j + \epsilon_{j,sp,t,r} \quad (4.4)$$

$$B_{j,t,r} = a + b_r + c_t + \alpha_j + \epsilon_{j,t,r} \quad (4.5)$$

where $H_{sp,j,t,r}$ was the maximum height of species sp in plot pair j and treatment t ; a , b_r , c_{sp} and d_t were the fitted coefficients. The fixed effects were the region, the species, and the treatment (fenced/unfenced). The unexplained (random) variance was divided into two components: the between-plot variance (σ_j) and the within-plot variance (σ_ϵ). The intercept, a , of these models corresponded to the average estimate for beech regeneration in fenced plots in the Ardenne (default factor levels).

The impact of browsing on seedling height growth was first assessed fitting Equation 4.6.

$$iH_{sp,j,t} = a + b_{sp} + c_t + d_{sp,t} + \alpha_j + \epsilon_{j,sp,t} \quad (4.6)$$

where $iH_{sp,j,t}$ was the height increment of species sp in plot pair j and treatment t . As the interaction between species and treatment was significant, additional models were fitted separately for each study species. In these models, the scores of the two first principal components (PC1) and (PC2) were

added as explanatory variables (Equation 4.7). We then tested whether browsing impacts depended on environmental conditions fitting Equation 4.7.

$$iH_{j,t,r,sp} = a_{sp} + b_{t,sp} + c_{sp} \cdot PC1_j + d_{sp} \cdot PC2_j + e_{t,sp} \cdot PC1_j + f_{t,sp} \cdot PC2_j + \alpha_j + \epsilon_{j,sp,t,r} \quad (4.7)$$

Two other approaches were tested to model the effect of browsing on seedlings height. For each plot pair and species, we computed the difference between paired height increments (unfenced and fenced plots): $\Delta iH_{j,sp} = iH_{t=fenced,j,sp} - iH_{t=unfenced,j,sp}$. A linear model was fitted to predict $\Delta iH_{j,sp}$ in response to the two principal components across species (Equation 4.8).

$$\Delta iH_{j,sp} = a + b_{sp} + c_{sp} \cdot PC1_j + d \cdot PC2_j + e_{sp} \cdot iH_{t=fenced,j} + \epsilon_{j,sp} \quad (4.8)$$

In addition, as it appeared that $\Delta iH_{j,sp}$ depended on $iH_{t=fenced,j}$, we fitted Equation 4.9 to directly model the height increment of unprotected seedlings in response to the height increment of protected seedlings (considered as an indicator of the potential growth) and the two principal components.

$$iH_{t=unfenced,j,sp} = a + b_{sp} + c_{sp} \cdot iH_{t=fenced,j} + d_{sp} \cdot PC1_j + e_{sp} \cdot PC2_j + \epsilon_{j,sp} \quad (4.9)$$

The biomass of the ground vegetation was estimated at the plot level. The fitted models (Equation 4.10) were then very similar to the ones used to model the height increment but without the species effect.

$$iB_{j,t,r} = a + b_t + c \cdot PC1_j + d \cdot PC2_j + \alpha_j + \epsilon_{j,sp,t,r} \quad (4.10)$$

Additionally, the reduction of the biomass increment in paired plots ($\Delta iB_j = iB_{t=unfenced,j} - iB_{t=fenced,j}$) was modelled in response to the treatment and principal components fitting Equation 4.11.

$$\Delta iB_j = iB_{t=unfenced,j} - iB_{t=fenced,j} = a + b_t + c \cdot PC1_j + d \cdot PC2_j + e_t \cdot PC1_j + \epsilon_{j,t} \quad (4.11)$$

Results and discussion

The two first principal components explained 41 % of the total variability of the explanatory variables (Figure 14). The first components depended mainly on estimates of red deer density whereas the second component depended on other environmental conditions.

Large scores on the first component were obtained for areas with low red deer density and, but to a lesser extent, high roe deer density. In the following, this principal component was inverted so to have large score in areas where red deer was abundant (Figure 15).

Large scores on the second component were obtained for plots at high elevation, far from roads and buildings, where the carrying capacity was low, wild boar population was small and the ground vegetation was less palatable. Such plots were mostly found in the large forest patches at high elevation in Ardenne.

In the following, for the sake of simplicity, we will sometimes refer to these gradients as gradients of red deer density and elevation. The reader must nevertheless keep in mind that other environmental characteristics were correlated to these variables.

hornbeam and maple (i.e., two palatable species). The height increments generally increased with the initial height of the seedlings, especially in fenced plots (Figure 16). In unfenced plots, the height increment was, for every study species but spruce, significantly lower in unfenced plots than in fenced plots (Table VII). This reduction was about 15 cm/yr for birch (60 %), 15 cm for rowan (83%), 11 cm/yr for hornbeam (65%), 6 cm/yr for maple (54%) and 4 cm/yr for beech (30%) and oak (57%).

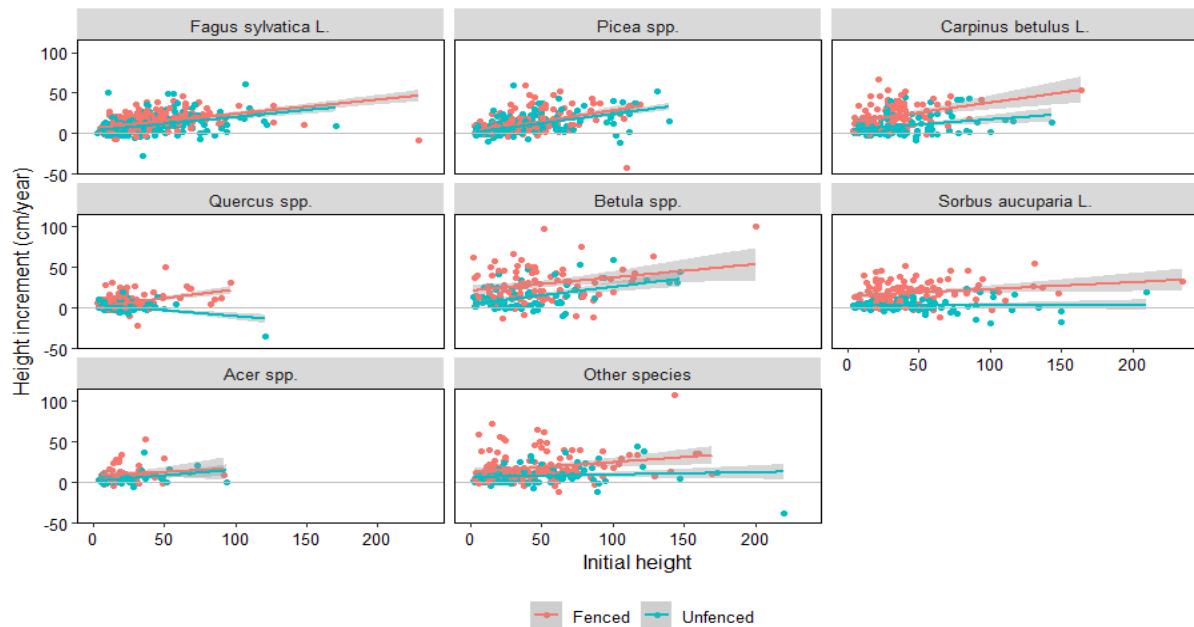


Figure 16. Relationships between height increment and regeneration initial height across treatments and species

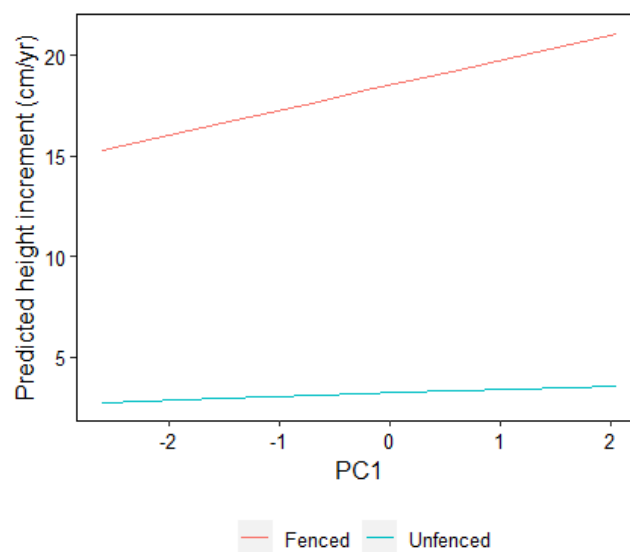
Fitting Equation 4.7 (not showed), significant relationships were found between seedling height growth, red deer density indicators (expressed by the first principal component, PC1) and environmental conditions (PC2). The relationships were nevertheless species and treatment specific. For example, the height increment of hornbeam significantly depended on PC1 and PC2 (Table VIII). Nevertheless, the interpretation of such a model was considered delicate. On the one hand, protected hornbeam seedlings grew faster where red deer were abundant ($P < 0.001$). On the other hand, unprotected seedlings grew significantly slower than protected seedlings ($b = -15,9$ cm/yr, $P < 0.001$) and the difference increased with the density of red deer ($P < 0.001$). PC1, or the density of red deer, affected then positively (indirect effect) and negatively (direct effect likely due to browsing) the growth of hornbeam seedlings. Considering the two effects, unprotected hornbeam seedlings grew slightly faster in area with large red deer population (Figure 17).

Table VII. Summary statistics of the linear mixed model of the height increment across treatments and species (Equation 4.6)

Predictors	Estimates	CI	p
(Intercept)	12.94	11.81 – 14.06	<0.001
species [Picea spp.]	-3.26	-4.92 – -1.59	<0.001
species [Carpinus betulus L.]	6.32	4.08 – 8.56	<0.001
species [Quercus spp.]	-6.13	-7.82 – -4.44	<0.001
species [Betula spp.]	12.12	9.86 – 14.39	<0.001
species [Sorbus aucuparia L.]	6.04	3.95 – 8.14	<0.001
species [Acer spp.]	-2.18	-5.09 – 0.73	0.142
species [Other species]	4.34	2.39 – 6.29	<0.001
species [Fagus sylvatica L.] × treatment [Unfenced]	-3.83	-5.19 – -2.47	<0.001
species [Picea spp.] × treatment [Unfenced]	-1.16	-2.84 – 0.52	0.175
species [Carpinus betulus L.] × treatment [Unfenced]	-11.44	-13.94 – -8.95	<0.001
species [Quercus spp.] × treatment [Unfenced]	-3.85	-5.72 – -1.97	<0.001
species [Betula spp.] × treatment [Unfenced]	-15.37	-18.20 – -12.54	<0.001
species [Sorbus aucuparia L.] × treatment [Unfenced]	-15.49	-18.03 – -12.96	<0.001
species [Acer spp.] × treatment [Unfenced]	-5.62	-9.27 – -1.97	0.003
species [Other species] × treatment [Unfenced]	-9.64	-11.95 – -7.33	<0.001
Random Effects			
σ^2	81.2		
$\tau_{00 \text{ plot}}$	47.65		
ICC	0.37		
N_{plot}	686		
Observations	2483		
Marginal R^2 / Conditional R^2	0.172 / 0.478		

Table VIII. Summary statistics of the linear mixed model of the height increment of hornbeam in response to treatment and the two first principal components scores (PC1 and PC2)

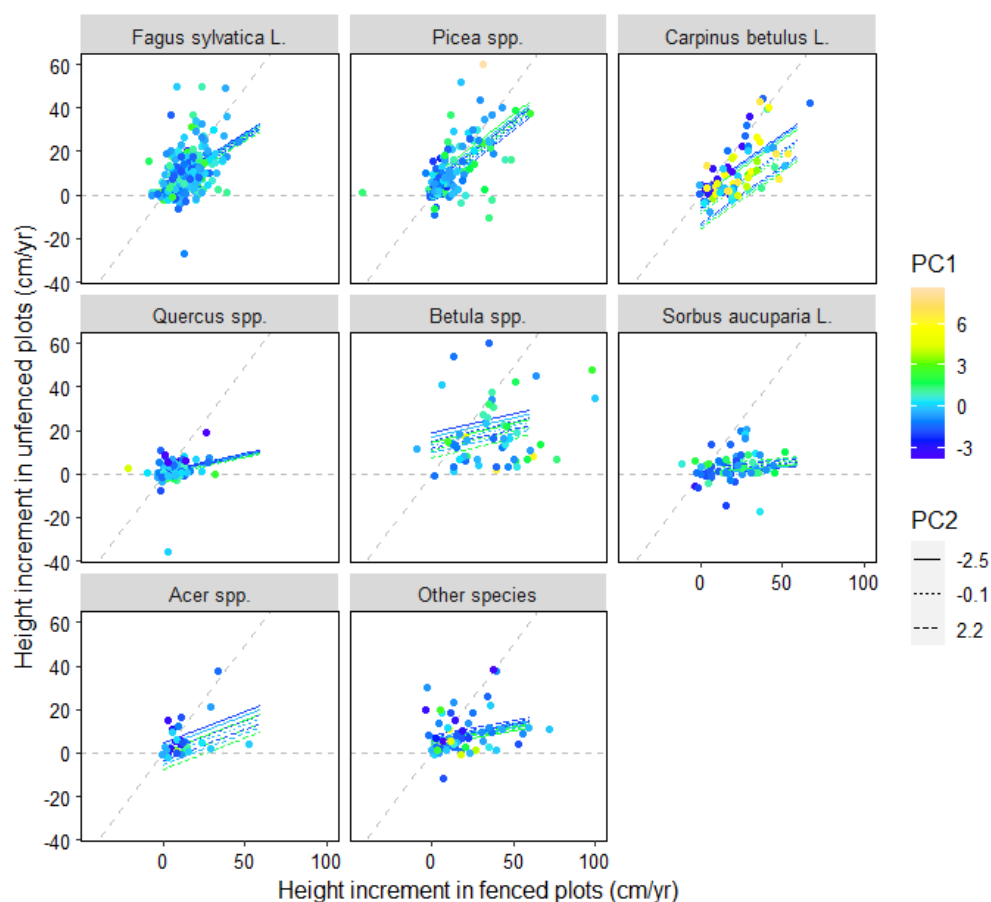
<i>Predictors</i>	<i>Estimates</i>	<i>CI</i>	<i>p</i>
(Intercept)	18.36	12.91 – 23.80	<0.001
treatment [Unfenced]	-15.88	-21.25 – -10.51	<0.001
PC1	1.26	0.56 – 1.96	<0.001
PC2	-0.84	-3.12 – 1.43	0.466
treatment [Unfenced] × PC1	-1.08	-1.73 – -0.43	0.001
treatment [Unfenced] × PC2	-2.5	-4.68 – -0.31	0.025
Random Effects			
σ^2	56.67		
$\tau_{00 \text{ plot}}$	99.64		
ICC	0.64		
N_{plot}	125		
Observations	208		
Marginal R^2 / Conditional R^2	0.258 / 0.731		

**Figure 17. Model prediction of hornbeam seedling height in response to PC1 which is correlated to red deer density**

All species together, the mean height increment differences, $\Delta iH_{j,sp}$, was 5.9 cm/yr. Significant species-specific differences were observed. For example, the increment reduction for hornbeam seedlings was positively correlated with $iH_{t=fenced,j}$, PC1 and PC2 (Table IX).

Table IX. Summary statistics of the linear model of the height increment reduction of hornbeam in response to treatment and the two first principal components scores (PC1 and PC2)

Predictors	Estimates	CI	p
(Intercept)	7.48	2.38 – 12.58	0.005
$iH_{t=fenced,j}$	0.47	0.34 – 0.61	<0.001
PC1	0.62	0.06 – 1.17	0.029
PC2	3.11	1.17 – 5.04	0.002
Observations	83		
R^2 / R^2 adjusted	0.444 / 0.423		

**Figure 18. Observations and model predictions of the regeneration height increments in unfenced plots in response to the height increments in fenced plots. The predictions were computed for three values (quantiles 10%, 50% and 90%) of the first and second principal component (PC1 and PC2)**

Then, the growth of unprotected seedlings was modelled with Equation 4.9 (Table X). With this model, the increment of unprotected seedlings depended on red deer density (PC1) only for hornbeam seedlings ($P = 0.023$). The growth of unprotected hornbeam, spruce and birch decreased also with the elevation (PC2). For example, for hornbeam, the effect of PC2 was greater than the effect of PC1 underlining the importance of local conditions in addition to the effect of ungulate density (Figure 18).

Table X. Summary statistics of the linear model of the height increment of unprotected seedlings response to the increment observed in fenced plots, species, PC1 and PC2 (Equation 4.9)

Predictors	Estimates	CI	p
(Intercept)	3.19	1.58 – 4.79	<0.001
species [Picea spp.]	0.95	-1.49 – 3.39	0.444
species [Carpinus betulus L.]	-10.66	-15.83 – -5.50	<0.001
species [Quercus spp.]	-2.91	-5.34 – -0.49	0.019
species [Betula spp.]	9.76	4.95 – 14.57	<0.001
species [Sorbus aucuparia L.]	-1.45	-5.77 – 2.87	0.511
species [Acer spp.]	-4.89	-11.62 – 1.84	0.154
species [Other species]	2.59	-0.80 – 5.97	0.134
species [Fagus sylvatica L.] × Fenced	0.47	0.36 – 0.57	<0.001
species [Picea spp.] × Fenced	0.58	0.48 – 0.68	<0.001
species [Carpinus betulus L.] × Fenced	0.53	0.39 – 0.66	<0.001
species [Quercus spp.] × Fenced	0.17	-0.05 – 0.38	0.128
species [Betula spp.] × Fenced	0.18	0.07 – 0.29	0.002
species [Sorbus aucuparia L.] × Fenced	0.07	-0.09 – 0.23	0.388
species [Acer spp.] × Fenced	0.29	0.01 – 0.57	0.04
species [Other species] × Fenced	0.14	0.02 – 0.26	0.027
species [Fagus sylvatica L.] × PC1	-0.34	-1.03 – 0.36	0.346
species [Picea spp.] × PC1	0.74	-0.04 – 1.52	0.063
species [Carpinus betulus L.] × PC1	-0.62	-1.15 – -0.08	0.023
species [Quercus spp.] × PC1	-0.25	-0.94 – 0.44	0.476
species [Betula spp.] × PC1	-1.11	-2.44 – 0.23	0.105
species [Sorbus aucuparia L.] × PC1	0.22	-1.49 – 1.93	0.799
species [Acer spp.] × PC1	-1.03	-2.92 – 0.86	0.285
species [Other species] × PC1	-0.7	-1.62 – 0.22	0.137
species [Fagus sylvatica L.] × PC2	-0.54	-1.25 – 0.18	0.139
species [Picea spp.] × PC2	-0.94	-1.79 – -0.09	0.030
species [Carpinus betulus L.] × PC2	-3.11	-4.97 – -1.25	0.001
species [Quercus spp.] × PC2	-0.18	-1.22 – 0.86	0.733
species [Betula spp.] × PC2	-1.51	-2.65 – -0.37	0.01
species [Sorbus aucuparia L.] × PC2	0.73	-0.66 – 2.11	0.302
species [Acer spp.] × PC2	-1.74	-4.65 – 1.18	0.243
species [Other species] × PC2	0.42	-0.78 – 1.63	0.49
Observations		896	
R ² / R ² adjusted		0.599 / 0.585	

On average, the initial biomass of the ground vegetation was about 52 g/m² but its variability was substantial (s.d. = 87 g/m²) as its estimates ranged between 0 and 992 g/m². On average, the initial biomass was greater in the unfenced plots, but the difference was not significant (15.9 g/m², $P = 0.165$). The initial biomass was also very poorly correlated to PC1 ($r = 0.075$) and PC2 ($r = 0.144$).

The biomass increments increased slightly with the initial biomass (Figure 19, Table XI). The average biomass increment was 22 g/m²/yr. It was lower than 26 g/m²/yr in 75% of the plots. The biomass increment was significantly lower in the unfenced plots (-9.51 g/m²/yr, $P < 0.001$, Table XI). The biomass increment depended both on PC1 and PC2. Once again, the use of this model seemed limited as the abundance of red deer (PC1) had positive and negative effects.

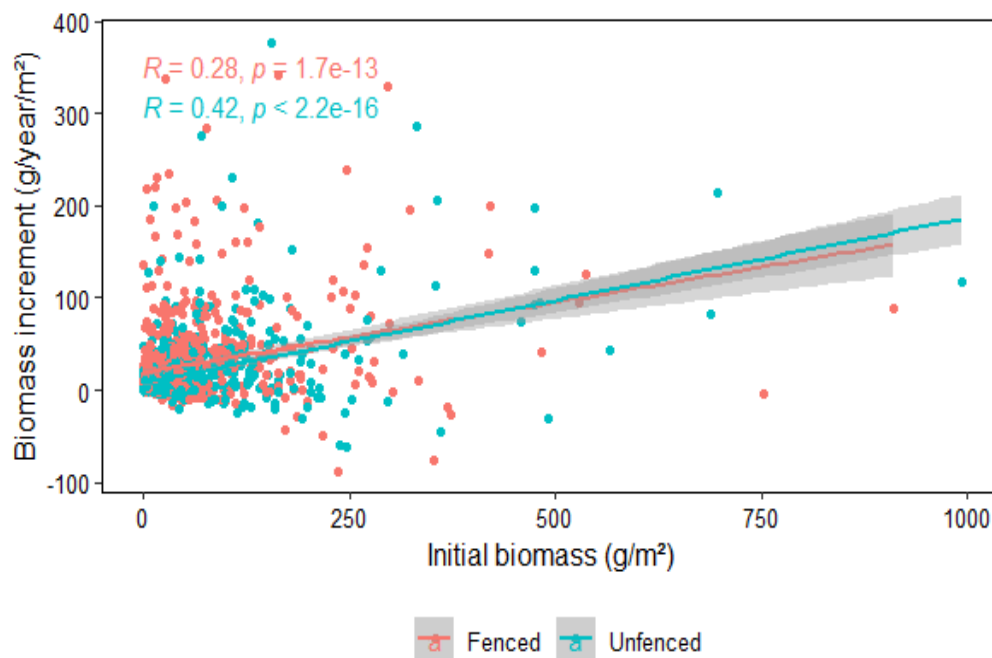


Figure 19. Relationships between the biomass increment and the initial biomass in fenced and unfenced plots

Conclusions

Several equations were tested to model the effect of ungulate browsing on tree regeneration and ground vegetation. Relationships between browsing impacts and wild ungulate density were sought after but such relationships were not clearly evidenced. Unfortunately, for some species, the growing conditions were more favourable where red deer was abundant. This indirect and positive effect of ungulate density on seedling growth was found difficult to disentangle from the direct effect of browsing. Protected birch and hornbeam seedlings grew particularly faster in areas with abundant red deer. This effect might originate from (i) a correlation between red deer densities and different unmeasured environmental characteristics, (ii) the result of deer browsing prior to plot installation inducing different understory history, and (iii) greater efforts of field workers to set up the plots in good growing conditions in the areas with large red deer populations.

Table XI. Summary statistics of the linear model of the biomass increment in response to the initial biomass, treatment, PC1 and PC2 (Equation 4.10)

Predictors	Estimates	CI	p
(Intercept)	18	14.72 – 21.29	<0.001
initial biomass	0.16	0.14 – 0.19	<0.001
treatment [Unfenced]	-9.51	-12.40 – -6.63	<0.001
PC1	3.32	1.85 – 4.78	<0.001
PC2	-3.37	-5.06 – -1.69	<0.001
treatment [Unfenced] × PC1	-2.43	-3.85 – -1.01	0.001
treatment [Unfenced] × PC2	0.91	-0.71 – 2.53	0.271
Random Effects			
σ^2	739.12		
$\tau_{00 \text{ plot}}$	842.15		
ICC	0.53		
N_{plot}	689		
Observations	1373		
Marginal R^2 / Conditional R^2	0.140 / 0.598		

With this work, the impacts of browsing can now be modelled using the mean species-specific reduction of height increment, i.e., the estimates of parameter $d_{sp,t}$ of Equation 4.6. This reduction corresponds to the mean height increment reduction (of species highest seedling) observed throughout the study area for relatively small seedlings (< 60 cm). Eventually, for taller seedlings, the relative value of the height increment reduction could be used instead of the absolute value. The effect of environmental conditions and ungulate density could be considered fitting species-specific model of the height increment of unprotected seedlings (Equation 4.9, e.g., Table X). These models could also be improved fitting non-linear equations.

The impact of browsing could also be modelled using estimate of biomass increment reduction (parameter b_t of Equation 4.10). This reduction corresponds to the mean biomass increment reduction observed throughout the study area for relatively small seedlings. To accurately apply this approach, further work is required to improve the estimates of ground vegetation biomass and to develop additional equations or algorithms to simulate the biomass consumption of the different regeneration cohorts.

Additional data and analyses of ungulate impacts on regeneration

With the additional measurements taken in 2022 in the regeneration dynamic monitoring plots, the length of apical shoots was modelled in response to seedling initial heights with Equation 4.12:

$$L_{i,j,sp,b} = a_{sp} \cdot h_{i,j,sp,b} + b_{sp,b} \cdot h_{i,j,sp,b} + \alpha_j + \epsilon_{i,j,sp,b} \quad (4.12)$$

where $L_{i,j,sp,b}$ was the length of the apical shoot of seedling i , in plot j , of species sp . $b_{sp,b}$ was the difference between normal and browsed shoot lengths. $h_{i,j,sp,b}$ was the initial height of the seedling, i.e. the height reached before budbreak. This model assumed that the shoot increments were proportional to seedling heights. The reduction of apical shoot length was significantly evidenced for beech, hornbeam and oak (Figure 20). The number of observations was likely too limited to evidence such an effect for the other species. The reduction of apical shoot length was the greatest for hornbeam seedlings and the smallest for spruce and rowan (Table XII).

The number of sampled seedlings and sites appeared too limited to fit general models and, particularly, to predict the probability of a given shoot to be browsed. We also had planned to estimate seedling initial biomass and biomass increment with only one census (measuring seedling height, diameter and the length of different apical and lateral shoots). This approach was finally found not accurate enough to evidence the effect of browsing on seedling biomass. Repeated measurements, that are logistically more demanding, are likely required to fit such a model. The collected data nevertheless confirmed and supplemented some earlier observations, particularly about the effect of browsing on seedling height growth.

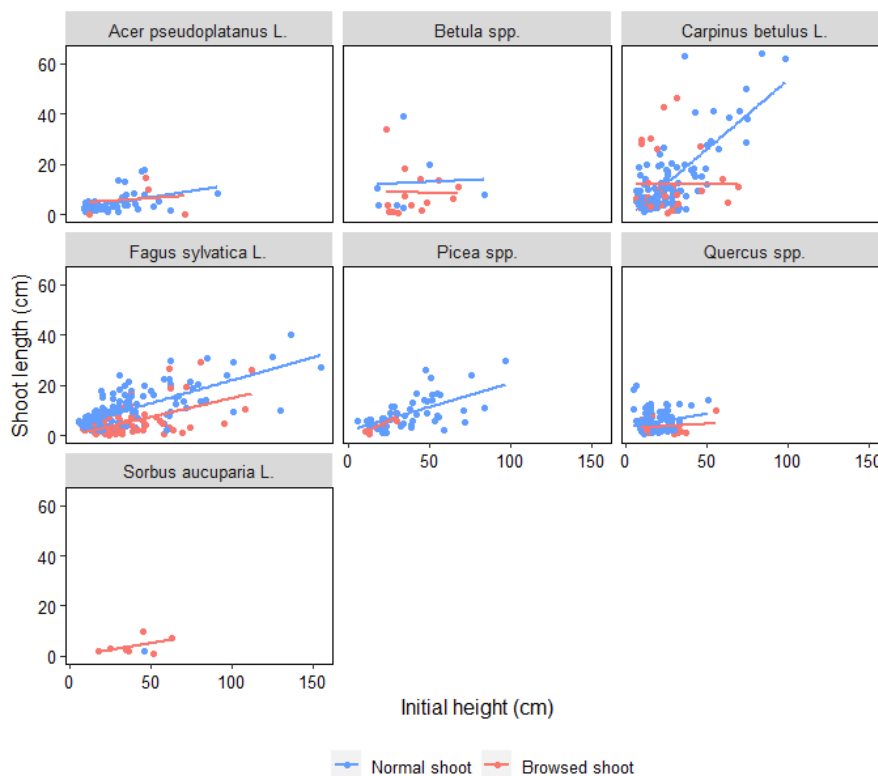


Figure 20. Relationships between apical shoot length and initial seedling height

Table XII. Summary statistics of the model of shoot length (Equation 4.12)

<i>Predictors</i>	<i>Estimates</i>	<i>CI</i>	<i>p</i>
a [Acer pseudoplatanus L.]	0.13	0.07 – 0.19	<0.001
a [Betula spp.]	0.26	0.16 – 0.36	<0.001
a [Carpinus betulus L.]	0.52	0.47 – 0.56	<0.001
a [Fagus sylvatica L.]	0.23	0.20 – 0.25	<0.001
a [Picea spp.]	0.19	0.15 – 0.23	<0.001
a [Quercus spp.]	0.25	0.18 – 0.32	<0.001
a [Sorbus aucuparia L.]	0.03	-0.22 – 0.28	0.832
b [Acer pseudoplatanus L.]	-0.01	-0.14 – 0.11	0.853
b [Betula spp.]	-0.07	-0.19 – 0.05	0.253
b [Carpinus betulus L.]	-0.18	-0.26 – -0.11	<0.001
b [Fagus sylvatica L.]	-0.09	-0.13 – -0.05	<0.001
b [Picea spp.]	0	-0.20 – 0.21	0.966
b [Quercus spp.]	-0.14	-0.27 – -0.02	0.027
b [Sorbus aucuparia L.]	0.06	-0.20 – 0.32	0.663
Random Effects			
σ^2	31.39		
$\tau_{00 \text{ plot}}$	9.59		
ICC	0.23		
N_{plot}	83		
Observations	664		
Marginal R ² / Conditional R ²	0.496 / 0.614		

Bark peeling

The drivers and characteristics of bark peeling damage on spruce trees have been relatively well described in the literature (Candaele *et al.*, 2021; Cukor *et al.*, 2019; Gill, 1992a; Gill, 1992b; Vospernik, 2006). We also have valuable information on the subsequent decay in the stems and well-detailed models of forest stand dynamics and forest management (Burneviča *et al.*, 2016; Čermák and Strejček, 2007; Vacek *et al.*, 2020). This information has already been implemented in HETEROFOR but some improvements and tests were still needed.

Although it was not planned within the initial activities of this project, we decided to assess the impact of bark peeling on entire timber production cycles of Norway spruce. This study was found necessary to test and improve our last developments, particularly about the impacts of ungulate damage and those used to assess the profitability of silvicultural routes (in Economics2 library), while answering to relevant questions. The complete description of this study has been published in the European Journal of Forest Research in 2023 and is available online (<https://hdl.handle.net/2268/301794>) (Ligot *et al.*, 2023). Here, only few key features are described.

Assessing the financial impact of bark peeling damage on timber production was interesting as it requires considering multiple variables and processes over a long period of time (>50 years).

Consequently, most studies have focused on certain processes but rarely made a comprehensive assessment of financial losses. Gill *et al.* (2000) illustrated how such an assessment could be made with elementary models, but acknowledged that their approach was limited and that further models had to be developed to estimate yield losses, particularly for Norway spruce. In line with what has been proposed to assess the economic impacts of browsing by roe deer (Rakotoarison, 2009; Ward *et al.*, 2004) or moose (Wam and Hofstad, 2007), an assessment can be made by modelling forest dynamics and interactions with ungulate populations (Weisberg and Bugmann, 2003). Once models are established, they can be used to predict the costs and revenues of different management strategies for various protective treatments and/or environmental conditions (e.g., ungulate density).

To fill this gap, we coupled a model of the forest dynamics and management of even-aged coniferous stands (GYMNOS) with models of bark peeling damage. We then conducted a virtual experiment to address several questions: does bark peeling damage substantially harm the profitability of Norway spruce plantations? Should rotation be shortened in the stands that are highly impacted by bark peeling damage? Is it more cost-effective to protect plantations with fences or to protect individual trees against bark peeling at the time of the first thinning (i.e., after some damage has already occurred)?

The cost of bark peeling damage was found to be substantial depending on the rate of bark peeling damage (*BSR*), discount rate (*r*), and, to a lesser extent, site index (*SI*, Figure 21). With high bark peeling rate (*BSR* = 10%) and without protection, around 85% of the trees harvested at the final cut contained decayed wood and the volume of this decayed wood accounted for 15% of stand volume.

Within the study area, the mean bark peeling rate was about 4% (Gheysen *et al.*, 2011). This rate also corresponds to the damage rate tolerated by the forest administration. In Southern Belgium, Norway spruce yields 14.7 m³/ha on average, which corresponds to a site index of 27 m (stand dominant height reached at 50 years of age). If we choose a discount rate of *r* = 2%, the average opportunity cost of bark peeling damage is 2 647 €/ha which corresponds to an annuity of 53 €/ha/year (Figure 21). These figures are high, corresponding to a loss of net revenue of 19%. This cost is also of the same order of magnitude as the plantation costs or hunting leases.

Forest managers may additionally be tempted to shorten the rotation in stands where bark peeling damage is observed because they are eager to start a new rotation. However, we found that the optimum rotation should either remain the same or be only slightly lengthened irrespective of the discount rate used. In old stands, new bark peeling damage becomes less likely (Gill *et al.*, 2000; Jerina *et al.*, 2008; Vospernik, 2006) and the spread of the decay is very low (Čermák *et al.*, 2004; Čermák and Strejček, 2007; Löffler, 1975). Considerations about the rotation length should therefore first consider the effects of the discount rate, site index and certainly also, though not examined here, the risk of future disturbance to stands and other ecosystem services.

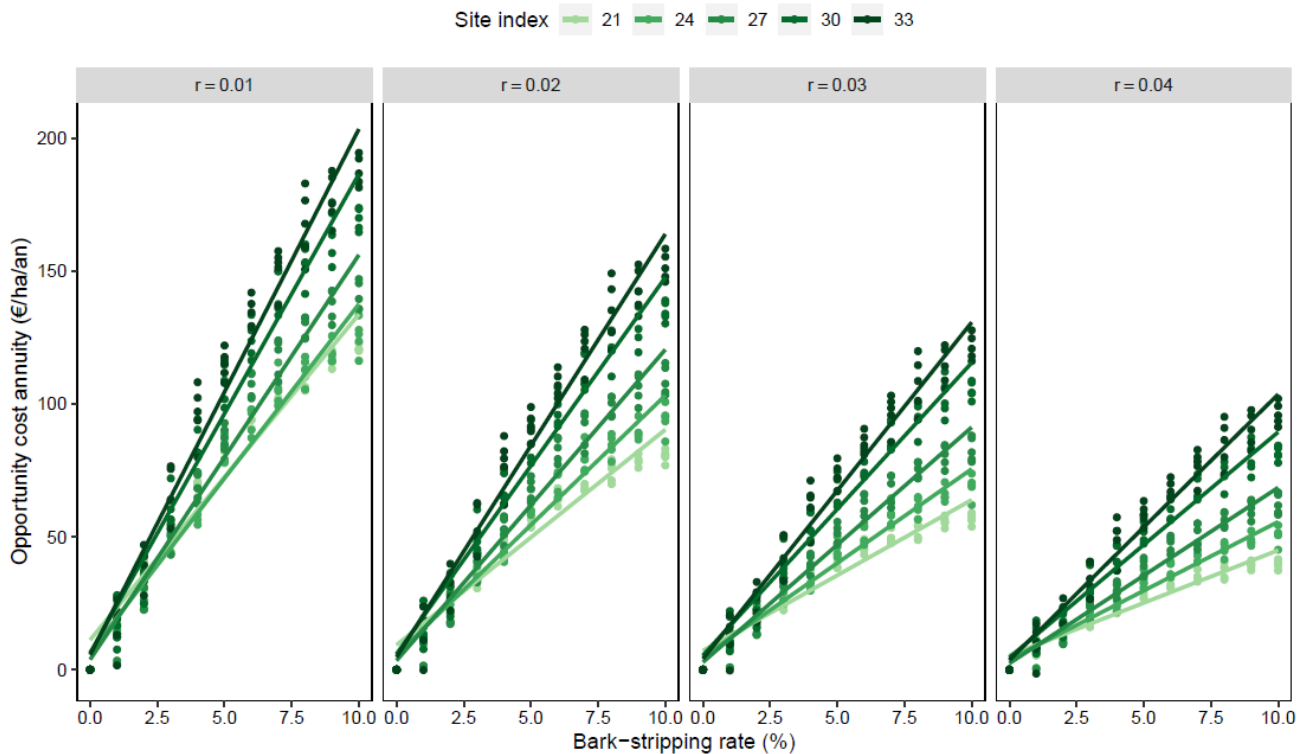


Figure 21. Relationships between the annuity of the opportunity cost of bark peeling damage, bark peeling rate, discount rate, and site index

Fencing to protect trees against bark peeling damage was found unlikely to be cost-effective. In most cases, its cost was appreciably greater than the opportunity cost of the damage. Moreover, we probably underestimated its cost because the fence maintenance costs were not counted. Fences in forests usually last about 15 years, much less than the time trees need protection against bark peeling damage (about 40 years). Fences were cost-effective only when the chosen discount rate was low ($r < 1\%$), the bark peeling rate high and/or likely when saplings need also to be protected from browsing (Jensen *et al.*, 2012).

Cheaper protections might however be cost-effective particularly in the most productive stands. In this study, we assumed that such individual protections were placed at the time of the first thinning (at 17-29 years of age). At that time, the trees are big enough to be pruned and their bark scraped to protect them against bark peeling. Nevertheless, a substantial proportion of the trees may already be damaged at that age (Candaele *et al.*, 2021; Gill, 1992b; Vospernik, 2006). In the simulations with high bark peeling rates, individual protections could be fitted on already damaged trees, so having no effect or a very small effect on future timber value. This occurred mostly in the less productive stands and when the bark peeling rate was very high. In the most productive stand, the first thinning occurs earlier, and enough healthy crop trees can probably be found making individual protection a valid solution. In less fertile stands, individual protection should be fitted several years before the first thinning.

Levels of wild ungulate populations have usually been adjusted to the damage levels, with limited regard to the actual cost of such damage. The model we propose in this study can be used to assess the cost of bark peeling damage balancing long-term revenues against short-term costs of protection

measures and long-term costs of bark peeling damage. Knowing the true cost of bark peeling damage is essential to improving the economic efficiency of deer and forest management.

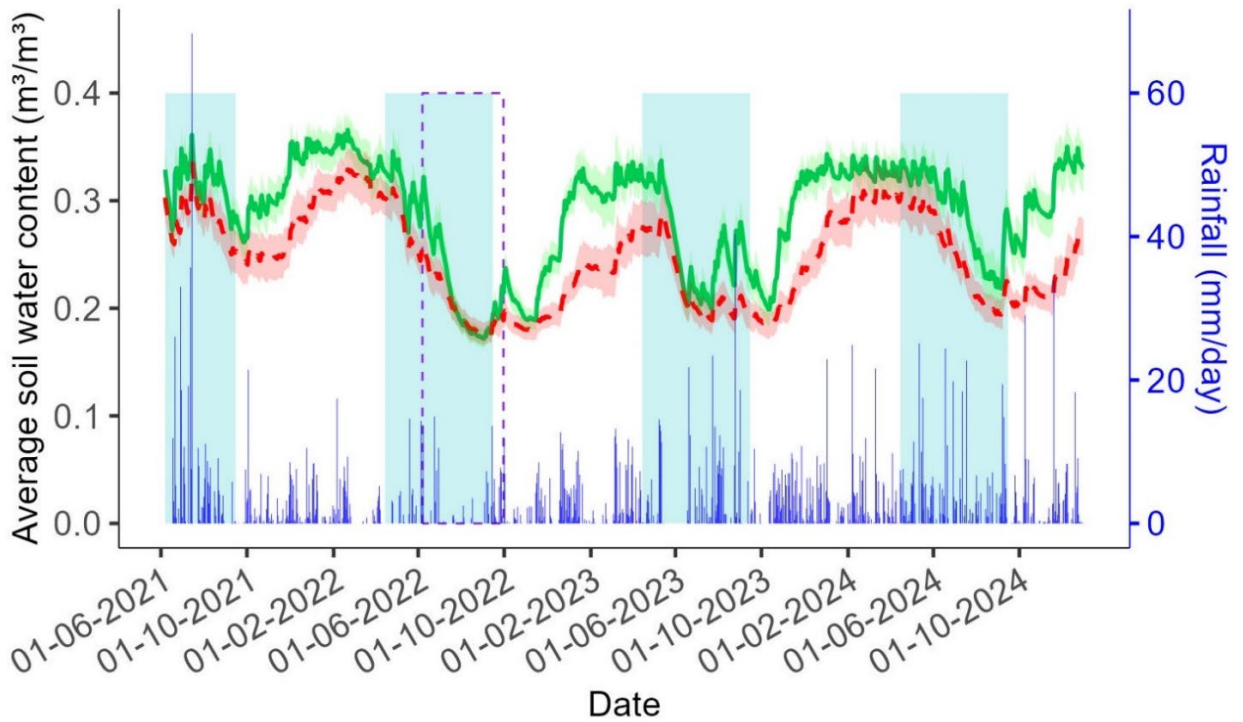
This study also demonstrated the use of the Economics2 library as well as the algorithms used to simulate the impact of ungulate damage.

4.2 Rainfall limitation experiment

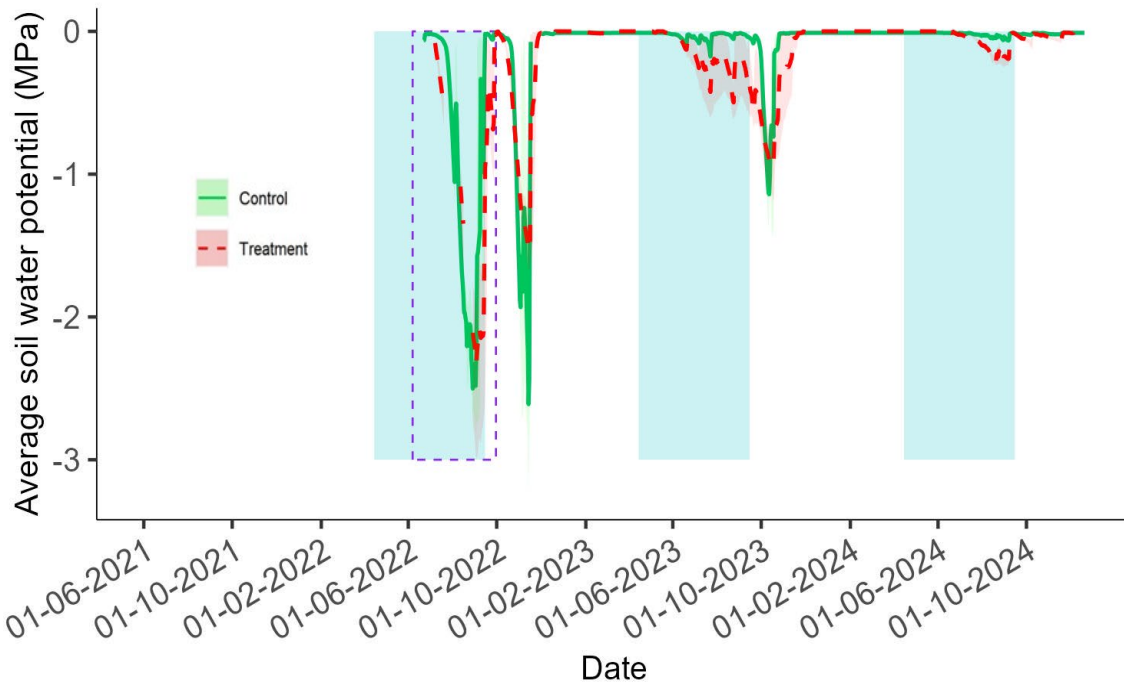
The temporal dynamics of the average volumetric soil water content (SWC) measured for the upper 30 cm soil layers in the experimental units of the rainfall limitation experiment is presented in Figure 22(a) for the 07/06/2021-31/12/2024 period. During most of the first growing season covered by these measurements (07/2021-08/2021), SWC values remained high given the large rainfall depth observed during that period, especially during July. Yet, systematically lower average SWC values were found in the 'treatment' units compared with the 'control' units, though the differences were sometimes limited. After a SWC decrease during a drier period in September 2021, larger differences were observed due to a faster SWC recharge in the control until reaching maximum SWC values in early spring 2022 where the treatment effect is again reduced. Then, a general SWC decrease occurred, especially in the treatment units for which temporary SWC recharge peaks due to rainfall events were much more attenuated in the treatment compared with the control. The SWC decrease was particularly pronounced for the severe drought period from 07/2022-09/2022 at the end of which very low SWC values around $0.18 \text{ m}^3/\text{m}^3$ were observed in both the control and the treatment. When the rain was back, the SWC recharge was again faster for the control, leading to much higher SWC values in the control compared with the treatment. In contrast to 2022, significant SWC differences among both modalities prevailed until the start of the 2023 growing season. Yet, the absence of rainfall for one month (from mid-May to Mid-June) induced a steep decrease of SWC and led again to low values (around $0.20 \text{ m}^3/\text{m}^3$) in all units which persisted until the end of July. Then, larger rainfall events enabled partial recharging of the soil with water in the control during the last part of the growing period while SWC values remained low for the treatment. This was followed by a new short dry period in early October, after which a general SWC increase occurred with a faster recharge in the control compared with the treatment, following a pattern similar to that observed during the previous dormant period. The first half of 2024 was characterized by regular rainfall, which kept the soil continuously close to saturation until mid-July. SWC then decreased, reaching minimum values in early September at levels comparable to those observed in the previous years, while remaining this time significantly higher on average in the control units than in the treatment units. However, precipitation events continued to occur and more sustained rainfall soon caused SWC to increase again. These results indicate that the roofs generally significantly reduce SWC, except when severe droughts take place and induce dryness in all experimental units. Moreover, the roof effect is particularly marked during the post-drought recharge periods. Figure 22(b) shows the temporal evolution of the soil water potential (SWP) measured in parallel to SWC using the tensiometer probes installed in the more intensively equipped beech zone (referred to as "Beech zone 3" in the following). For 2022, similar patterns are observed for the control and the treatment units, with a progressive decrease during the severe drought period, followed by a rapid increase once rainfall occurs again (see Figure 23(a) for a more detailed view of this period). Yet, the decrease started earlier in the treatment while, like for

SWC, the recovery was somewhat delayed compared with the control. Then, a new peak, more pronounced in the control, arose during autumn before reaching values constantly close to zero until June 2023. During the 2023 growing season, SWP showed only little variations and remained close to zero in the control. In contrast, somewhat lower average SWP values were observed in the treatment, though associated with a large variability among probes. A pronounced SWP decrease occurred in both modalities after the growing period, in early October, and then reached near-zero values. The regular rainfall during 2024 maintained SWP continuously close to zero, with only a limited decrease in the treatment units at the end of the vegetation period.

Similarly as depicted above for SWP (see Figure 22(b) and Figure 23(a)), the stem water potential measured on seedlings during the 2022 growing period decreased progressively during the drought before increasing during the subsequent rainfalls (Figure 23(b)). Nevertheless, stem water potential variations were much more pronounced for the control compared with the treatment, giving rise to more negative stem water potential values for the seedlings in the control and to increasing differences between both units as the drought progressed. These results would indicate that the seedlings under the roof were less stressed than those in the control. Several hypotheses can be made to explain these quite unexpected results. A first hypothesis could be that seedlings of both modalities presented contrasted fine root abundances and distributions. Such differences could result from a higher root mortality by anoxia for the seedlings in the control that were subject to higher SWC levels during the preceding wet summer of 2021 and/or from the development of fine roots in more deeper soil horizons by the seedlings under the roof as an adaptation to the drier conditions. Another explanation would be that the seedlings in the treatment unit were exposed to less stressful conditions due to the lower radiation reaching them compared with the control unit, as attested by the PAR measurements presented in Figure 23(c). These lower radiation levels in the treatment unit would partly arise from the interception of a part of the radiation by the roof structure but might also result from contrasted light environments for the two modalities within the stand, although these were only a few meters apart. The analysis of the hemispherical photos taken above each unit (and above the roof in the case of the treatment unit) revealed that, for the period corresponding to those measurements, the average percentage of the incident PAR radiation that reached the treatment unit was around 3% while it amounted to 9% for the control unit (Figure 24(a)). This indicates that the differences in radiation levels between both units would mainly arise from a 'location' effect and that the 'roof' effect would be relatively minor. Given these different exposures to radiation, the seedlings under the roof would have been subject to a lower atmospheric demand for water than in the control.



(a)



(b)

Figure 22. Temporal variation of (a) soil volumetric water content and (b) soil water potential measured in the 'control' and the 'treatment' units of the rainfall limitation experiment. Lines are daily average values and shaded areas around the lines are corresponding 95% confidence intervals. Results presented in subfigure (a) consider all experimental zones while data in subfigure (b) only concern to the more intensively equipped beech zone. The green shaded areas delimit for each year the period between 15/04 and 15/09, corresponding approximately to the vegetation period, the dashed purple line delimits the measurement period covered by Figure 23. Daily incident rainfall depth is also provided in subfigure (a).

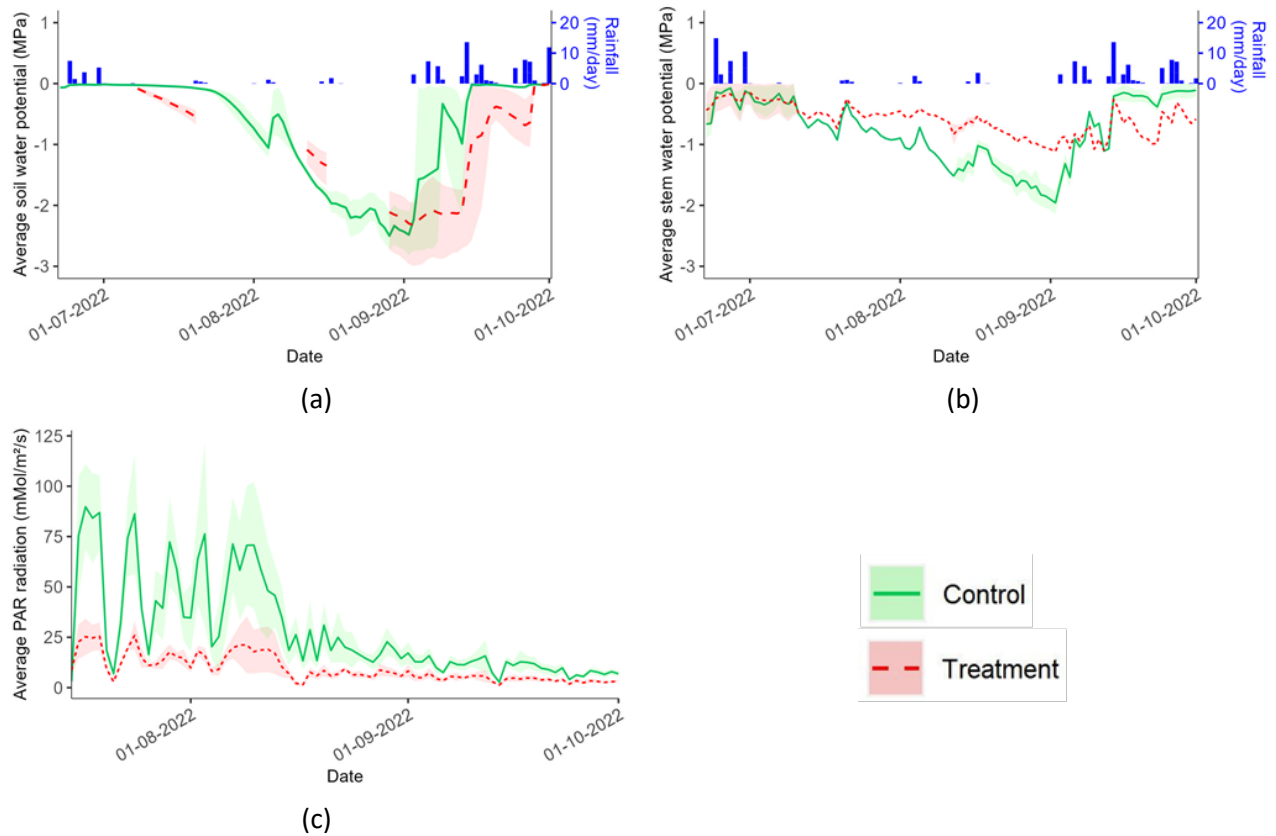


Figure 23. Temporal variation of (a) soil water potential, (b) seedling stem water potential and (c) photosynthetically active radiation (PAR) measured in the 'control' and the 'treatment' units of the more intensively equipped beech zone ("Beech zone 3") of the rainfall limitation experiment. Lines are daily average values and shaded areas around the lines delimit minimum and maximum measured values. The measurement period corresponds to the time window bounded by the dashed purple line in Figure 22. Daily incident rainfall depth is also provided in subfigures (a-b)

Finally, a lack of control of the measurement variability due to the low number of repetitions (i.e., 1 or 2 repetitions for each modality, depending on the period) might also partly explain such results. In other respects, these results would argue in favour of the practice of regeneration under cover, in the shelter of adult trees, than through clearcuttings in which more stressful conditions would occur for the seedlings. It is worth to note, that the differences in transmitted radiation percentages among the control and the treatment units were much less pronounced and not systematic for the five other experimental zones (Figure 24(a)). Regarding leaf water potential (Figure 24(b)), which was measured in all experimental units using the Scholander bomb, higher values (i.e., less negative values) for beech tended to be observed in zones which received the least radiation (see Figure 24(a)). Such observations agree with those made above for stem water potential between the control and the treatment units of the beech zone 3. Yet, such a trend was not found for oak and, for both species, the treatment effect was systematically not significant (Figure 24(b)). In other respects, the somewhat higher leaf water potential values observed for beech compared with oak might be explained by contrasting responses of both species when facing drought. Indeed, beech is acknowledged to limit the variations of water potential through rapid stomata closure when dry conditions appear (isohydric strategy) while oak is known to keep its stomata open and maintain high photosynthetic but also transpiration rates for longer periods, leading thereby to a significant decrease of water potential under stressful conditions (anohydric strategy).

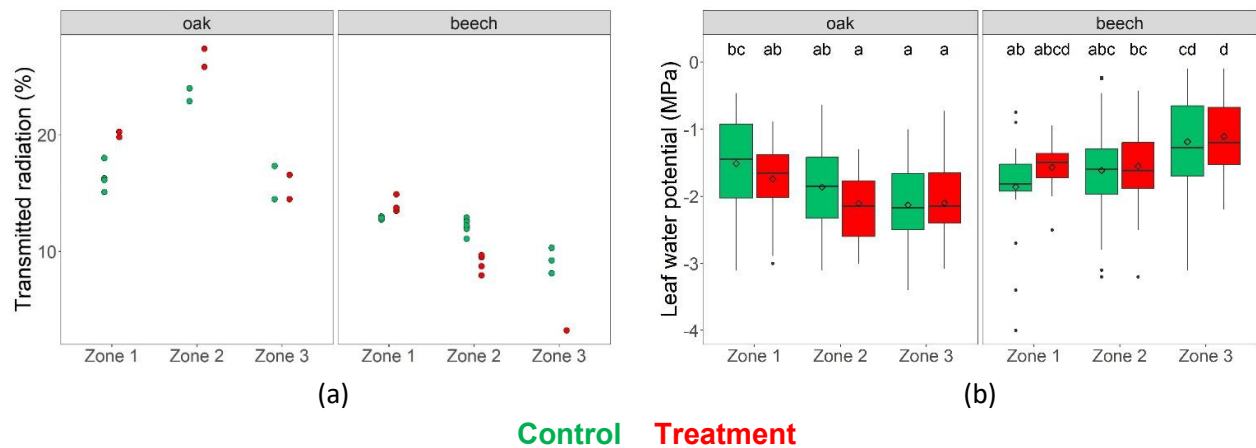


Figure 24. Comparison among experimental zones and treatments (a) of transmitted radiation estimated from hemispherical photographs analysis and (b) of seedling leaf water potential measured with the Scholander pressure bomb. Repetitions shown for each zone × treatment combination in subfigure (a) are results from either different photographs or different image thresholding options for a given photograph. Different letters in subfigure (b) indicate statistically significant differences ($P \leq 0.05$)

Results from the dendrometric measurements performed on the 32 seedlings selected in each experimental unit are presented in Figure 25. As mentioned above, apical shoot increment was measured for each year (Figure 25(b)) while collar diameter measurements were not performed in 2024 (Figure 25(a)). So as to avoid the influence of the size effect on growth in the comparisons among treatments, growing years and species, increment data are presented in relative values.

A significant decrease in collar diameter relative increment was observed between 2021 and 2022 for both species, while relative increment values were comparable between 2022 and 2023. A similar pattern was observed for relative shoot increment in the same years, with the exception that for beech the decrease in increment values was more pronounced between 2022 and 2023 than between 2021 and 2022. A significant increase in relative shoot increment occurred for oak in 2024 compared to 2023, reaching an intermediate level between 2023-2024 and 2021. In contrast, for beech, relative shoot increment continued to decrease in 2024, although not significantly. The decline in growth between 2021 and 2022 would arise from the contrasted meteorological conditions characterising those years, especially with regard to rainfall amount and the resulting soil water content level, large rainfall depths and permanently high soil water contents having occurred during the growing period 2021 and inversely for 2022 (see Figure 22(a)). The persistence of the relative increment values measured for 2023 at levels generally similar to those for 2022 indicated that seedling growth did not respond positively to the more favourable conditions of soil water availability for the 2023 growing season compared with 2022 (see Figure 22). This might be explained by prolonged adverse effects of the 2022 severe drought on the 2023 growth of the collar diameter for both species and of the apical shoot for oak. The resumption of more sustained apical shoot relative increment for oak in 2024 suggested a lessening of these adverse effects and a recovery of seedling vitality for this species. In contrast, the results for the apical shoot of beech would rather indicate a delayed effect of water deficit on growth, with the main reduction of shoot increment being observed in 2023 instead of 2022. Another explanation for the generally low level of growth in 2023 could be the dry period at the start of the growing season on that year (see Figure 22(a)). Yet, the temporality of the shoot growth (shoot

increment was measured a first time in July and repeated during the dormant season) showed that most of the increment occurred before July in 2023, no or only negligible additional growth was observed during the second part of the growing season despite the partial SWC recharge. Furthermore, such a hypothesis of reduced growth due to temporary water shortage does not hold for 2024 given the sustained water supply over the growing season for that year. Beyond the delayed effect of water deficit, the continuation of low increment values for beech in 2024 would arise from the particularly low level of radiation observed for 2024. The lower values of relative apical shoot increment found for oak in 2024 compared to 2021 could also be explained by this lack of light in 2024.

In other respects, the treatment effect was systematically not significant for both dendrometric variables and both species, whatever the year. For 2021 and 2022, this could notably be explained by the quite similar SWC levels observed in the control and the treatment units over those two years. Nevertheless, the same observations also apply to 2023 and 2024 despite the relatively better soil water availability for the control compared with the treatment for those years as reflected (i) by the higher SWC values in the former modality (see Figure 22(a)) and (ii), for 2023, by the lower SWP values in the treatment compared with the control (see Figure 22(b)). Yet, these differences of water availability among treatments remained quite limited and were most likely not sufficient to induce differences in growth between modalities.

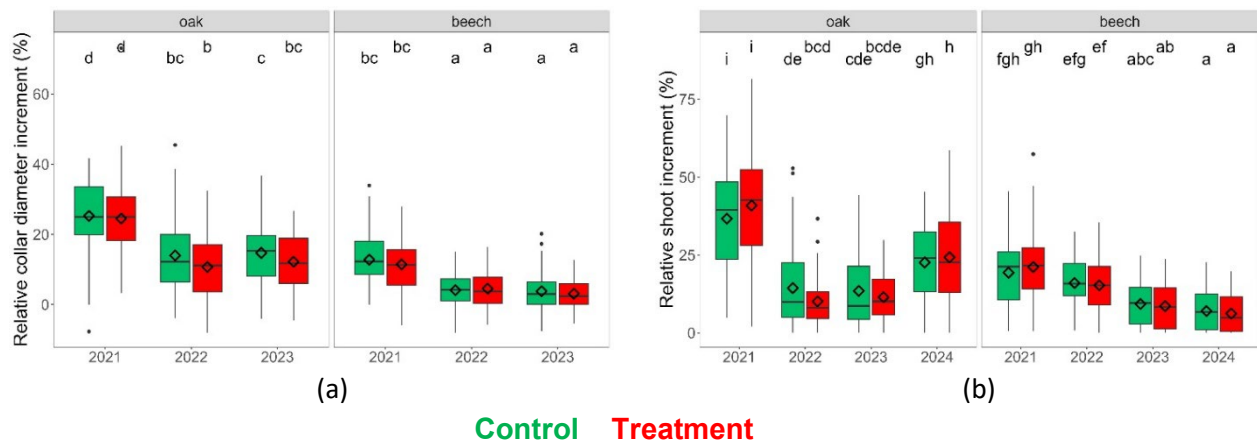


Figure 25. Comparison of measurements of seedling (a) collar diameter increment and (b) terminal shoot increment among years and treatments. Different letters indicate statistically significant differences ($P \leq 0.05$)

To further investigate and quantify the effects on seedling growth of the different factors considered in this experiment, the following mixed-effect model was fitted for both species:

$$iShoot_{resid} \sim SWC_{growing} + Treat + Zone + SWC_{growing} \times Treat + SWC_{growing} \times Zone + Treat \times Zone + SWC_{growing} \times Treat \times Zone + \alpha + \varepsilon \quad (4.13)$$

in which shoot increment is expressed as a function of average soil water content over the growing season ($SWC_{growing}$), the treatment ($Treat$: control vs roof units), the experimental zone ($Zone$) and the seedling individual (α). The three first explanatory variables were set as fixed effects while the seedling individual was considered as random term. In this model, shoot increment corresponds to

$$iShoot_{resid} = iShoot_{meas} - iShoot_{pred} \quad (4.14)$$

with $iShoot_{meas}$ being the measured yearly shoot increment and $iShoot_{pred}$ is the yearly increment predicted based on the relationship established for each species by Ligot *et al.* (2013a), relating seedling height growth to the percentage of above canopy light at the seedling level ($PACL$) and the seedling total height. This transformation removed from the data the effects on seedling growth of individual size and of differences in light levels between experimental units and zones. Thereby, a positive $iShoot_{resid}$ value would indicate an observed above-average increment, and inversely for a negative $iShoot_{resid}$ value. Transmitted radiation, determined from the hemispherical photographs (see Figure 24(a)), was used as $PACL$ values in Ligot *et al.* (2013a) equation.

The fitting results are presented in Figure 26 and Table XIII. For oak, the average soil water content over the growing season showed a positive effect on shoot increment, as indicated by the increasing $iShoot_{resid}$ values as $SWC_{growing}$ increased. This effect was more pronounced in the treated units than in the control units, suggesting that soil water content had a stronger influence on seedling growth under limited water supply. In addition, for a given soil water content, height growth in the treated units was on average systematically higher than in the control unit. This observation can be interpreted as the result of a protective effect of the roof on the underlying seedlings by maintaining a more favourable microclimate, notably during extreme weather events such as late frosts or heat waves. In other respects, as aforementioned, it may also result from the adaptation of the seedlings under the roofs to drier conditions through the development of roots at greater depths, making them more resilient to drought than the seedlings in the control units. Similar observations apply to beech. In this case, however, the SWC effect was much less marked than for oak and appeared as not significant in the control units. For both species, the treatment and the zone effects accounted for 1% and 4% of the total variability, respectively. Inter-individual variability represented 8% and 12% of the total variability for oak and beech, respectively (Table XIII). Finally, the dominant contribution of residual variability observed for each species indicates that a large part of measured seedling growth variability is influenced by factors other than those considered in the fitted model. These factors would notably include the atmospheric evaporative demand, which is governed by air temperature, relative humidity, wind and radiation. These variables were not directly measured at our experimental site and did not necessarily vary concomitantly with soil water availability.

Table XIII. Percentage of seedling residual height growth total variability explained by each factor considered in the mixed-effect model 4.13

Effect	Oak	Beech
$SWC_{growing}$	24%	5%
<i>Treat</i>	1%	1%
<i>Zone</i>	4%	4%
α	8%	12%
<i>Residuals</i>	63%	78%

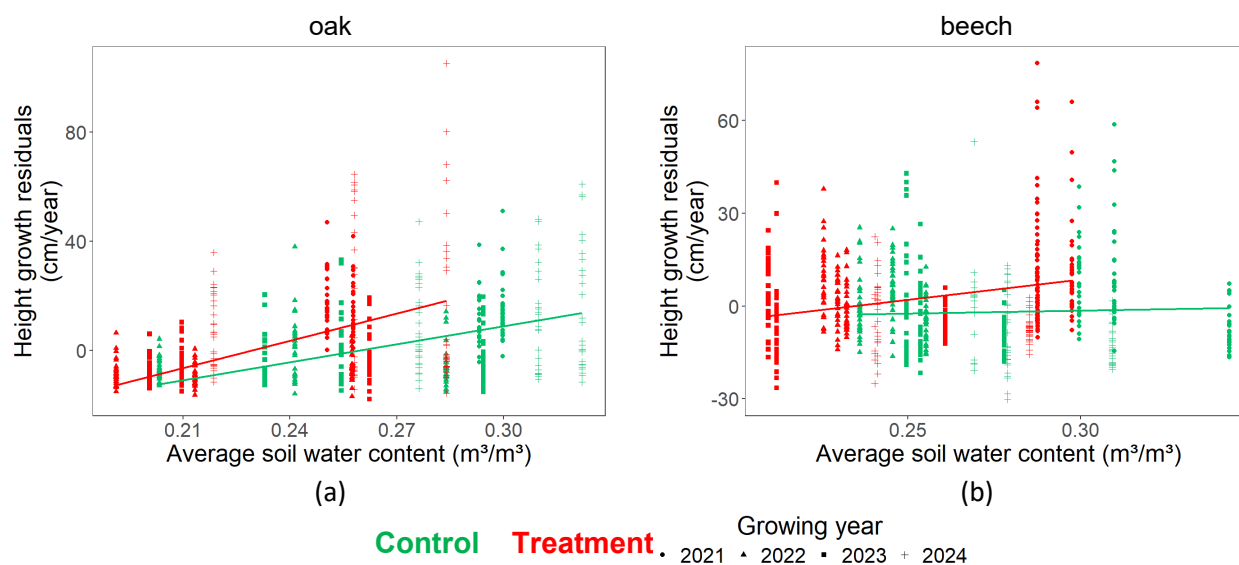


Figure 26. Influence of the average soil water content during the growing season and of the rainfall limitation treatment on seedling residual height growth (see Equation 4.14)

4.3 Establishment of climate projection scenarios

Validation of the disaggregation procedure

The disaggregation methods as currently presented were validated using a leave-one-out method (see Task 1.6). The results are shown in Table XIV wherein a comparison is also made with temporal downscaling methods provided in literature. It appears that the proposed methods perform as good or mostly better than those reported in literature.

Table XIV. Validation results as obtained in different studies and in our study (last row) for incoming solar radiation (RS), temperature (T), precipitation (P), relative humidity (RH) and wind speed (W). The scores used include the correlation (r) and the root mean squared error (RMSE)

Study	R _s		T		P		RH		W	
	r	RMSE	r	RMSE	r	RMSE	r	RMSE	r	RMSE
Bregaglio <i>et al.</i> (2010)	-	-	-	-	-	-	0.04-0.46	11.25-19.75	-	-
Debele <i>et al.</i> (2007)	-	-	0.97	2.37	0.35-0.55	0.58-0.88	0.51	19.12	0.48-0.77	2.5-3.7
Fadhel <i>et al.</i> (2017)	-	-	-	-	-	3.44-3.46	-	-	-	-
Förster <i>et al.</i> (2016)	0.94	46.6	0.96	1.94	-	-	0.49	15.08	0.72	1.33
Lu and Qin (2014)						1.98-4.06				
Our study	0.96	57.1	0.98	1.42	0.41	0.51	0.63	14.20	0.82	0.88

Note that this table only compares the statistical performances of disaggregation schemes, while computational efficiency is an important factor for analysing century-long data which is the case for the REG+ project.

Evaluation of the bias correction methods

To evaluate the performance of the bias correction methods (additive/scaling and quantile mapping), we computed the Mean Absolute Error (MAE) between the models and observational data for both the uncorrected and bias-corrected datasets. The MAE is applied to each site and model separately. Table XV presents the average MAE computed across the eleven sites and eleven CMIP6 models for the six variables that we bias-corrected.

The additive and scaling methods reduce the average (site and model) bias of near-surface relative humidity, total precipitation, short-wave incoming radiation, near-surface wind speed, near-surface air temperature, near-surface minimum air temperature by 4.23%, 0.2 mm day⁻¹, 14.28 W m⁻², 0.42 m s⁻¹, 1.05 °C and 1.67 °C, respectively. It corresponds to a reduction of the initial bias of 68%, 29%, 69%, 51%, 63% and 73%, respectively. The quantile mapping (ISIMIP3) method reduces the average (site and model) bias of near-surface relative humidity, total precipitation, short-wave incoming radiation, near-surface wind speed, near-surface air temperature, near-surface minimum air temperature by 4.26%, 0.23 mm day⁻¹, 14.5 W m⁻², 0.42 m s⁻¹, 1.04 °C and 1.67 °C, respectively. It corresponds to a reduction of the initial bias of 69%, 33%, 70%, 51%, 62% and 73%, respectively. Table XV indicates that the two bias-corrections systematically reduce the model climatological biases for all variables. Also, the additive/scaling and quantile mapping approaches display similar performances. This was expected, as the MAE only provides bias-correction performances for the climatological mean of the distribution. We evaluated other aspects of the distribution. For this purpose, boxplots representing the daily distributions of the six corrected variables are presented in Figure 27 (additive/scaling corrections) and Figure 28 (quantile mapping correction). Key aspects of the correction performances and their limitations are outlined below.

Table XV. Validation of the bias-correction methods using the MAE. The MAE is applied to monthly-mean climatological values. Only the average MAE computed for the 11 sites and 11 models is presented. Results for each variable are divided into 2 columns, one for the uncorrected (raw) and one for the bias-corrected (BC) data over the validation period. For the first correction, the additive method is used for air temperature and minimum air temperature while the scaling method is used for the other variables

Correction	Near-surface relative humidity (%)		Precipitation (mm day ⁻¹)		Short-wave incoming radiation (W m ⁻²)		Wind speed (m s ⁻¹)		Air temperature (°C)		Minimum air temperature (°C)	
	Raw	BC	Raw	BC	Raw	BC	Raw	BC	Raw	BC	Raw	BC
Additive/scaling	6.19	1.96	0.69	0.49	20.6	6.32	0.82	0.40	1.67	0.62	2.28	0.61
Quantile mapping	6.19	1.93	0.69	0.46	20.6	6.10	0.82	0.40	1.67	0.63	2.28	0.61

Near-surface relative humidity

Near-surface relative humidity is not adequately represented by some climate models. Models like CMCC-ESM2, INM-CM4-8, and INM-CM5-0 produce consistently low relative humidity values. Models like ACCESS-ESM1-5, CMCC-ESM2, INM-CM4-8, INM-CM5-0, and IPSL-CM6A-LR display an excessively wide inter-quartile range. The scaling correction helps mitigate the aforementioned problems. However, the correction doesn't always improve the median value of the distribution in models like MPI-ESM1-2-LR and IPSL-CM6A-LR. Additionally, this correction does not accurately represent extreme

values in some models. In particular, the right tail of the distribution is characterized by values exceeding 100% in all models except CanESM5 and IPSL-CM6A-LR. These values, which surpass 100%, are already present in the raw dataset and are not introduced by the correction. The method does not remove these values but, instead, the scaling factor applied can make them even larger.

The scaling correction also occasionally generates negative values (ACCESS-ESM1-5: 112 days, MPI-ESM1-2-HR: 52 days, MPI-ESM1-2-LR: 5 days out of 10958). Negative values are found for all sites, but Baileux, Louvain-la-Neuve and Uccle. The scaling factor calculated based on (100%-relative humidity) proves to be highly sensitive to consistent disparities between model outputs and observational data. While scaling factors exhibit only minor variations around a value of 1 for relative humidity, values greater than 3 are possible for (100%-relative humidity). Such a high coefficient results in significant adjustments to (100%-relative humidity), which can surpass 100%. This leads to bias-corrected relative humidity values turning negative after transformation.

The ISIMIP3 method provides better results for relative humidity. This correction improves the median value of the distribution in all models. Besides, there are no values above 100% (because there are no supersaturated values in the observations). The lowest simulated values also agree with observations.

Total precipitation

The errors in GCM daily precipitation afflict the entire intensity spectrum. In many cases there are artificially large amounts of drizzle in the models, i.e. days with low precipitation, while the observations suggest a larger number of dry days. The mean of the distribution is also biased, and the observed high precipitation events are not properly reproduced (Dai, 2006). This is in essence what Figure 27 and Figure 28 show.

Figure 27 shows that the scaling correction only reduces the bias in the median in half of the models (ACCESS-ESM1-5, IPSL-CM6A-LR, MPI-ESM1-2-HR, MPI-ESM1-2-LR and MRI-ESM2-0), while the median is systematically improved using ISIMIP3. The value of the lower quartile, which is different from 0 in most models, shows that the correction does not significantly increase the number of dry days (see Table XVI). This is because the scaling correction does not provide separate corrections for precipitation occurrence and intensity. This distinction is implemented in ISIMIP3.

The scaling method was found effective for correcting the bias in high precipitation simulations of the EURO-CORDEX RCMs in Europe (Hosseinzadehtalaei *et al.*, 2020) and the CMIP5 GCMs in Belgium (Hosseinzadehtalaei *et al.*, 2017). Figure 27 agrees with those two studies. It shows that the upper quartile (75th percentile) of the modelled distribution gets closer to the observations. Nevertheless, extremes are not systematically better represented (ACCESS-CM2 and MRI-ESM2-0) using the scaling method. The ISIMIP3 method do not solve this problem. Contrary to the scaling method, ISIMIP3 does not produce extremely high values (183 mm day⁻¹ for ACCESS-CM2, 175 mm day⁻¹ for INM-CM5-0), but the highest value of the distributions is systematically underestimated. Reasons for this limitation are not clear and we can only formulate some hypotheses. It is possible that parametric quantile mapping for precipitation is not always appropriate for correcting the right queue of the distribution. In a lesser extent, the imperfect generation of pseudo future observations (refer to the ISIMIP3

protocol) can also limit the quality of the adjustment. In fact, the distributions over the calibration and validation periods might be different and the underlying climate change signal might differ on models and observations.

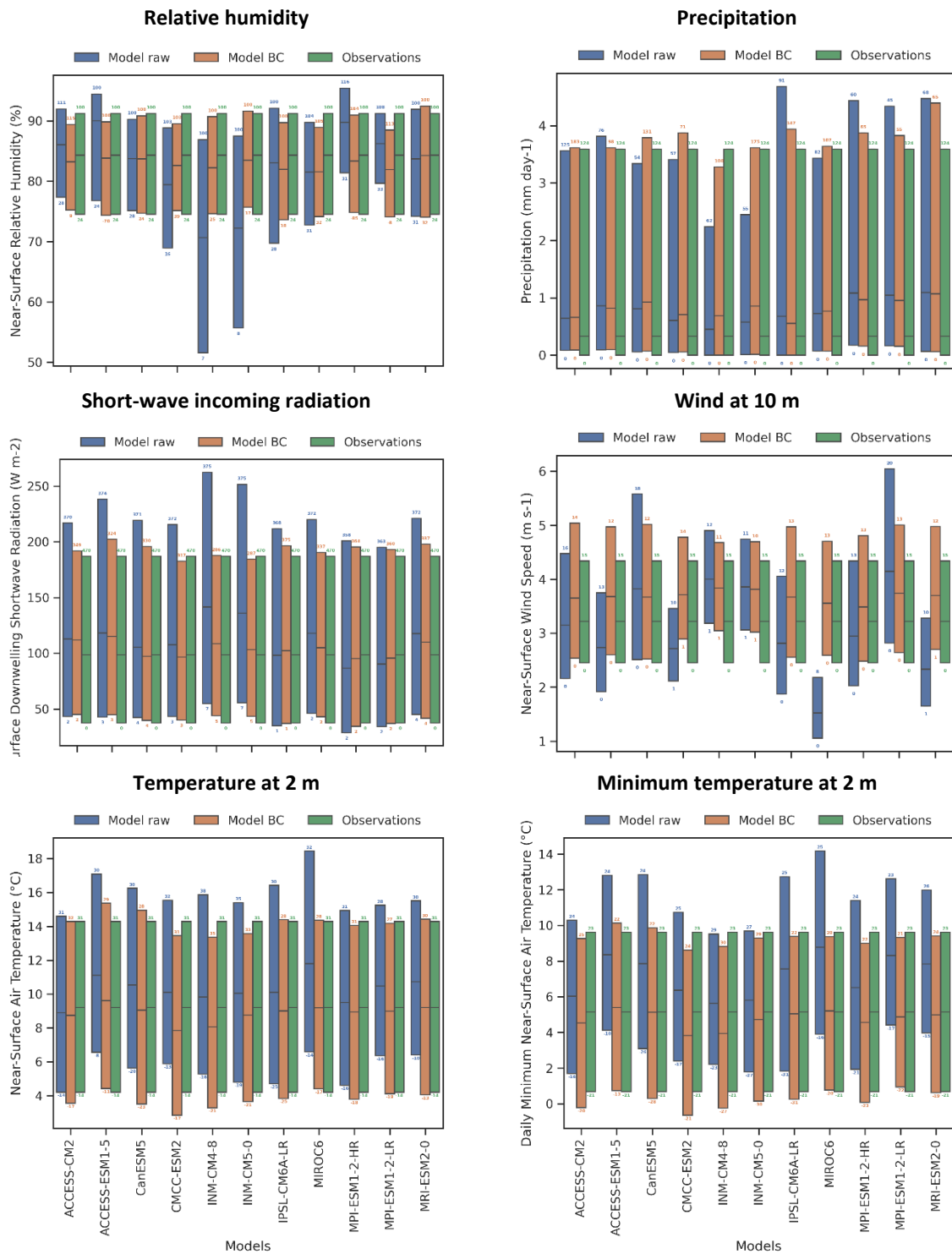


Figure 27. Boxplots for the raw and bias-corrected (additive for temperatures and scaling for the others) daily model data. Each box represents the distribution over the 11 sites. Raw data, bias-corrected data, observations are in blue, orange and green, respectively. Variables shown are the near-surface relative humidity, the total precipitation, the surface downwelling shortwave radiation, the near-surface wind speed, the near-surface temperature and the minimum near-surface temperature. Numbers at the bottom and top of each box are the minimum and maximum distribution values, respectively

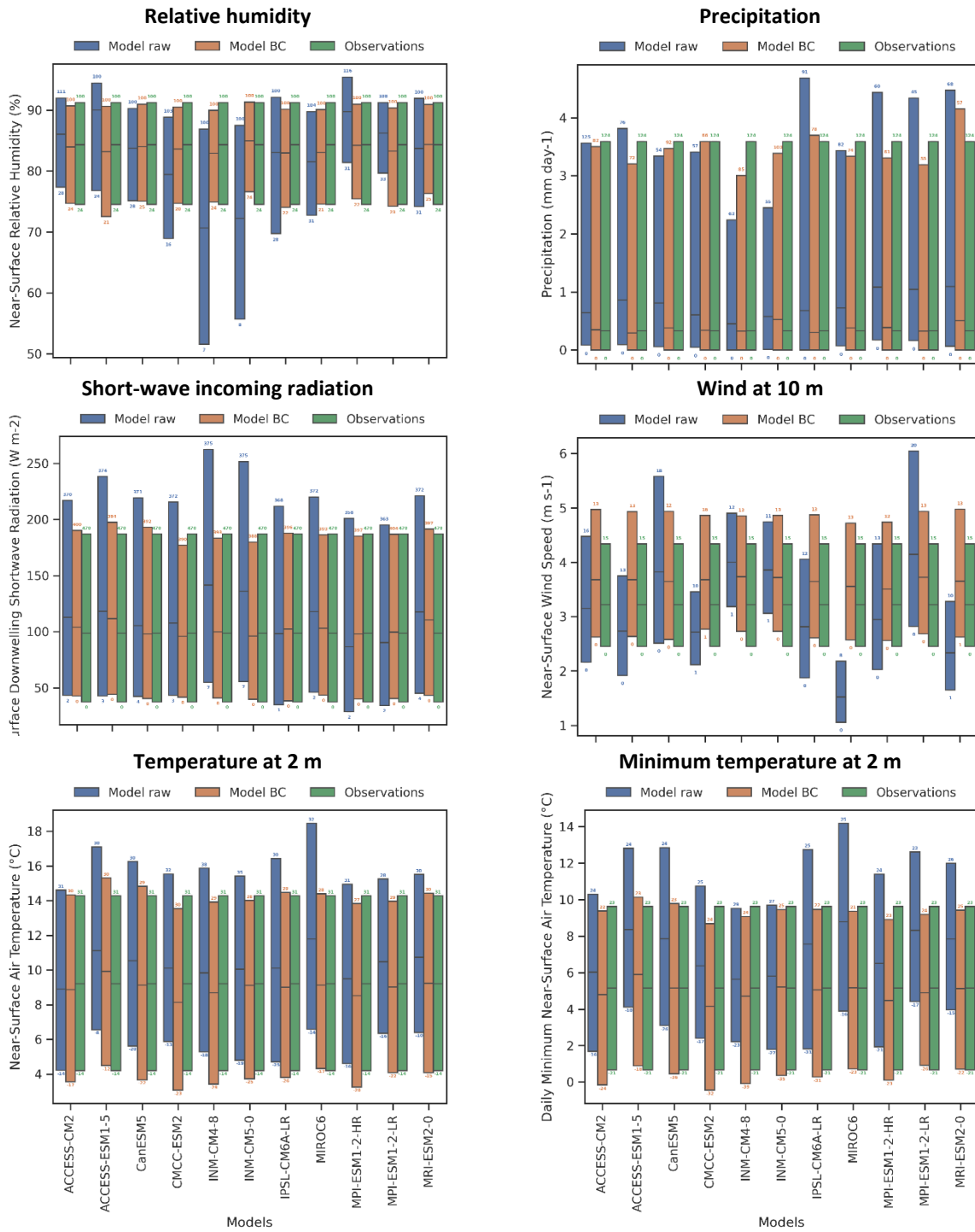


Figure 28. Boxplots for the raw and bias-corrected (ISIMIP3 method) daily model data. Each box represents the distribution over the 11 sites. Raw data, bias-corrected data, observations are in blue, orange and green, respectively. Variables shown are the near-surface relative humidity, the total precipitation, the surface downwelling shortwave radiation, the near-surface wind speed, the near-surface temperature and the minimum near-surface temperature. Numbers at the bottom and top of each box are the minimum and maximum distribution values, respectively

Table XVI. Number of dry days in the raw and bias-corrected (scaling and quantile mapping corrections) model data over the validation period 1992-2021. Values are averaged over the 11 sites. The number of dry days is calculated based on daily occurrence counts of $Pr < 0.1 \text{ mm day}^{-1}$

Correction	ACCESS-CM2	ACCESS-ESM1-5	CanESM5	CMCC-ESM2	INM-CM4-8	INM-CM5-0	IPSL-CM6A-LR	MIROC6	MPI-ESM1-2-HR	MPI-ESM1-2-LR	MRI-ESM2-0	Observations
Raw	3 021	2 808	3 188	3 399	3 985	3 667	4 290	3 033	2 279	2 324	3 013	4 630
Scaling	2 957	2 781	3 044	3 248	3 748	3 424	4 370	2 993	2 351	2 365	3 030	4 630
Quantile mapping	4 556	4 910	4 550	4 562	4 766	4 367	4 779	4 559	4 600	4 769	4 318	4 630

Near-surface wind speed

The ISIMIP3 method rarely outperforms the scaling method. Improvements compared with the raw data are only apparent for models which show the larger biases (MIROC6, MRI-ESM2-0). The limited improvements seen for both methods primarily pertain to the holdout method, where the first half of the data is used for calibration and the second half for validation. In fact, the observed wind speed shows a negative trend over the validation period. As none of the models capture this trend, the imprint of this trend is not incorporated into the pseudo observations used to correct the model over the validation period.

Near-surface temperature

Both corrections demonstrate comparable performance, consistently enhancing the first, second, and third quartiles of the distribution, with few exceptions. However, both methods noticeably struggle to improve the lowest values of the distribution in models that simulate a bias-low minimum value compared with observations.

Dry spell duration

As mentioned in Maraun (2016), often marginal aspects of the correction are evaluated, typically calibrated to match observations. Consequently, the performance of a bias correction might be overestimated. One should therefore evaluate aspects which have not been calibrated. For this reason, we evaluated the dry spell length distribution, an important parameter for forests. We focus on the ISIMIP3 correction, as the occurrence of dry days is not corrected with the scaling method.

The dry spell length distribution is presented in Figure 29 for two dry-day criteria: $Pr < 0.1 \text{ mm day}^{-1}$ and $Pr < 1 \text{ mm day}^{-1}$. For the sake of brevity, we show the distributions for MPI-ESM1-2-LR only, which is enough to discuss the general features. Some statistics of the dry spell length distribution are given in Table XVII. Figure 30 shows that MPI-ESM1-2-LR satisfactorily reproduces the shape of the distribution, which is also true for the other models. Most differences between the simulated and observed distributions are found for $Pr < 0.1 \text{ mm day}^{-1}$. Using this criterion, CMIP6 models tend to underestimate the number of dry spells for all spell lengths, which is a consequence of the drizzle effect. Model data

better agree with the observations when a 1 mm day⁻¹ threshold is used to detect dry sequences. Also, most of the models simulate drier single-days than observed for a 1 mm day⁻¹ threshold, while the opposite situation occurs when a 0.1 mm day⁻¹ threshold is used.

The bias-correction modifies the mean dry spell length, which is almost systematically improved whatever the criterion (see Table XVII). Improvements for the dry spell length variance are more contrasted where the added value of the ISIMIP3 correction is found for the 0.1 mm day⁻¹ criterion. Improvements in the longest dry spell length also depend on the chosen criterion. For the 0.1 mm day⁻¹ threshold, the longest dry spell length gets closer to the observations in 9 of the 11 models. For the 1 mm day⁻¹ threshold, the longest dry spell length deviates more from the observations in 5 of the 11 models. Differences between the two criteria is a direct consequence of the threshold used for adjusting the dry-day frequency (0.1 mm day⁻¹, see Table III).

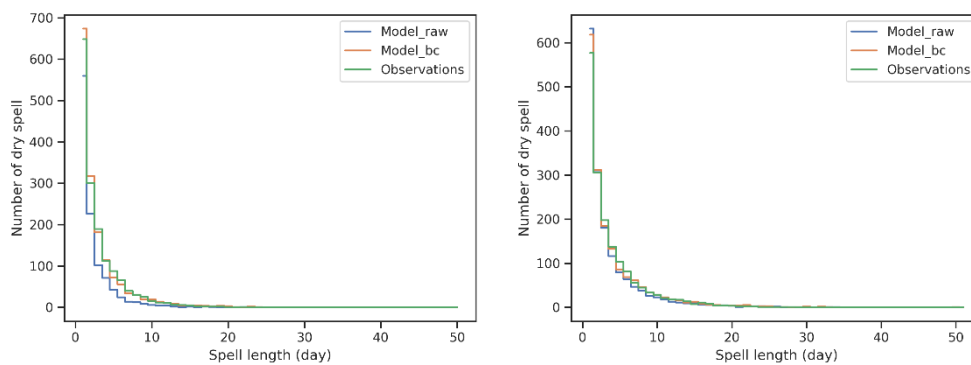


Figure 29. Dry spell length distribution in the raw model data (blue), bias-corrected (ISIMIP3 correction) model data (orange) and observations (green) over the period 1992-2021. A day is considered as dry if $Pr < 0.1 \text{ mm day}^{-1}$ (left) or $Pr < 1 \text{ mm day}^{-1}$ (right). Remember that the dry-day frequency is adjusted using the criterion $Pr < 0.1 \text{ mm day}^{-1}$. Only the site-mean distribution is presented for MPI-ESM1-2-LR

Table XVII. Dry spell length (DSL) statistics for the raw CMIP6 data, the bias-corrected (ISIMIP3 correction) model data and the observations over the validation period 1992-2021. A dry spell is defined as a set of consecutive days with daily rainfall amounts below thresholds of 1 mm day⁻¹. The upper (lower) row is for the raw (bias-corrected) model values. Only the mean distribution over the 11 sites is presented. For raw model data, the mean is computed over independent sites.

	ACCESS-CM2	ACCESS-ESM1-5	CanESM5	CMCC-ESM2	INM-CM4-8	INM-CM5-0	IPSL-CM6A-LR	MIROC6	MPI-ESM1-2-HR	MPI-ESM1-2-LR	MRI-ESM2-0	Observations
DSL mean	3.62	3.57	3.46	3.75	4.10	3.67	3.53	3.39	3.28	3.51	3.10	3.84
	3.87	3.93	3.57	3.91	3.76	3.49	3.73	3.57	3.81	3.92	3.44	
DSL standard deviation	4.01	4.29	4.04	4.07	4.67	3.85	3.74	3.40	3.41	3.99	3.06	3.98
	4.25	4.35	3.89	4.29	3.77	3.51	3.81	3.60	4.10	4.49	3.47	
Longest DSL	36	43	43	67	44	43	49	36	37	50	31	45
	38	42	39	67	32	31	49	36	47	51	31	

Climate change signals

A document was made by RMI that includes a graphical representation of the climate-change signals of the 11 CMIP6 models. In addition, for each model and each variable the signals were tabulated. This may facilitate the choice of GCM data that will be used to force the forest model. In this report, we present the climate change signals simulated by the six models that we selected (see Task 3.1). Changes are identified by comparing raw projected values to present-day values. We compute changes for three-time horizons in the 21th century. As changes are mostly important for trees during the vegetation growing season, we focus on this period in the following. The vegetation growing season includes days between the 15th of April and the 15th of November.

Figure 30 shows the diversity of model responses to climate change for the four SSP scenarios. Contrasted signals are found among the variables that we analysed.

For the near-surface temperature, all models agree on the sign of the changes. They simulate a warming irrespective of the scenario and the period investigated. Projections suggest that temperatures across Europe, Belgium in particular, will continue to increase at a higher rate than the global average as reported in IPCC (2021) (not shown). The effect of scenarios on temperature is visible from the middle of the century, when they start differentiating. It can be seen that the model uncertainty increases with lead time and also with more severe scenarios as reported in previous studies (Tabari and Willems, 2022). Changes in temperature will equally affect the growing and the vegetation dormant seasons (not shown).

The model responses for precipitation exhibit stark contrasts depending on the period of the year (i.e., growing or dormant season) and the specific scenario under investigation. Across all scenarios and future periods, models consistently indicate an increase in precipitation during the dormant vegetation period. Conversely, a trend towards decreased precipitation during the growing vegetation period emerges from the middle of the century in most models. Under the SSP5-8.5 scenario, relative changes in precipitation reach up to -20%. However, noteworthy exceptions exist, with certain models projecting an augmentation in precipitation towards the end of the century for scenarios SSP1-2.6 and SSP2-4.5 for the growing season. This underscores the necessity of incorporating multiple models in impact studies, as exemplified in REG+. To complement the analysis for precipitation, we examined modifications in the distribution of consecutive dry days for the vegetation growing season. The distribution is summarized in three categories. The first category counts the number of consecutive days reporting no precipitation ($Pr < 1$ mm) for droughts that do not exceed one week, the second the number of consecutive days with no rain for droughts lasting between one and two weeks. The third category reports consecutive dry days for droughts lasting more than two weeks. As illustrated in Figure 31, the number of consecutive dry days for droughts lasting less than one week is projected to decrease by the end of the century. This reduction is consistently simulated by all models across all scenarios, with the magnitude of the decline amplifying with forcing levels. This decline stems from a general reduction in the occurrence of droughts spanning one to seven days. Conversely, opposing trends are anticipated for droughts lasting longer than two weeks, with models predicting an increase in the number of consecutive dry days, leading to more frequent and prolonged long-term droughts. Furthermore, in this category, the severity of the scenario plays a significant role, with more severe

scenarios resulting in increased frequency and duration of droughts (not shown). Additionally, the projected number of consecutive dry days under the SSP5-8.5 scenario by the end of the century corresponds to relative changes ranging between 140% and 200% compared to the last three decades.

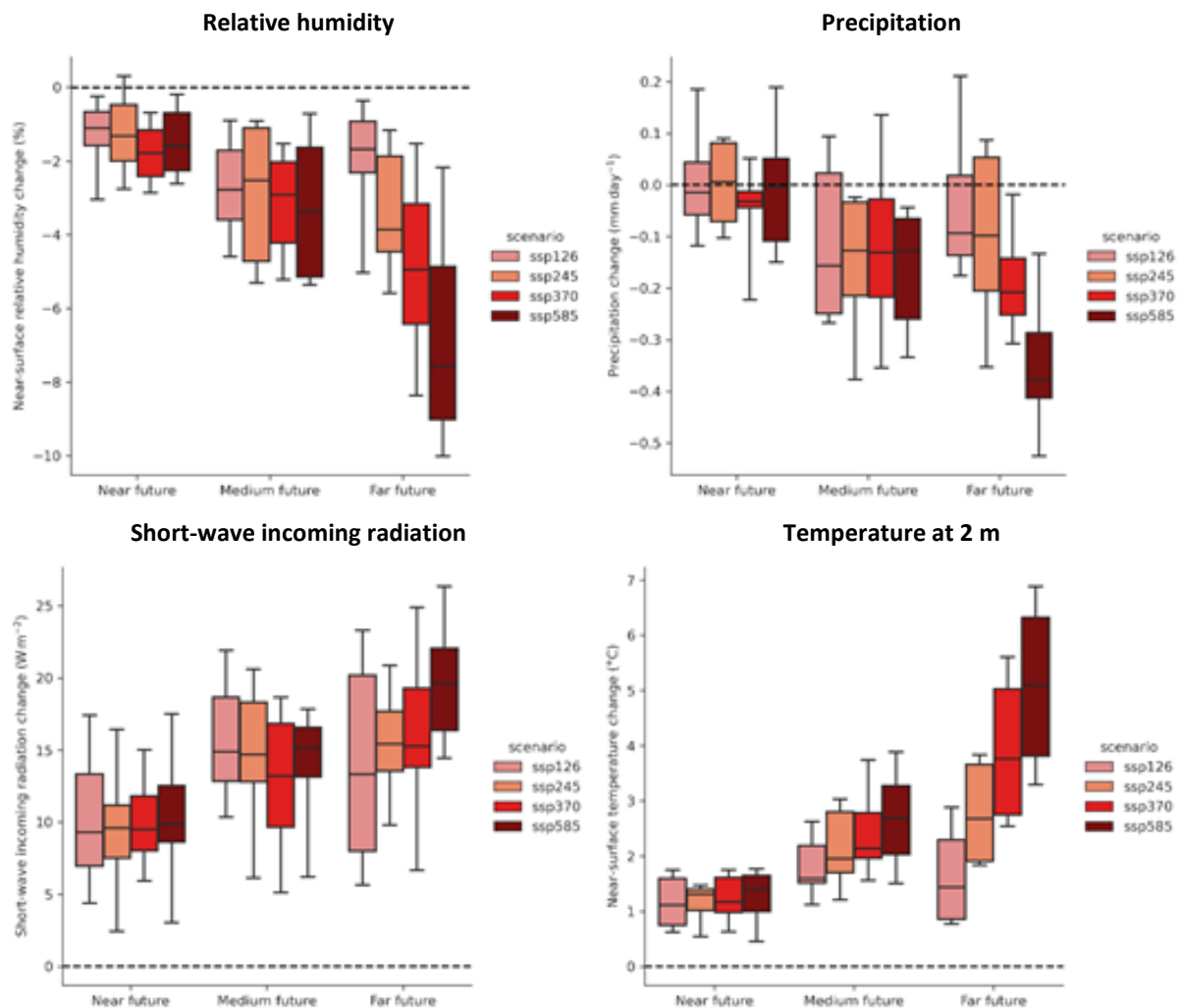


Figure 30. Boxplots representing the climate change signals (in absolute value) for the vegetation growing season in the six selected models for 4 SSP scenarios and three periods in the future. Changes are relative to 1976-2014 and are averaged over model independent forest sites. Near future: 2015-2040, medium future: 2041-2070, far future: 2071-2100. Variables shown are the near-surface relative humidity, the total precipitation, the surface downwelling shortwave radiation and the near-surface temperature

The relative humidity is projected to decrease towards the end of the century. All models agree on the sign of the changes, but they simulate responses of various amplitudes. On average over the last 30 years of the century, the relative humidity could change by 2 to 10% for scenario SSP5-8.5. This reduction is not limited to Belgium (Douville and Willett, 2023; Sherwood and Fu, 2014). It is simulated in many continental areas with the strongest changes occurring at northern mid-latitudes. Although continental drying projected by the CMIP6 models is highly model dependent, Douville and Willett (2023) showed that it is systematically simulated by models that best agree with observed historical warming and relative humidity observations. The reduction in relative humidity is expected to increase the evaporative demand, therefore amplifying the water stress for plants in periods with

little or no precipitation. This effect might be mitigated by the stomatal response of plants to an increase in CO₂ concentration (Douville *et al.*, 2020), as differences in total evapotranspiration anomalies over land and ocean areas suggest (Douville and Willett, 2023).

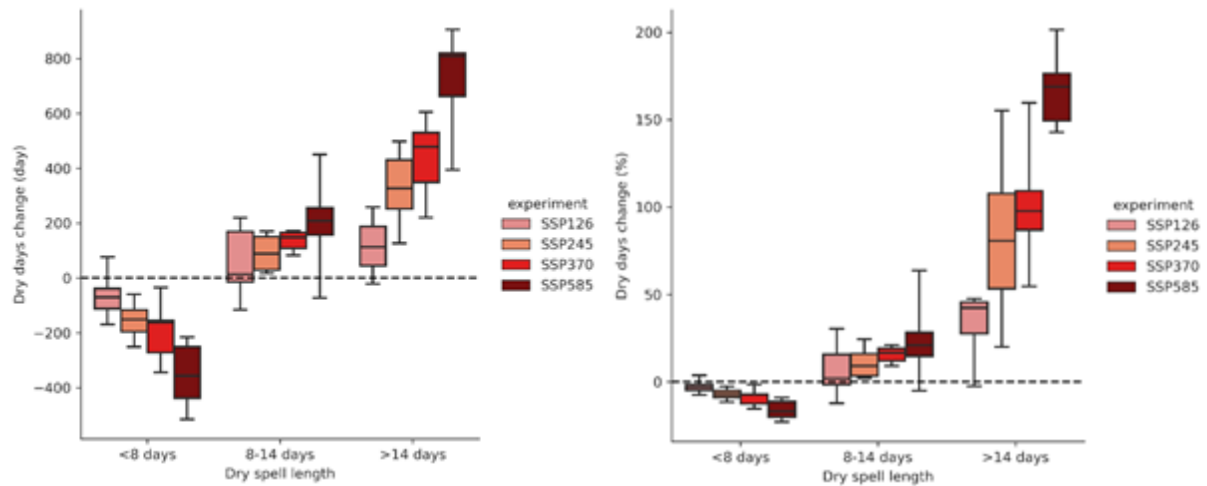


Figure 31. Boxplots representing the absolute (left) and relative (right) changes in the distribution of consecutive dry days between the end of the century (2071-2100) and the present period (1976-2014 period) for the vegetation growing season in the six selected models for 4 SSP scenarios. Changes are averaged over model independent forest sites. The distribution is limited to 3 categories counting the number of consecutive dry days for droughts shorter than one week, between one and two weeks and longer than two weeks. A day is considered as dry if the cumulated precipitation does not exceed 1 mm

Short-wave incoming radiation is projected to increase during summertime for the three-time horizons that we investigated. In winter, there is a tendency for a limited increase, but at least one model simulates a decrease for each period and scenario. The model uncertainty is found to be high compared with the scenario uncertainty, in agreement with the study of Drugé *et al.* (2021) which reported a minor influence of the scenario on the direct aerosol radiative forcing. Anthropogenic aerosols are known to induce radiative climate changes. The release of sulphate aerosols in the past decades led to an increased scattering of shortwave radiation, but also to indirect changes in the albedo of clouds, their lifetime and their precipitation ability (Bellouin *et al.*, 2020; Myhre *et al.*, 2013). Globally, the aerosol optical depth increased from pre-industrial times up to 1990, slowly decreasing afterwards due to a sulphate mass concentration decrease partially compensated by a nitrate concentration increase (Drugé *et al.*, 2021). Compared with our reference period (1976-2014), future scenarios thus provide lower concentrations in aerosols over Europe leading to a reduction of the aerosol optical depth. The increase in the shortwave incoming radiation at ground is also explained by a higher temperature of the atmosphere. Any water vapor in the air is less prone to condense into clouds (see for instance Svennevik *et al.* (2024)). An analysis of the total cloud cover percentage for the vegetation growing season reveals a negative fraction change for all the models and the scenarios (not shown) consistent with an increase in incoming shortwave radiation at the surface.

No significant changes in wind speed (calculated for the full year) over the 21st century is expected according to current models and scenarios (Figure 32). Relative changes are generally constrained within a 5% range and there remains ambiguity regarding the sign of these changes. The SSP1-2.6

scenario stands out as models for this scenario consistently predict a systematic decrease in wind speed towards the latter half of the century, accompanied by an unexplained negative peak around mid-century. For the last 30 years of the century, all scenarios but SSP2-4.5 predict a limited reduction of wind speed, which potentially less damage to trees.

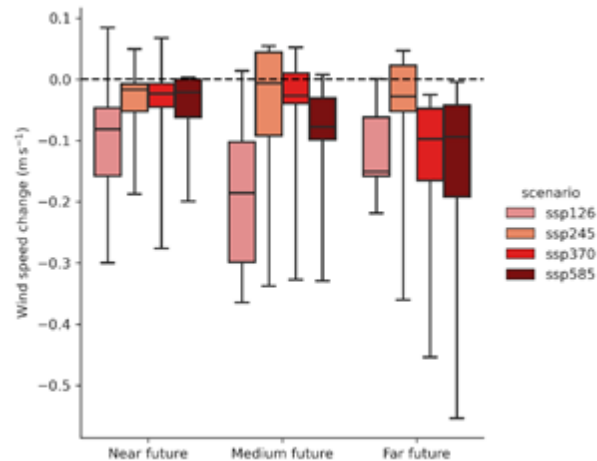


Figure 32. Boxplots representing the climate change signals (in absolute value) for wind speed in the six selected models for 4 SSP scenarios and three periods in the future. Changes are relative to 1976-2014 and are averaged over model independent forest sites. Near future: 2015-2040, medium future: 2041-2070, far future: 2071-2100

4.4 Simulation experiment results

4.4.1. Effects of silvicultural route and ungulate browsing

To synthesize our results while retaining as much information as possible, we aggregated a wide range of indicators into five categories: productivity, profitability, sustainability, carbon, and resilience. For each category, a Principal Component Analysis (PCA) was performed, and the first principal component (PC1) was used as a synthetic score (SI3). The productivity category includes variables related to tree growth, stand dynamics, and biomass production, such as basal area, gross primary production (GPP), and net primary production (NPP). Profitability indicators measure the short-term economic performance of the forest stands through metrics like net present value (NPV) and annual revenue. Sustainability focuses on long-term forest value and volume. Carbon indicators quantify carbon storage and emissions in different forest components, including above- and below-ground biomass, deadwood, and wood products. Finally, resilience indicators encompass forest structural and species diversity, species distribution, and responses to environmental stressors such as drought and wind damage. These indicators provide a comprehensive assessment of forest dynamics and performance under different management and environmental conditions.

To assess the effects of silvicultural and environmental factors on each of the five scores (productivity, profitability, sustainability, carbon, and resilience), an analysis of variance (ANOVA) was performed, with the score as the response variable. The model included interactions between the silvicultural scenario, the climate change scenario (SSP), and the ungulate pressure scenario. A stepwise model

selection using backward elimination was applied to identify the most parsimonious model, retaining only significant predictors. Post hoc pairwise comparisons were conducted using estimated marginal means (EMMs) to evaluate the effects of different factors on each score. The EMMs were extracted from the full model, including all interactions, rather than the most parsimonious model. This approach was chosen to illustrate the effects of all factors, not just those identified as significant in the model selection process.

The productivity score varied significantly across silvicultural scenarios ($p < 0.05$), ungulate densities ($p < 0.001$), and SSP ($p < 0.001$). Additionally, there was a significant interaction between silvicultural scenarios and ungulate densities ($p < 0.001$) (Table XVIII). Productivity was greater with OAK, followed by DIV then BAU. It increased with the severity of climate change (from SSP1 to SSP3). Productivity generally decreased with ungulate density, but this effect depended on the silvicultural scenario. The impact of ungulate density was the lowest with BAU, while in OAK and DIV, high ungulate pressure drastically reduced productivity (Figure 33 and Figure 34).

The profitability score varied significantly with silvicultural scenarios ($p < 0.01$) and SSP ($p < 0.05$) (Table XVIII). Profitability was higher with DIV and BAU than with OAK. It increased with SSP levels (Figure 33 and Figure 34).

The sustainability score varied significantly across silvicultural scenarios ($p < 0.001$), ungulate densities ($p < 0.001$), and SSP ($p < 0.001$). There was also a significant interaction between silvicultural scenarios and ungulate densities ($p < 0.001$) (Table XVIII). In contrast to the short-term profitability score, the long-term sustainability score was clearly reduced with high ungulate pressure. Sustainability was greater with BAU and OAK than with DIV. As with productivity, sustainability was least affected by ungulate density under the BAU scenario. In contrast, sustainability declined more sharply under the OAK and DIV scenarios, particularly at high ungulate pressure (Figure 33 and Figure 34).

Similarly to the sustainability score, the carbon score varied significantly across silvicultural scenarios ($p < 0.001$), ungulate densities ($p < 0.001$), and SSP ($p < 0.001$). Additionally, there was also a significant interaction between silvicultural scenarios and ungulate densities ($p < 0.001$) (Table XVIII). Carbon storage was highest with BAU, followed by OAK and then DIV. It increased with SSP levels but decreased with higher ungulate pressure. Like the productivity and sustainability scores, the impact of ungulate density on carbon score was lowest under the BAU scenario. In contrast, high ungulate pressure drastically reduced the carbon score under the OAK and DIV scenarios (Figure 33 and Figure 34).

The resilience score varied significantly across silvicultural scenarios ($p < 0.001$), ungulate densities ($p < 0.001$), and there was a significant interaction between silvicultural scenarios and ungulate densities ($p < 0.001$) (Table XVIII). As expected, resilience was highest under DIV, far surpassing both OAK and BAU, with OAK still outperforming BAU. It decreased with higher ungulate pressure, but the effect was weakest with BAU. In DIV and OAK, high ungulate pressure drastically reduced resilience (Figure 33 and Figure 34).

Overall, BAU maximized economic and carbon benefits, and OAK maximized productivity and long-term economic benefits, while DIV prioritized resilience. High ungulate pressure generally worsened all indicators under OAK and DIV (Figure 34).

Table XVIII. Results of the analyses of variance (ANOVA) for each score: productivity, profitability, sustainability, carbon, and resilience

Model	Factor	Df	Sum Sq	Mean Sq	F value	Pr(>F)	
Productivity	Silvicultural Scenario	2.0	26.1	13.0	4.0	0.020	*
	SSP	2.0	123.1	61.5	18.7	<0.001	***
	Ungulate Densities	3.0	311.2	103.7	31.6	<0.001	***
	Silvicultural Scenario x Ungulate Densities	6.0	254.0	42.3	12.9	<0.001	***
	Residuals	202.0	663.6	3.3			
Profitability	Silvicultural Scenario	2.0	54.5	27.3	6.7	0.001	**
	SSP	2.0	28.6	14.3	3.5	0.031	*
	Residuals	211.0	855.2	4.1			
Sustainability	Silvicultural Scenario	2.0	77.6	38.8	21.6	<0.001	***
	SSP	2.0	57.5	28.8	16.0	<0.001	***
	Ungulate Densities	3.0	145.3	48.4	26.9	<0.001	***
	Silvicultural Scenario x Ungulate Densities	6.0	82.2	13.7	7.6	<0.001	***
	Residuals	202.0	363.3	1.8			
Carbon	Silvicultural Scenario	2.0	132.3	66.1	18.8	<0.001	***
	SSP	2.0	106.8	53.4	15.2	<0.001	***
	Ungulate Densities	3.0	191.2	63.7	18.1	<0.001	***
	Silvicultural Scenario x Ungulate Densities	6.0	95.3	15.9	4.5	<0.001	***
	Residuals	202.0	711.1	3.5			
Resilience	Silvicultural Scenario	2.0	252.6	126.3	47.7	<0.001	***
	Ungulate Densities	3.0	323.0	107.7	40.7	<0.001	***
	Silvicultural Scenario x Ungulate Densities	6.0	94.6	15.8	6.0	<0.001	***
	Residuals	204.0	539.9	2.6			

Degrees of freedom (Df), Sum of square (Sum sq), Mean square (mean sq), F-value and p-value for each factor (silvicultural scenario, ssp and ungulate density), for each combination of factors and for residuals. *** indicates a p-value less than 0.001, ** corresponds to a p-value between 0.001 and 0.01, * represents a p-value between 0.01 and 0.05

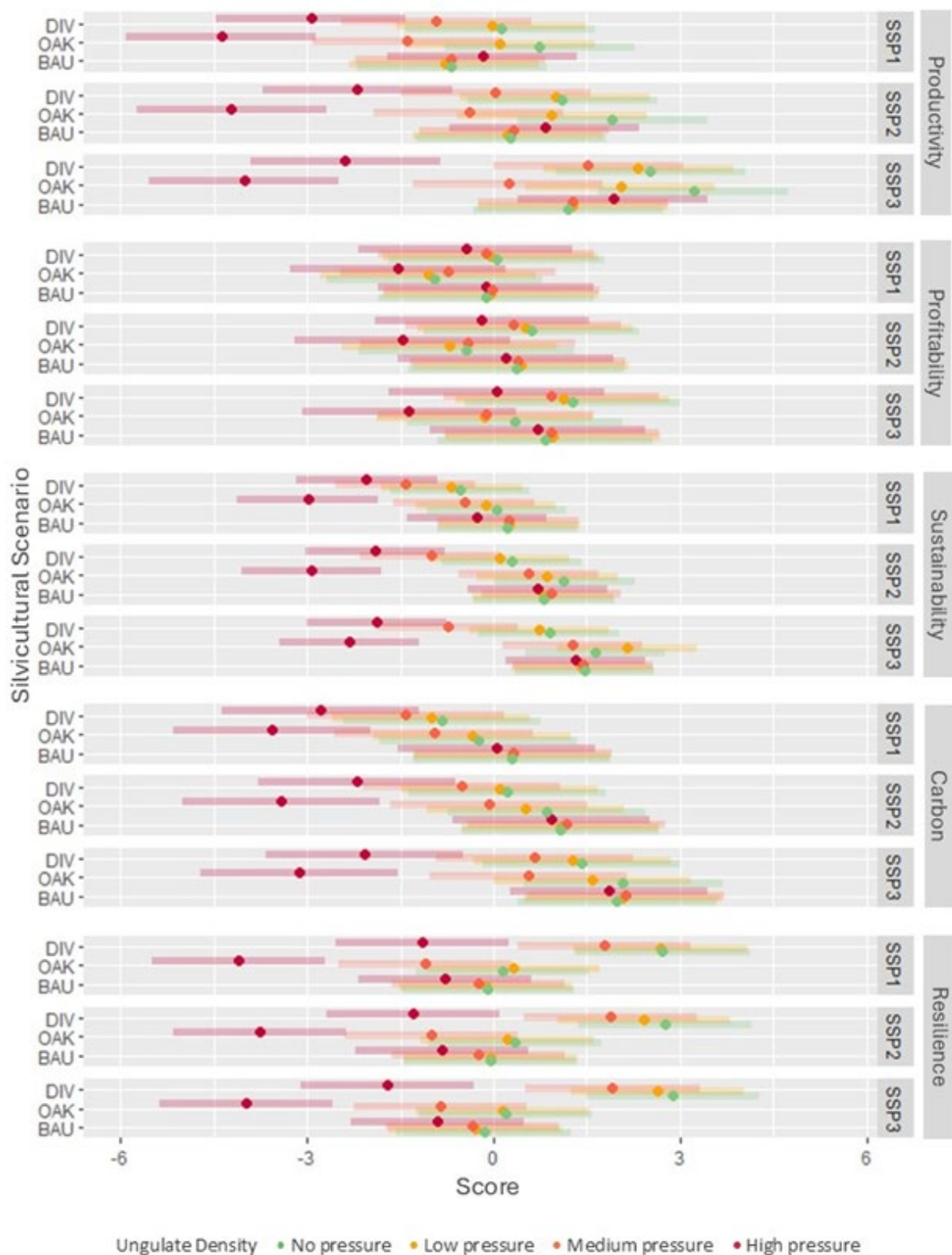


Figure 33. Estimated marginal means and 95% confidence intervals for the five simulation scores relating to productivity, profitability, sustainability, carbon and resilience. Simulations were run for all combinations of silvicultural scenario (DIV, OAK, BAU), climate scenario (SSP1, SSP2, SSP3) and ungulate density (no pressure, low pressure, medium pressure, high pressure)

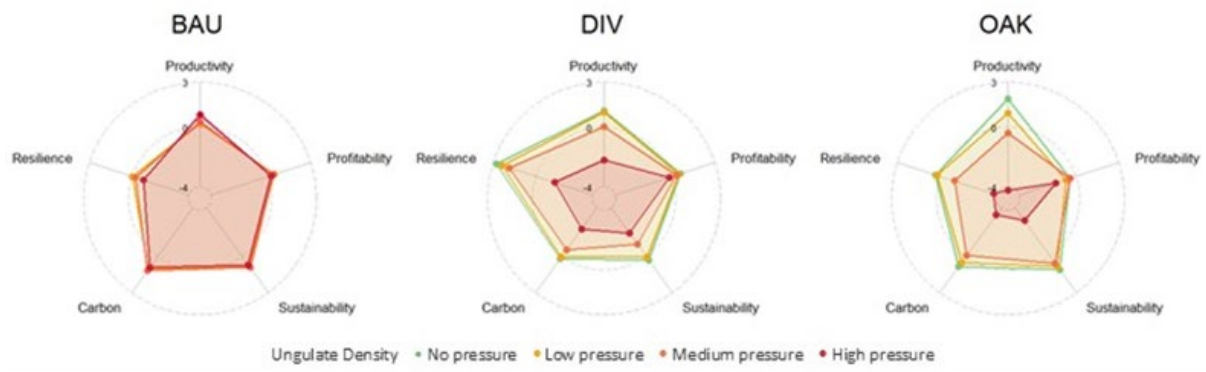


Figure 34. Estimated marginal means for the five scores (productivity, profitability, sustainability, carbon and resilience), for each silvicultural scenario (DIV, OAK, BAU), only for SSP2 and with four ungulate densities (no pressure, low pressure, medium pressure, high pressure)

4.4.2. Climate change impacts and uncertainties

The indicators provided by the simulations were grouped by type as follows (see Table I for a description of indicator computation):

- carbon cycle indicators: average and variation of stable and active carbon stocks (StableC, ActiveC), average and variation of carbon stock in living biomass (LivingBiom), average and variation of carbon stock in products in use (ProdInUse), average and variation of carbon stock in litter (LitterC), total fossil fuel carbon emissions (FossilFuelC tot), total material and energy substitution (Substitution tot), carbon balance (Carbon balance, determined from the preceding components), average carbon stock (Carbon stock, computed as the sum of StableC avg, ActiveC avg, LivBiom avg, LitterC avg and ProdInUse avg), gross primary production (GPP);
- water balance indicator: average rainfall (Rainfall), total, tree and seedling average transpiration (Transpi), total, tree and seedling average transpiration deficit (DefTranspi), average deep drainage (DeepDrain), water use efficiency (WUE, defined as the ratio between GPP and transpiration), net water balance determined from the preceding fluxes (Water balance);
- productivity indicators: seedling, tree and total gross and net primary production (GPP, NPP), average harvested volume (Vol harv), average basal area and volume production (Vol prod, G prod);
- profitability indicators: total net present value (NPV), net present value of trees (NPV trees), calculated internal rate of return (IRR calc), initial, final, average and variation of stand market value (SMV), average harvested volume (Vol harv), average income (Income), average profit (Profit);
- diversity indicators: average Simpson index (Simpson), average Shannon index (Shannon), average score based on dendro microhabitats (DMH), average species richness (Species richness), average aggregation index (Aggregation), average mixture index (Mixture), average differentiation indexes for trunk circumference at breast height and for total height (DiffC130, DiffHtot);

- resilience indicators: average number of recruited trees (NhaRecr), average percentage of undamaged trees following storms (WindUndam perc) and average percentage of dead trees (Dead perc).

Figure 35 presents biplots for the first two components of the PCAs carried out on each group of indicators. The first component generally explained more than 50% of the variance in the data, except for water balance indicators where it accounted for 42% of the variance. In most cases, a limited number of indicators showed dominant contributions to the first component and one of them was selected as representative of the corresponding group and used for the subsequent analyses. Therefore, the indicators chosen for carbon cycle, water balance, productivity, profitability, diversity and are GPP, total transpiration, volume production, profit and the Simpson index, respectively. The exception is resilience, for which none of the three considered indicators showed a dominant contribution to the first ACP component, and the interpretation of this component based on its correlations with the indicators was not straightforward. As a result, in this latter case, each indicator was considered individually below.

The following mixed model was fitted for each indicator selected from the ACPs:

$$\begin{aligned} Indicator_{avg} \sim & Silvi + Climate + CO_2 + Silvi \times Climate + Climate \times CO_2 + Silvi \times CO_2 \\ & + Silvi \times Climate \times CO_2 + \alpha + \beta \times Silvi + \beta \times Climate + \beta \times CO_2 + \varepsilon \quad (4.15) \end{aligned}$$

in which the silvicultural scenario (*Silvi*), the climate scenario (*Climate*), the modality (i.e., variable or constant) of atmospheric CO₂ temporal evolution (*CO₂*) were set as fixed effects, considering all interaction combinations among them. To reduce the number of model parameters while taking their effects into account, the site (α) and the climate model (β) were included as random terms. The site was considered as a random factor, while the climate model was defined as random coefficients to account for its possible interactions with the fixed effects. *Indicator_{avg}* is the average indicator value, averaged either over the whole simulation period or over sub-periods.

Figure 36 shows, for each indicator, the comparison of mean values over the 120-year simulation period between the silvicultural and climate scenarios and for the two CO₂ modalities. The significance of the differences between means was tested using contrasts based on the statistical model defined in Equation 4.15. Contrasts were performed separately for the CO₂ modalities and their results are presented by letters at the top of each graph, with common letters indicating non-significant differences among compared means (uppercase and lowercase letters refer to variable and constant CO₂, respectively).

When considering a variable CO₂ concentration, the average yearly GPP increases significantly as the radiative forcing associated with the climate scenario increases. This is due to the well-documented CO₂ fertilization effect, corresponding to an increased rate of photosynthesis with elevated levels of atmospheric CO₂. However, it is important to note that the effect of CO₂ fertilization might be overestimated in these simulations as they did not account for potential nutrient limitations that could have constrained the GPP increase. On the other hand, if the CO₂ concentration is kept constant, GPP tends to decrease with increasing radiative forcing in future climate projection scenarios. Yet, significant differences only appear between the more extreme scenarios (i.e., SSP126 and SSP585) for

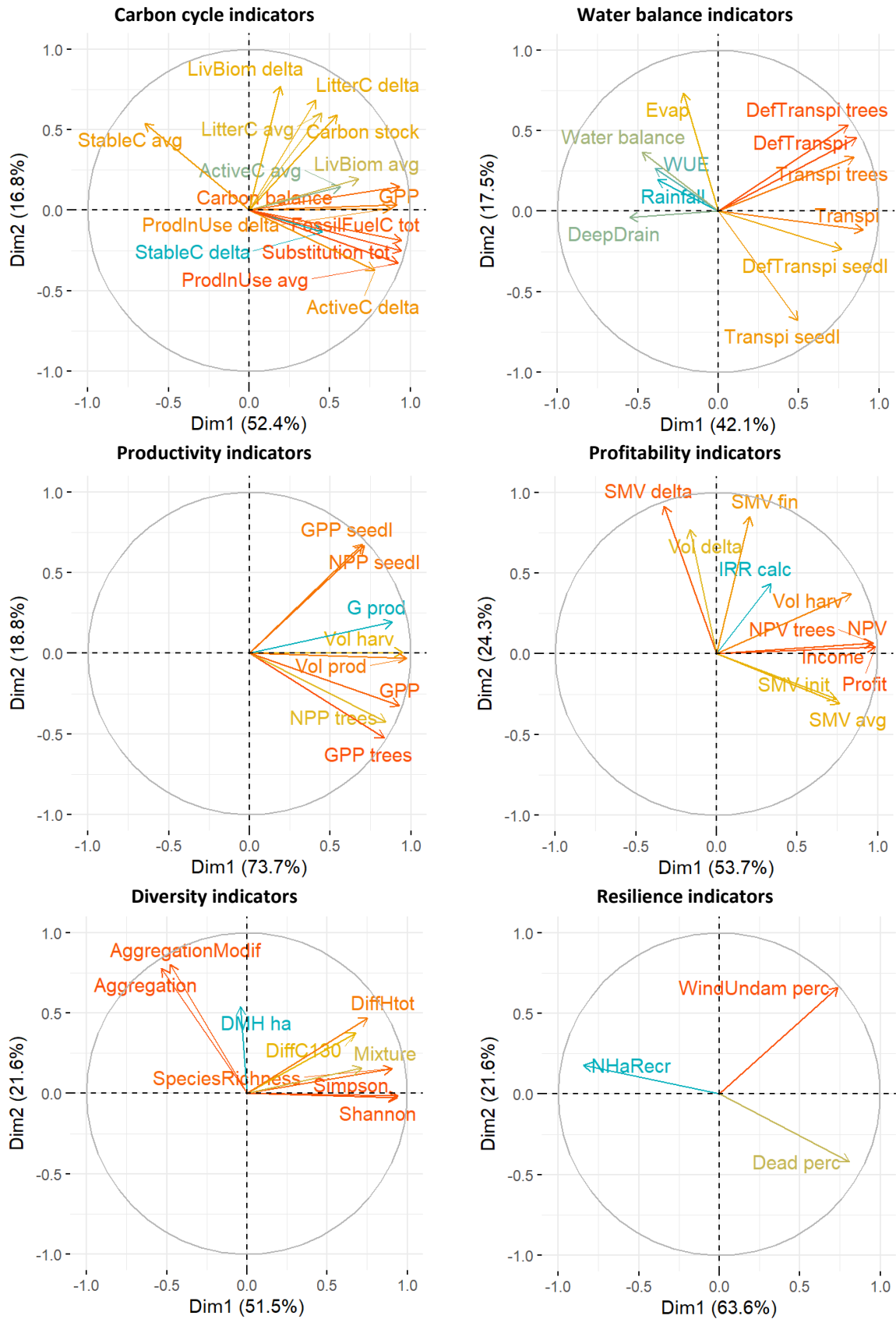


Figure 35. Biplots of the principal component analyses performed on indicators from the simulation experiment investigating the impacts of climate change

a given silvicultural route. These results in the absence of CO₂ variation would arise from an earlier stomatal closure triggered by an increase in water stress due to the rise in mean temperature accompanying the increase in radiative forcing, thereby reducing assimilation and GPP. Compared to the historical scenario, GPP under constant CO₂ is significantly higher for SSP126 and SSP245 for all silvicultural routes, and for SSP370 for the Diversity route. Regardless of the climate scenario and the CO₂ modality, the ranking of the silvicultural routes in terms of average GPP is as follows: BAU > OAK > DIV. However, differences between BAU and OAK are only significant for SSP370 and SSP585 under constant CO₂, while differences between OAK and DIV are significant in all cases except for SSP585 under variable CO₂.

For variable CO₂ concentration, average yearly transpiration decreases with increasing forcing of the SSP climate scenarios, while differences are not significant between SSP370 and SSP585. This trend, which is the opposite of GPP, indicates lower water consumption per unit of carbon assimilated, reflecting greater water use efficiency as CO₂ atmospheric concentration increases. Under constant CO₂, transpiration shows similar levels for all SSP scenarios, with no significant difference, and is also comparable to that of SSP126 under variable CO₂, while values are significantly higher than those for historical climate. The ranking of silvicultural routes according to transpiration is the same as for GPP (i.e., BAU > OAK > DIV), with significant differences only observed between BAU and DIV for the historical and SSP126 scenarios for both CO₂ modalities, and between BAU and OAK for SSP245, SSP370 and SSP585 under variable CO₂.

As observed for GPP, the average volume production increases significantly with the severity of the climate scenario under variable CO₂ concentration, while it is only slightly affected by the climate scenario under constant CO₂ concentration. Again, this difference between the two CO₂ modalities is due to the CO₂ fertilization effect, and the caveats mentioned above for GPP also apply here as the simulations did not take into account nutrient limitations. In contrast to GPP, volume production for both CO₂ modalities is in most cases significantly higher for OAK and DIV than for BAU, and the differences between the two former silvicultural routes are systematically not significant, although slightly higher values are generally found for DIV compared to OAK.

When variable CO₂ concentration is considered, the average yearly profit also increases significantly as the radiative forcing of the climate scenario increases. This is related to the stimulation of productivity through the fertilization effect of CO₂ which has a direct impact on profit by increasing the volume of harvested wood and, as a result, the income from timber sales. However, as mentioned above for GPP and volume production, this fertilizing effect of CO₂ could be limited by nutritional constraints. In the case of constant CO₂, non-significant differences in profit are observed between the climate scenarios for a given silvicultural route and, similarly as for GPP and volume production, profit even tend to decrease slightly as radiative forcing increases. Comparing the silvicultural routes for given climate scenario and CO₂ modality, the lowest and highest average profit values are systematically observed for the OAK and for the DIV routes respectively, with the BAU route showing intermediate profit levels. Nevertheless, differences between BAU and DIV are not significant for all climate scenarios when CO₂ is considered as constant. For variable CO₂, the amplitude of the difference in average profit between BAU and OAK decreases with increasing radiative forcing and becomes

insignificant for the SSP370 and SSP585 scenarios. This pattern of differences among silvicultural routes differs from that observed for GPP and volume production. Indeed, beyond the harvested volume, the profit is also a function of timber prices. These prices depend on the species and dimensions of the harvested trees, which are modulated by the silvicultural treatment.

The Simpson index, which increases with increasing species diversity, systematically presents the lowest and highest average values for the BAU and DIV silvicultural routes, respectively, with intermediate values for the OAK route. For a fixed silvicultural route, differences between climate scenarios and CO₂ modalities are always non-significant, although the average index value tends to decrease slightly with increasing radiative forcing, more particularly when variable CO₂ is considered.

The climate scenario and the CO₂ modality have a limited impact on the percentage of basal area of trees that remained undamaged during storms. The largest differences for this indicator are observed between BAU and the other two silvicultural routes, with average values close to 94% for the former route against around 90% for the latter ones. Furthermore, the OAK route presents a wider range of values, with percentages of undamaged trees down to 65%.

For the number of recruited trees, the major differences occur among silvicultural routes with the lowest and highest mean values systematically observed for the BAU and the DIV routes, respectively. In addition, for these two routes, recruitment tends to increase with increasing radiative forcing (i.e., increasing CO₂ concentration) under variable CO₂ while it remains stable under constant CO₂. In contrast, for OAK, the indicator average value is not significantly affected whatever the climate scenario and the CO₂ modality.

The percentage of dead trees, expressed on a tree number basis, is always significantly higher for the BAU treatment compared with the two others silvicultural routes which generally show no significant differences, except for SSP585 under variable CO₂ where the DIV route presents a significantly higher average mortality percentage than the OAK route. Under constant atmospheric CO₂ concentration, the mortality percentage remains stable among climate scenarios for a given silvicultural route. In contrast, under variable CO₂, mortality increases significantly with increasing radiative forcing of the climate scenario. These results suggest an increase in tree mortality due to a more pronounced concurrence associated with stimulated growth under the effect of CO₂ fertilization. The extreme values observed for most modalities pertain to the site of Chimay which, for unclear reason, presents much higher mortality percentages but with variations similar to those of the other study cases. When expressed in terms basal of area, the pattern differs from that based on tree number. In particular, for given silvicultural route, average values remain more stable among climate scenarios under variable CO₂, although the ranking of silvicultural routes according to average values is respected. It is also important to note that the mortality percentage is consistently low, with all average values lower than 0.5% of the basal area and some values around 1% in the worst cases.

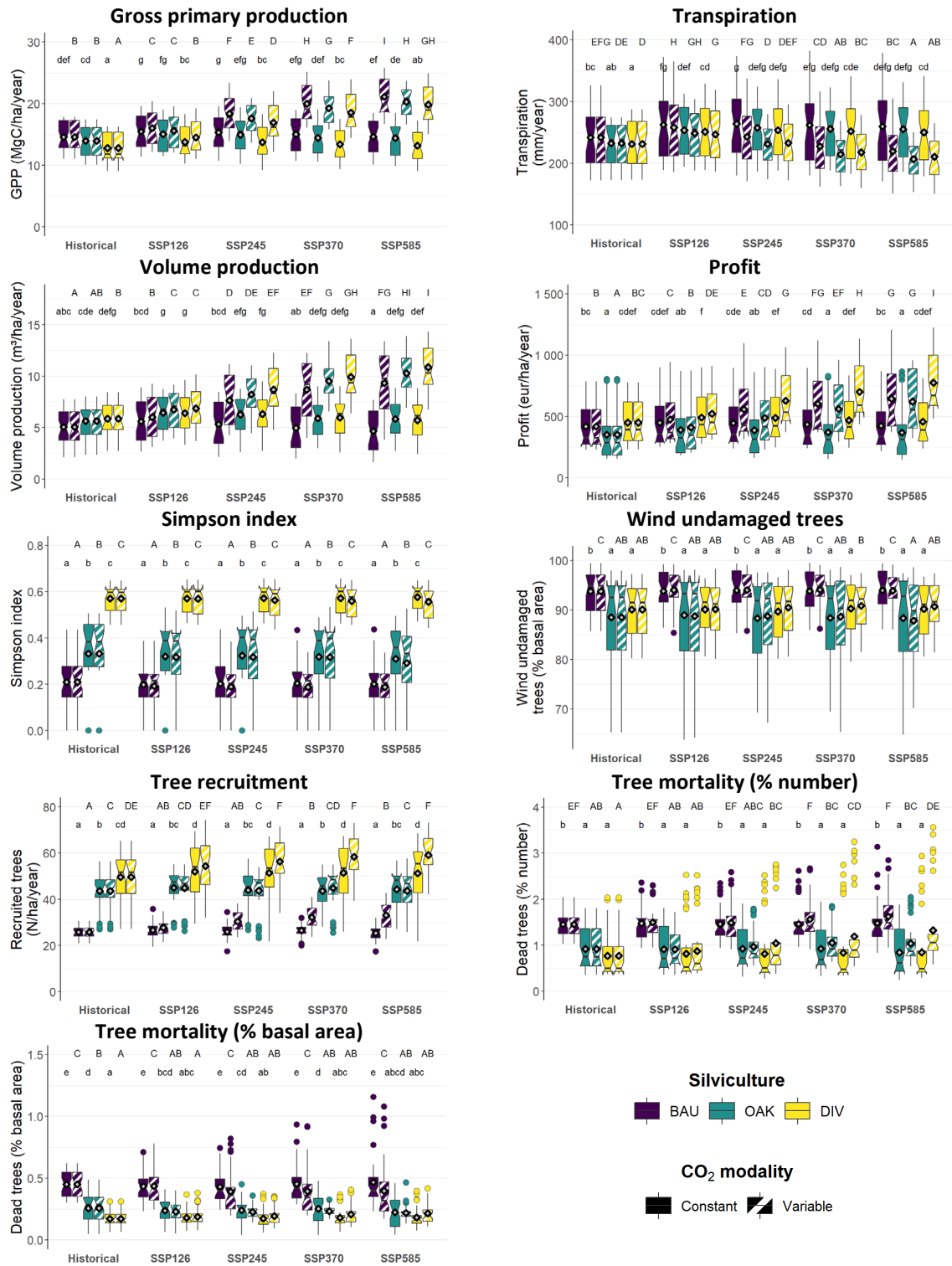


Figure 36. Comparison of the indicator values from the simulation experiment investigating the impacts of climate change among the investigated silvicultural and climate scenarios and the CO₂ modalities. Each individual point corresponds to the average value of the indicator computed over the 120 years of a Site x Silviculture x Climate x Climate model x CO₂ modality simulation (i.e., 1 080 averages values for each indicator). For each boxplot, the notch represents the median value while the lower and upper ends correspond to the first (Q1) and the third (Q3) quartiles, respectively, which delimit the interquartile range (IQR); the extremities of the whiskers correspond to the minimum and maximum values determined as Q1 - 1.5×IQR and as Q3 + 1.5×IQR, respectively; the points represented below and beyond these minimum and maximum values are considered as extreme values; the diamond symbol represents the general average value

The radar charts shown in Figure 37 provide a general overview of the average values of the studied indicators for each silvicultural route and of their variations as a function of the climate scenario and of the CO₂ modality. Comparing silvicultural routes, DIV presents in each case higher values than the two other routes for volume production, profit, tree recruitment and, as expected, the Simpson diversity index, while it is always among the lowest values for tree mortality, GPP and transpiration. BAU maximizes transpiration, GPP, wind resistance and tree mortality while it presents the lowest values for the volume production and the Simpson index. OAK systematically minimizes profit and wind resistance, and presents values intermediate to BAU and DIV for the other indicators. These results for silvicultural route comparison are in agreement with those reported above for the simulation experiment investigating the effects of silviculture and ungulate browsing. Given the influence of atmospheric CO₂ concentration on productivity and stomatal regulation, the effects of climate change dominate the silvicultural route effects for GPP, profit and transpiration when variable atmospheric CO₂ concentration is considered, with pronounced increases of the values of first two indicators with increasing radiative forcing (i.e., CO₂ concentration) and inversely for the transpiration. On the other hand, climate change has only limited impacts on the other indicators.

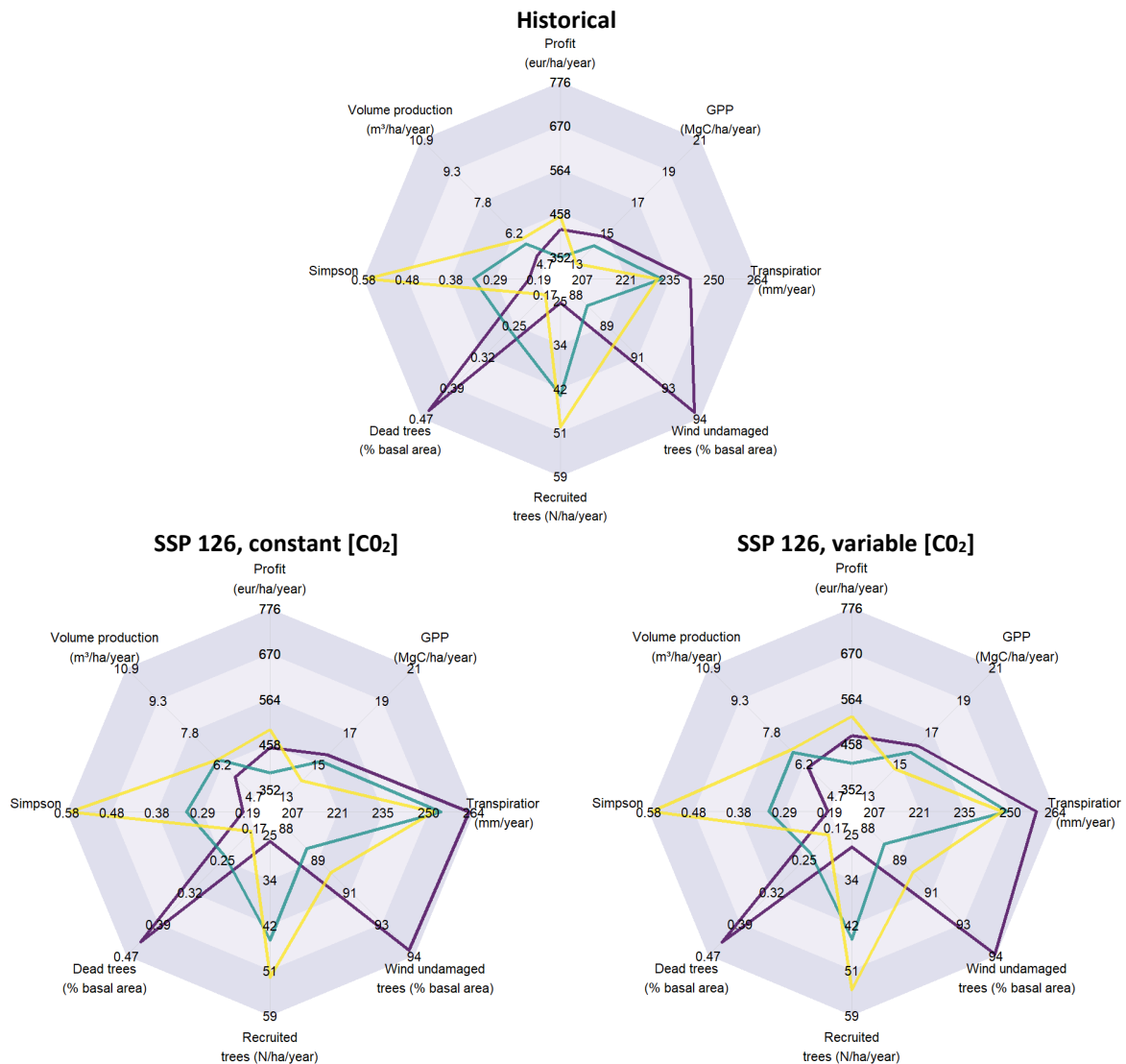


Figure 37. Average indicator values for the three silvicultural routes (BAU, OAK, DIV), four climate scenarios (Historical, SSP126, SSP245, SSP585) and considering constant or variable atmospheric CO₂ concentration

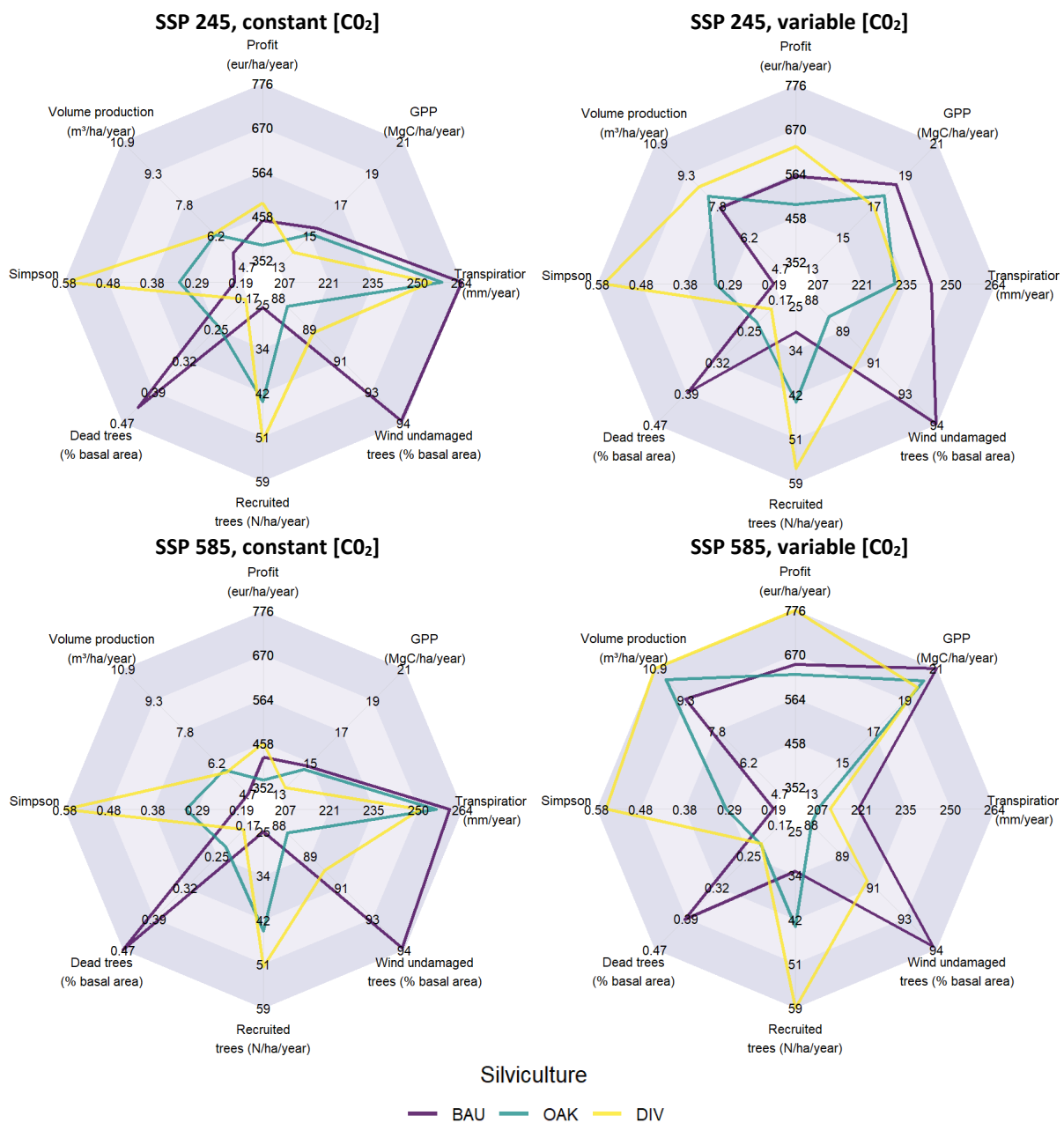


Figure 38. Average indicator values for the three silvicultural routes (BAU, OAK, DIV), four climate scenarios (Historical, SSP126, SSP245, SSP585) and considering constant or variable atmospheric CO₂ concentration (continued)

Figure 38 shows the distribution of indicator variance across the studied factors, derived from the statistical model outlined in Equation 4.15. The distribution is presented for the entire 120-year simulation period, as well as for three 40-year sub-periods (2016-2055, 2056-2095, 2096-2135). Over the full period, the site effect explained over 70% of the variance for transpiration and profit, 67% for wind undamaged percentage, 50% for GPP and volume production, around 30% for the Simpson index and tree mortality and 12% for tree recruitment. For the latter three indicators, the silvicultural route was the dominant factor explaining the variability, accounting for 62% for the Simpson index variance and around 50% for both tree recruitment and mortality. The effects of CO₂ modality (i.e., constant vs.

variable atmospheric concentration) and the climate scenario (SSP) showed noticeable contributions to variability for volume production, GPP, transpiration and profit, with these two factors explaining around 3% and 7% of the variance for the two latter indicators, 7% and 10% for GPP, and up to 9% and 24% for volume production. The climate model explained 5% of the variance for transpiration and around 3% and 2% for GPP and volume production respectively, while contributing to less than 1% for the other indicators. Finally, the 'residual' contribution, corresponding to the part of the variance unexplained by the preceding factors, ranged between 6% for profit and 35% for tree recruitment. This residual effect is partly due to stochasticity introduced in the HETEROFOR model to account for uncertainties in some of the modelled processes and for the randomness involved in silvicultural operations (e.g., selection of the trees to be harvested during logging). Additionally, a part of residual variance would also arise from the fact that the stands of the case studies used as the initial stages for the simulations presented contrasting characteristics (see Table IV) and, as a result, the stands in the simulations do not evolve in phase among the different sites for a given combination of silvicultural route x climate scenario x climate model x CO₂ modality, thus introducing variability in the indicators not explained by the studied factors.

Furthermore, variance distribution among factors showed variation across the three 40-year sub-periods. The pattern and magnitude of these variations depended on the indicator. For GPP and transpiration, the contributions of the climate scenario and the CO₂ modality increased from the first to the last sub-periods. These results reflect growing divergences in climate scenarios over time and their impact on these two processes, especially when variable CO₂ concentration was considered given its effect on growth and water use efficiency as discussed above. The residual variance also increased over time, along with the contributions of the climate scenario and CO₂ modality, compensating for the decline in the site effect contribution. Nevertheless, the site effect generally remained the dominant contributor to the variance for both indicators. The contributions of the climate model and the silvicultural route showed little variation across sub-periods, remaining similar to values observed for the complete period. As a corollary to the observations for GPP, the contributions of the climate scenario and CO₂ modality to profit variance also increased with time, especially for the final sub-period. While the site remained the main contributor for profit, its variance contribution was higher in the second sub-period compared to the first and last. For the Simpson index, the contribution of the silvicultural route to the variance strongly increased over time, accompanied by a decrease in the site contribution. Similar trends were observed for wind resistance, although the increase in silvicultural route contribution was less pronounced due to a larger part of residual variance in the final two sub-periods. Conversely, for tree recruitment, the contribution of silviculture decreased over time, while the site effect increased. The residual component consistently accounted for more than 40% of the variance for this indicator. Finally, for tree mortality, the contribution of the silvicultural route increased from the first to the second sub-periods and then stabilized, while the site contribution slightly decreased over time.

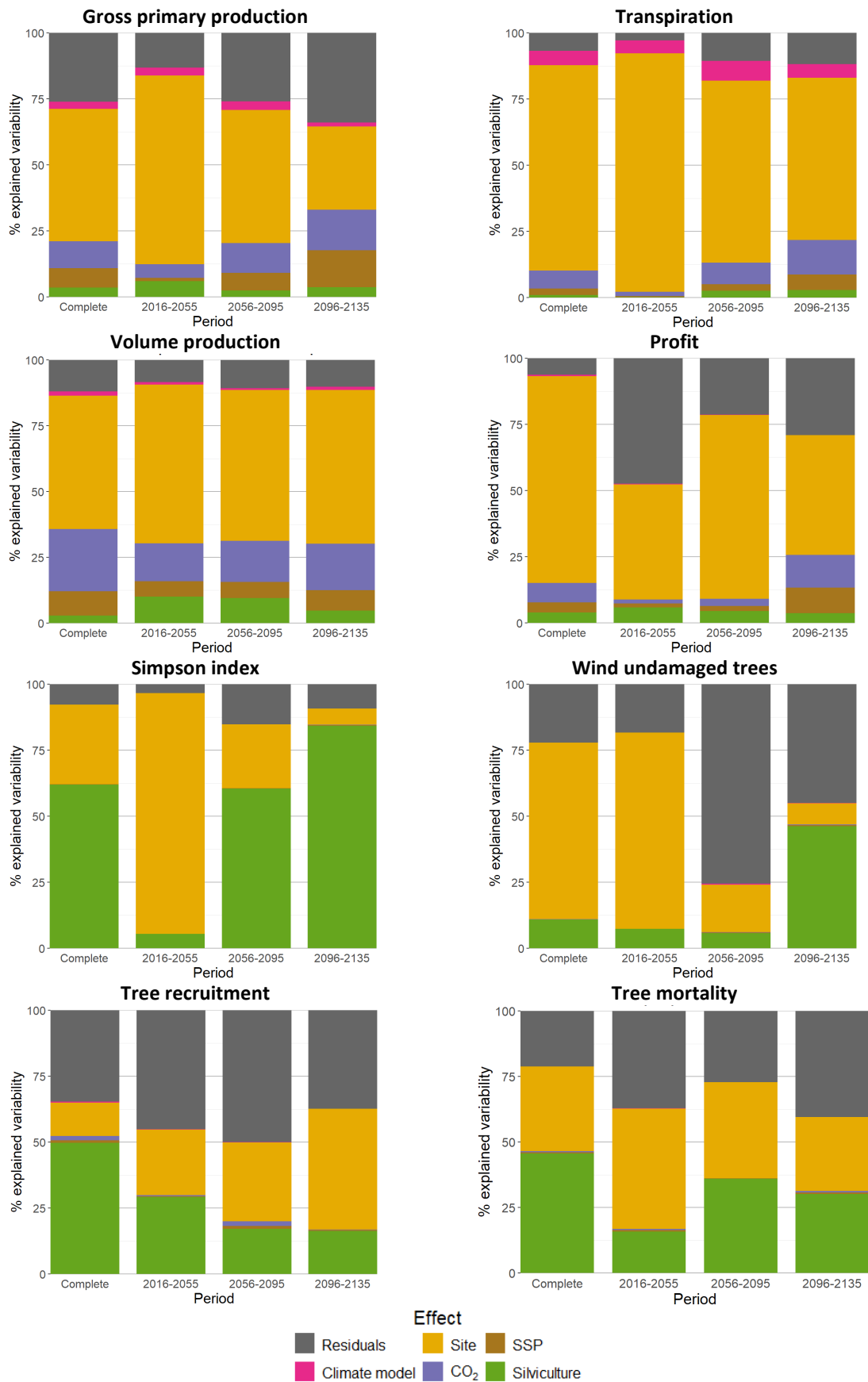


Figure 39. Decomposition of the indicator variance among the investigated factors, comparing the full 120-year simulation period and three 40-year sub-periods

To further examine the climate change impact, the variation in the value of each indicator resulting from climate was quantified as follows:

$$\Delta relInd_{Silv.SSP.CM.CO2} = \frac{Ind_{Silv.SSP.CM.CO2,[2070-2100]} - Ind_{Silv.Hist.CM.CO2,[2070-2100]}}{Indicator_{Silv.Hist.CM.CO2,[2070-2100]}} \times 100 \quad (4.16)$$

where $Ind_{Silv.SSP.CM.CO2,[2070-2100]}$ is the mean yearly value for indicator Ind over the 2070-2100 period for simulation with silvicultural route, $Silv$, climate scenario, SSP , climate model, CM , and CO_2 modality, CO_2 , and $Ind_{Silv.Hist.CM.CO2,[2070-2100]}$ is the corresponding mean indicator value for the simulation performed using the historical climate scenario.

This relative variation of index value was represented in Figure 39 as a function of the corresponding change in mean air temperature ($Temp$) during the growing season (set as extending from 15/04 to 15/09):

$$\Delta Temp_{SSP.CM.CO2,[2070-2100]} = Temp_{SSP.CM.CO2,[2070-2100]} - Temp_{Hist.CM.CO2,[2070-2100]} \quad (4.17)$$

The relationship between indicator relative variation and temperature change was particularly marked for GPP, volume production and transpiration under variable atmospheric CO_2 concentration. GPP and volume production showed a positive correlation with temperature change, while a negative correlation was observed for transpiration. These results are in line with the observed increase in both GPP and water use efficiency as radiative forcing rises (i.e., as CO_2 concentration increases when it is considered as variable) reported above (see Figure 36). Indeed, the rise in radiative forcing is coupled with an increase in average temperature. The trends were similar for all silvicultural routes, although the increase in GPP with rising temperature change was slightly more pronounced for DIV compared to BAU and OAK. Additionally, an influence of the climate model was observed, with the MPI-ESM1-2-LR, MPI-ESM1-2-HR and MRI-ESM2-0 models showing results that differ from those of the three other models. This discrepancy is due to differences in temperature change for a given radiative forcing between the two model groups, the first three models showing a temperature change peaking around 4°C while it is almost the double for the last three models. When CO_2 concentration was held constant, the relationships between relative changes in GPP, volume production and transpiration and temperature change were much less pronounced, and the direction of the correlations tended to revert compared to when CO_2 was variable, which is also in agreement with the results reported above. For the other indicators, the relationships between the two variables were generally weak. A noticeable observation was the stability of the Simpson index and wind undamaged percentage values for DIV, with relative change values consistently close to zero, in contrast to the much greater dispersion observed for the two other silvicultural routes. In other respects, although the correlation with temperature change was weak, the relative change in tree recruitment showed differing levels across silvicultural routes, with BAU showing on average higher values compared to OAK and DIV (note the logarithmic scales used for this indicator, as well as for tree mortality).

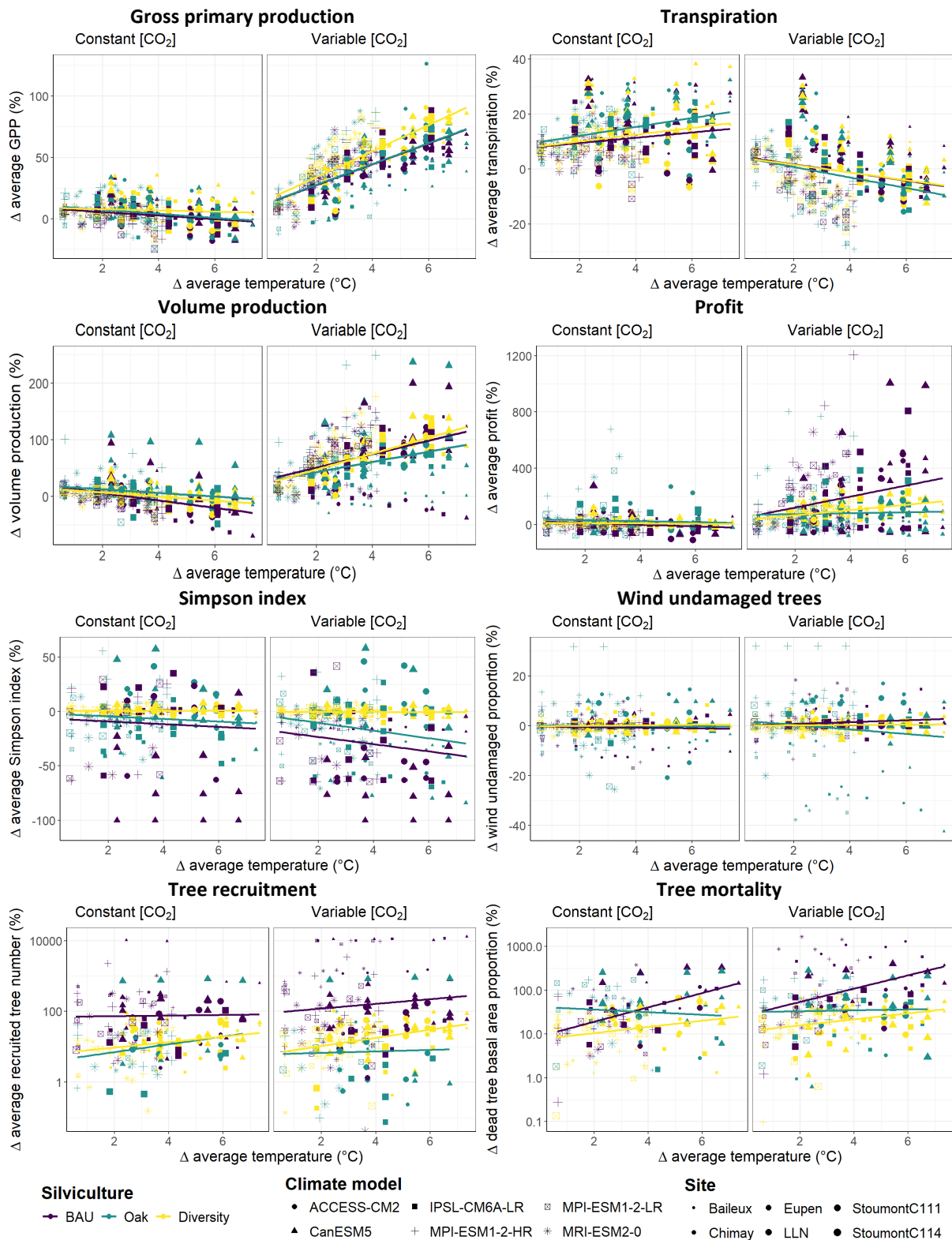


Figure 40. Relative variation between the mean value of the indicator for the simulation years 2070 – 2100 for each Site x Silviculture x SSP x Climate model x CO₂ modality and the corresponding mean value simulated considering the ‘historical’ climate scenario (see Equation 4.16) as a function of the respective change in mean air temperature during the growing season. Note the logarithmic scale of the y-axis for the tree recruitment and tree mortality indicators to improve the readability of the graphs

4.5 Support to decision making

The simulation experiments conducted in this project used a range of indicators to assess the strengths and weaknesses of three contrasted forest regeneration and silvicultural management strategies:

- (1) maintaining an even-aged stand through shelterwood regeneration with limited silvicultural interventions, referred to as business as usual (BAU),
- (2) promoting sessile oak regeneration via targeted clearings (OAK),
- (3) improving stand composition and structural diversification through natural regeneration and enrichment plantations (DIV).

The evaluation focused on each strategy's capacity to sustain ecosystem services and enhance forest resilience under the dual pressures of climate change and ungulate browsing. In the absence of ungulate pressure, the DIV (diversified) strategy demonstrated several strengths—not only in terms of biodiversity and resilience, as evidenced by higher recruitment rates and lower mortality, but also in productivity and profitability, outperforming the other two silvicultural approaches. However, DIV showed the weakest performance in carbon storage, whereas the BAU (business-as-usual) strategy delivered the highest values for this indicator. BAU also recorded the highest levels of transpiration, wind resistance, and tree mortality, while scoring lowest in terms of tree recruitment and biodiversity. In contrast, the OAK strategy stood apart from both DIV and BAU, with lower wind resistance and profitability, and generally intermediate—though often on the lower end—values across the other indicators.

The future climate scenario had a pronounced impact on productivity, profitability, and carbon storage, all of which increased with the severity of the scenario. These upward trends, favourable from both an economic perspective and in terms of climate change mitigation through enhanced carbon sequestration, are primarily driven by the rising atmospheric CO₂ concentrations. This phenomenon, known as the CO₂ fertilization effect, stimulates photosynthesis and boost forest productivity. However, these benefits must be interpreted with caution. Nutrient limitations and an increased likelihood of climate-related disturbances—such as wildfires, pest outbreaks, or disease—were not accounted for in the simulations and could potentially offset the positive effects of CO₂ fertilization. At the same time, transpiration was found to decrease significantly with rising CO₂ levels, indicating improved water-use efficiency. While reduced transpiration can be advantageous for water resource conservation and forest physiological functioning, it also lessens the forest's cooling effect on the atmosphere due to decreased evaporative water loss.

Another key finding from the simulation experiment is the significant—and often overriding— influence of site conditions on the indicators assessed. Site-specific characteristics, and particularly the initial stand attributes such as species composition, structural complexity, and stand density, play a critical role in shaping future stand dynamics, the delivery of ecosystem services, and overall forest resilience. The fact that the influence of initial stand characteristics persists throughout the simulation—even as it diminishes over time—highlights the strong inertia of forest ecosystems. Silviculture plays a crucial role in shaping forests into more resilient ecosystems, equipping them to better withstand future changes and disturbances—though these transformations take time.

Moreover, the most effective silvicultural strategies vary from site to site, reinforcing the idea that there is no one-size-fits-all solution.

Our results highlight the substantial and often underestimated influence of ungulate pressure on forest dynamics. At high densities, ungulates consistently reduced productivity, resilience, and economic sustainability across all climate pathways and management scenarios. Their impact was at least as significant as that of climate change for most performance indicators. Notably, the OAK and DIV scenarios were particularly vulnerable to browsing, with frequent regeneration failures and canopy openings observed under intense pressure. In contrast, the BAU scenario remained largely unaffected, likely due to its reliance on species and structural compositions less palatable to ungulates. These results suggest that, in areas with high ungulate densities, diversification efforts may be seriously compromised, as browsing pressure hinders regeneration success and increases protection costs. Effective ungulate management is therefore essential to ensure the feasibility and success of adaptive silvicultural strategies, particularly those aiming to enhance forest diversity and resilience.

The developments arising from this project have contributed significantly to the ongoing discourse on forest policy. By highlighting the vulnerability of forest ecosystems to climate change and by quantifying the costs and benefits of various adaptation strategies, the project provides valuable evidence to inform future policy directions.

In recent years, several policy initiatives have been implemented in Wallonia to enhance the resilience of forests. Among them, the "Forêt résiliente" subsidy scheme has notably supported the diversified regeneration of forest plots recently subjected to clear-cutting following bark beetle infestations. However, this measure was limited in scope and applied primarily to conifer stands affected by pest outbreaks.

Our project expands this perspective by anticipating the potential decline of broadleaved stands, particularly beech forests, which may increasingly suffer from severe dieback under changing climate conditions. Through experimental trials and comparative analysis, we assessed the effectiveness of various preemptive silvicultural strategies aimed at enhancing the resilience of these ecosystems. This proactive approach provides a scientific foundation for future forest policies that could be modelled after the scenarios tested in this research.

Moreover, our findings clearly identify the ecological and economic costs associated with overabundant ungulate populations, notably through bark peeling and browsing damage. These pressures not only threaten forest regeneration but also compromise the adaptive capacity of forest ecosystems in the face of climate change. These insights are highly relevant to the regional forest management agenda.

Indeed, following the *Assises de la Forêt* (Forest Roundtables), the first strategic axis of the new Regional Forest Strategy, adopted in May 2024, explicitly aims to adapt forest management practices to strengthen resilience, ensure regeneration, and safeguard the continuity of key native tree species in Wallonia. Our research directly supports these priorities and offers concrete, science-based recommendations for their implementation.

4.6 Additional project-related benefits

The extensive enhancements made to the HETEROFOR model—enabling it to assess the impact of various silvicultural strategies on ecosystem service provision and stand resilience under changing environmental conditions and intense ungulate pressure—will prove highly valuable for future simulation studies of a similar nature. During the project, several new modules were developed to enhance the model’s capabilities, including a tree hydraulics module to account for water stress during droughts and heatwaves, a soil organic carbon module, and the coupling with an existing forest product life cycle tool (CAT) to enable a comprehensive carbon budget. Additionally, a module addressing ungulate impacts was introduced. New tools were also created to support the implementation of silvicultural interventions (interveners) and to generate model outputs, including a range of indicators related to ecosystem services and forest resilience. Finally, a disaggregation procedure was also implemented to allow the use of daily meteorological data—instead of relying solely on hourly data—by converting them into the hourly variables required by the model.

These enhancements will significantly broaden the potential applications of HETEROFOR, both in fundamental research and in training and R&D contexts. The model is already being utilized in projects across Europe and North America. We also plan to integrate it more extensively into the training of forestry bioengineers, in combination with educational field tools such as marteloscopes.

This project provided a valuable opportunity to strengthen collaborations between Gembloux AgroBioTech (ULiège), the Earth and Life Institute (UCLouvain), and the Royal Meteorological Institute (RMI), while also fostering closer ties with key forest management stakeholders, including landowners, managers, trainers, and researchers. In addition, collaborations within the forest modelling community have been strengthened and newly established through the CAPSIS modelling platform and its user network, as well as via the PROCLIAS COST action.

5. DISSEMINATION AND VALORISATION

Scientific conference

Ligot G., Candaele R., Fichet V., Licoppe A., Lejeune P., 2023. Ungulates and succession dynamics reduce tree species richness in temperate uneven-aged forests. Presented at the Uneven-aged silviculture: insights into forest adaptation in times of global change, Mendel university in Brno, Brno, Czechia.

Ligot G., Gheysen T., Perin J., Candaele R., de Coligny F., Licoppe A., Lejeune P., 2023. From the simulation of forest plantation dynamics to the quantification of bark-stripping damage by ungulates. Presented at the FOREM 2023, Grenoble, France.

Jonard M., André F., Ligot G., Candaele R., 2023. Régénération des forêts dans un climat changeant. Presented at the FOREM 2023, Grenoble, France.

Ligot G., Charles G., 2024. Can silviculture be instrumental to increase carbon sequestration? Presented at the FOREM 2024, Nancy, France.

Guignabert A., Jonard M., Messier C., André F., de Coligny F., Doyon F., Ponette Q., 2024. La sylviculture adaptative à l'échelle du peuplement améliore-t-elle la résilience des forêts tempérées face à des perturbations multiples ? Presented at the FOREM 2024, Nancy, France.

Ligot G., Claessens H., 2024. Status and drivers of oak population decline in Western European forests. Presented at the IUFRO 26th world congress, Forest & society towards 2050, Stocholm, Sweden.

Ligot G. 2024. Compétition interspécifique dans les régénérations naturelles en peuplement irrégulier : dispositifs d'études en Wallonie. Presented at Atelier Régénération en futaie irrégulière, Nogent-sur-Vernisson, 21-23 August 2025. France.

Pau M., Jonard M., André F., Ligot G. 2025 Diversification forestière face aux changements globaux et à la pression des ongulés : une expérience de simulation. Poster presented at Carrefour Forestier, 21 March 2025, Libin, Belgium.

Pau M., Jonard M., André F., Ligot G. 2025 Diversification forestière face aux changements globaux et à la pression des ongulés : une expérience de simulation. Presented at FOREM, CEFE CNRS, Montpellier, France.

Other talks

Candaele R., Jonard M., André F., Ligot G., 2021. Régénération des forêts dans un climat et un environnement changeants. Presented at the Cerfs, biches, chevreuils... Une question d'équilibre, 17 September 2021, Stoumont, Belgium.

Candaele R., Ligot G., Licoppe A., Fichet V., Lievens J., André F., Jonard M., Lejeune P., 2021. Les ongulés sauvages menacent-ils la diversité des forêts futures? Presented at the Journée d'étude et conservations de la faune en milieux tempérés et tropicaux, 25 October 2021, Gembloux, Belgium.

Ligot G. 2024. Situation et facteurs de déclin du chêne dans les forêts d'Europe occidentale. Presented at the Séminaire Pro Silva, 19 June 2024, On-line.

Ligot G. 2025 Impact économique de la gestion des peuplements mélangés. Presented at Rencontres Filière bois, 15 April 2025, Libramont, Belgium.

6. PUBLICATIONS

Peer-reviewed scientific papers

Ligot G., Gheysen T., Perin J., Candaele R., de Coligny F., Licoppe A., Lejeune P., 2023. From the simulation of forest plantation dynamics to the quantification of bark-stripping damage by ungulates. European Journal of Forest Research. <https://doi.org/10.1007/s10342-023-01565-w>

Candaele R., Ligot G., Licoppe A., Lievens J., Fichet V., Jonard M., André F., Lejeune P., 2023. Interspecific Growth Reductions Caused by Wild Ungulates on Tree Seedlings and Their Implications for Temperate Quercus-Fagus Forests. Forests 14, 1330. <https://doi.org/10.3390/f14071330>

Barrere J., Ligot G., Boulanger V., Collet C., Courbaud B., de Coligny F., Mårell A., Saïd S., Balandier P., 2024. Oak regeneration facing deer browsing: Can competition between saplings offset the diversion effect? A simulation experiment. *Ecological Modelling* 489, 110608. <https://doi.org/10.1016/j.ecolmodel.2023.110608>

Guignabert A., Jonard M., Messier C., André F., de Coligny F., Doyon F., Ponette Q., 2024. Adaptive forest management improves stand-level resilience of temperate forests under multiple stressors. *Science of The Total Environment*, 948, 174168. <https://doi.org/10.1016/j.scitotenv.2024.174168>

Popularization papers

Charles G., Ligot G., Claessens H., Fortin M., De Mil T., 2024. La sylviculture peut-elle contribuer à combattre le changement climatique ? *Sylva Belgica* 33, 2.

Marchi S., Jonard M., André F., Ghilain N., Goosse H., 2024. Quel climat futur pour nos forêts ? *Sylva Belgica* 5, 30.

Ligot G., Gheysen T., Perin J., Candaele R., Licoppe A., Claessens, H., Lejeune, P., 2023. Quel est le coût des dégâts d'écorcement dans les plantations d'écipéa ? *Forêt.Nature* 168, 39.

7. ACKNOWLEDGEMENTS

The authors thank the Belgian Federal Science Policy Office (BELSPO) for financing the current research in the frames of the BRAIN REGE+ project (contract B2/212/P1/REG+). The authors thank the Université catholique de Louvain, the University of Liège (Gembloux Agro-Bio Tech) and the Royal Meteorological Institute for providing the needed infrastructure. This work was supported by forestry field data acquired under the ICP Forests (UNECE) and the Accord-cadre de recherches et de vulgarisation forestières (SPW) programmes or collected by the "Département de la Nature et des Forêts" (DNF, SPW), and by climate projection and historical series originated from the Coupled Model Intercomparison Project Phase 6 (CMIP6) and the CORDEX.be projects. We are grateful to C. Barvaux (DNF, SPW) and T. Thyron (UCLouvain) for granting us access to forest sites to supplement our datasets. We also thank F. de Coligny, manager and main developer of the Computer-Aided Projection of Strategies In Silviculture (Capsis) platform, for his assistance in implementing new functionalities in the HETEROFOR model.

The follow-up committee of the project was composed of the following members: De Waele Valérie (Researcher, DEMNA), Licoppe Alain (Premier Attaché, DEMNA), Colson Vincent (Head of the small private property support unit, OEWB), Cléda Martin (Director, DNF), Barvaux Catherine (Chief of cantonment, DNF), Benoît Cassart (Qualified attaché, DNF), de Wouters Philippe (Director of the Royal Forestry Society of Belgium, SRFB), Nicolas Dassonville (Training and R&D manager, SRFB), Timal Grégory (Forestry researcher and trainer & Forestry expert, CDAF), Sanchez Christine ('Pro Silva' forestry trainer, Forêt.Nature), Monville Marie (Forest alderwoman, Stoumont), Balandier Philippe (Research director, INRAe), Deleuze Christine (Modelling research and development manager, ONF), Hamdi Rafiq (Researcher, RMI), Ghilain Nicolas (Researcher, ULiège & RMI), Terlinden Michel (Forestry expert), de Viron Jean-Charles (Chief operating officer of an insurance company specialised in the forestry sector, AMIFOR).

REFERENCES

- Adair E.C., Parton W.J., Del Grosso S.J., Silver W.L., Harmon M.E., Hall S.A., Burke I.C., Hart S.C. (2008). Simple three-pool model accurately describes patterns of long-term litter decomposition in diverse climates. *Global Change Biology*, 14: 2636-2660.
- Alderweireld M., Burnay F., Pitchugin M., Lecomte H. (2015). Inventaire Forestier Wallon. Résultats 1994 - 2012. SPW, DGO3, DNF, Direction des Ressources forestières, Jambes, pp. 236.
- Asbeck T., Großmann J., Paillet Y., Winiger N., Bauhus J. (2021). The Use of Tree-Related Microhabitats as Forest Biodiversity Indicators and to Guide Integrated Forest Management. *Current Forestry Reports*, 7: 59-68.
- Balandier P., Marquier A., Casella E., Kiewitt A., Coll L., Wehrlen L., Harmer R. (2013). Architecture, cover and light interception by bramble (*Rubus fruticosus*): A common understorey weed in temperate forests. *Forestry*, 86: 39-46.
- Ball J.T., Woodrow I.E., Berry J.A. (1987). A Model Predicting Stomatal Conductance and its Contribution to the Control of Photosynthesis under Different Environmental Conditions. *Progress in Photosynthesis Research: Volume 4 Proceedings of the VIIth International Congress on Photosynthesis Providence, Rhode Island, USA, August 10–15, 1986*. Springer Netherlands, Dordrecht, pp. 221-224.
- Bellouin N., Quaas J., Gryspeerdt E., Kinne S., Stier P., Watson-Parris D., Boucher O., Carslaw K.S., Christensen M., Danianu A.L., Dufresne J.L., Feingold G., Fiedler S., Forster P., Gettelman A., Haywood J.M., Lohmann U., Malavelle F., Mauritsen T., McCoy D.T., Myhre G., Mülmenstädt J., Neubauer D., Possner A., Rugenstein M., Sato Y., Schulz M., Schwartz S.E., Sourdeval O., Storelvmo T., Toll V., Winker D., Stevens B. (2020). Bounding Global Aerosol Radiative Forcing of Climate Change. *Reviews of Geophysics*, 58.
- Berg B., Ekbohm G., Johansson M.B., McLaugherty C., Rutigliano F., De Santo A.V. (1996). Maximum decomposition limits of forest litter types: A synthesis. *Canadian Journal of Botany*, 74: 659-672.
- Berger U., Piou C., Schiffers K., Grimm V. (2008). Competition among plants: Concepts, individual-based modelling approaches, and a proposal for a future research strategy. *Perspectives in Plant Ecology, Evolution and Systematics*, 9: 121-135.
- Boulanger V. (2010). Pression d'herbivorie et dynamique des communautés végétales : influence à court et moyen termes des populations de cervidés sur la diversité des communautés végétales en forêt. Université Henri Poincaré, Vandoeuvre-lès-Nancy, France, pp. 285p.
- Bravo F., Fabrika M., Ammer C., Barreiro S., Bielak K., Coll L., Fonseca T., Kangur A., Löf M., Merganičová K., Pach M., Pretsch H., Stojanović D., Schuler L., Peric S., Rötzer T., Del Río M., Dodan M., Bravo-Oviedo A. (2019). Modelling approaches for mixed forests dynamics prognosis. Research gaps and opportunities. *Forest Systems*, 28.
- Bregaglio S., Donatelli M., Confalonieri R., Acutis M., Orlandini S. (2010). An integrated evaluation of thirteen modelling solutions for the generation of hourly values of air relative humidity. *Theoretical and Applied Climatology*, 102: 429-438.
- Brunner L., Pendergrass A.G., Lehner F., Merrifield A.L., Lorenz R., Knutti R. (2020). Reduced global warming from CMIP6 projections when weighting models by performance and independence. *Earth System Dynamics*, 11: 995-1012.
- Burneviča N., Jansons Ā., Zaļuma A., Kļaviņa D., Jansons J., Gaitnieks T. (2016). Fungi inhabiting bark stripping wounds made by large game on stems of *Picea abies* (L.) Karst. in Latvia. *Baltic Forestry*, 22: 2-7.
- Candaele R., Lejeune P., Licoppe A., Malengreaux C., Brostaux Y., Morelle K., Latte N. (2021). Mitigation of bark stripping on spruce: the need for red deer population control. *European Journal of Forest Research*, 140: 227-240.

- Candaele R., Ligot G., Licoppe A., Lievens J., Fichet V., Jonard M., André F., Lejeune P. (2023). Interspecific Growth Reductions Caused by Wild Ungulates on Tree Seedlings and Their Implications for Temperate Quercus-Fagus Forests. *Forests*, 14: 1330.
- Carreau J., Ben Mhenni N., Huard F., Neppel L. (2019). Exploiting the spatial pattern of daily precipitation in the analog method for regional temporal disaggregation. *Journal of Hydrology*, 568: 780-791.
- Carvalho D., Cardoso Pereira S., Rocha A. (2021). Future surface temperatures over Europe according to CMIP6 climate projections: an analysis with original and bias-corrected data. *Climatic Change*, 167: 10.
- Čermák P., Glogar J., Jankovský L. (2004). Damage by deer barking and browsing and subsequent rots in Norway spruce stands of Forest Range Mořkov, Forest District Frenštát p. R. (the Beskids Protected Landscape Area). *Journal of Forest Science*, 50: 24-30.
- Čermák P., Strejček M. (2007). Stem decay by *Stereum sanguinolentum* after red deer damage in the Českomoravská vrchovina Highlands. *Journal of Forest Science*, 53: 567-572.
- Champagne E., Raymond P., Royo A.A., Speed J.D.M., Tremblay J.P., Côté S.D. (2021). A Review of Ungulate Impacts on the Success of Climate-Adapted Forest Management Strategies. *Current Forestry Reports*, 7: 305-320.
- Charles G. (2023). Evaluation de l'influence de la sylviculture sur le bilan carbone de la filière forêt-bois wallonne. Liège Université - Gembloux Agro-Bio Tech, Gembloux, pp. 58p.
- Chen C.T., Knutson T. (2008). On the verification and comparison of extreme rainfall indices from climate models. *Journal of Climate*, 21: 1605-1621.
- Churski M., Bubnicki J.W., Jędrzejewska B., Kuijper D.P.J., Cromsigt J.P.G.M. (2017). Brown world forests: increased ungulate browsing keeps temperate trees in recruitment bottlenecks in resource hotspots. *New Phytologist*, 214: 158-168.
- Clark P.J., Evans F.C. (1954). Distance to Nearest Neighbor as a Measure of Spatial Relationships in Populations. *Ecology*, 35: 445-453.
- Courbaud B., Larrieu L., Kozak D., Kraus D., Lachat T., Ladet S., Müller J., Paillet Y., Sagheb-Talebi K., Schuck A., Stillhard J., Svoboda M., Zudin S. (2022). Factors influencing the rate of formation of tree-related microhabitats and implications for biodiversity conservation and forest management. *Journal of Applied Ecology*, 59: 492-503.
- Courbaud B., Pupin C., Letort A., Cabanettes A., Larrieu L. (2017). Modelling the probability of microhabitat formation on trees using cross-sectional data. *Methods in Ecology and Evolution*, 8: 1347-1359.
- Couvreux V., Ledder G., Manzoni S., Way D.A., Muller E.B., Russo S.E. (2018). Water transport through tall trees: A vertically explicit, analytical model of xylem hydraulic conductance in stems. *Plant Cell and Environment*, 41: 1821-1839.
- Cukor J., Vacek Z., Linda R., Vacek S., Marada P., Šimůnek V., Havránek F. (2019). Effects of bark stripping on timber production and structure of Norway Spruce forests in relation to climatic factors. *Forests*, 10.
- Dai A. (2006). Precipitation characteristics in eighteen coupled climate models. *Journal of Climate*, 19: 4605-4630.
- de Wergifosse L., André F., Beudez N., de Coligny F., Goosse H., Jonard F., Ponette Q., Titeux H., Vincke C., Jonard M. (2020). HETEROFOR 1.0: a spatially explicit model for exploring the response of structurally complex forests to uncertain future conditions – Part 2: Phenology and water cycle. *Geosci. Model Dev.*, 13: 1459-1498.
- de Wit C.T. (1978). Simulation of assimilation, respiration and transpiration of crops. Wageningen: Pudoc.

- Debele B., Srinivasan R., Yves Parlange J. (2007). Accuracy evaluation of weather data generation and disaggregation methods at finer timescales. *Advances in Water Resources*, 30: 1286-1300.
- Diacre M. (2022). Quantification et modélisation de l'appétence des semis des principales essences ligneuses pour les ongulés. Liège Université - Gembloux Agro-Bio Tech, Gembloux, pp. 36p.
- Dobor L., Baldo M., Bílek L., Barka I., Máliš F., Štěpánek P., Hlásny T. (2024). The interacting effect of climate change and herbivory can trigger large-scale transformations of European temperate forests. *Global Change Biology*, 30.
- Douville H., Decharme B., Delire C., Colin J., Joetzjer E., Roehrig R., Saint-Martin D., Oudar T., Stchepounoff R., Voltaire A. (2020). Drivers of the enhanced decline of land near-surface relative humidity to abrupt 4xCO₂ in CNRM-CM6-1. *Climate Dynamics*, 55: 1613-1629.
- Douville H., Willett K.M. (2023). A drier than expected future, supported by near-surface relative humidity observations. *Science Advances*, 9: ade6253.
- Drugé T., Nabat P., Mallet M., Somot S. (2021). Future evolution of aerosols and implications for climate change in the Euro-Mediterranean region using the CNRM-ALADIN63 regional climate model. *Atmospheric Chemistry and Physics*, 21: 7639-7669.
- Dufrêne E., Davi H., François C., le Maire G., Le Dantec V., Granier A. (2005). Modelling carbon and water cycles in a beech forest Part I : Model description and uncertainty analysis on modelled NEE. *Ecological Modelling*, 185: 407-436.
- Edelmann P., Weisser W.W., Ambarlı D., Bässler C., Buscot F., Hofrichter M., Hoppe B., Kellner H., Minnich C., Moll J., Persoh D., Seibold S., Seilwinder C., Schulze E.D., Wöllauer S., Borken W. (2023). Regional variation in deadwood decay of 13 tree species: Effects of climate, soil and forest structure. *Forest Ecology and Management*, 541.
- Ehret U., Zehe E., Wulfmeyer V., Warrach-Sagi K., Liebert J. (2012). HESS Opinions "should we apply bias correction to global and regional climate model data?". *Hydrology and Earth System Sciences*, 16: 3391-3404.
- Fadhel S., Rico-Ramirez M.A., Han D. (2017). Uncertainty of Intensity–Duration–Frequency (IDF) curves due to varied climate baseline periods. *Journal of Hydrology*, 547: 600-612.
- Filière Bois Wallonie (2024). *Panorabois Wallonie 2024.*, Marche-en-Famenne, pp. 114 p.
- Förster K., Hanzer F., Winter B., Marke T., Strasser U. (2016). An open-source MEteoroLOGical observation time series DISaggregation Tool (MELODIST v0.1.1). *Geoscientific Model Development*, 9: 2315-2333.
- Füldner K. (1995). Zur Strukturbeschreibung in Mischbeständen. *FORSTARCHIV*, 66: 235-240.
- Gheysen T., Brostaux Y., Hébert J., Ligot G., Rondeux J., Lejeune P. (2011). A regional inventory and monitoring setup to evaluate bark peeling damage by red deer (*Cervus elaphus*) in coniferous plantations in Southern Belgium. *Environmental Monitoring and Assessment*, 181: 335-345.
- Gill R., Webber J., Peace A. (2000). *The Economic Implications of Deer Damage - A review of current evidence: Forest Research Agency. Surrey.*
- Gill R.M.A. (1992a). A review of damage by mammals in north temperate forests: 1. Deer. *Forestry*, 65: 145-169.
- Gill R.M.A. (1992b). A review of damage by mammals in north temperate forests: 3. Impact on trees and forests. *Forestry*, 65: 363-388.
- Gleckler P.J., Taylor K.E., Doutriaux C. (2008). Performance metrics for climate models. *Journal of Geophysical Research Atmospheres*, 113.
- Hanewinkel M., Kuhn T., Bugmann H., Lanz A., Brang P. (2014). Vulnerability of uneven-aged forests to storm damage. *Forestry*, 87: 525-534.
- Hempel S., Frieler K., Warszawski L., Schewe J., Piontek F. (2013). A trend-preserving bias correction – The ISI-MIP approach. *Earth System Dynamics*, 4: 219-236.

- Hilmers T., Biber P., Knoke T., Pretzsch H. (2020). Assessing transformation scenarios from pure Norway spruce to mixed uneven-aged forests in mountain areas. *European Journal of Forest Research*, 139: 567-584.
- Hosseinzadehtalaei P., Ishadi N.K., Tabari H., Willems P. (2021). Climate change impact assessment on pluvial flooding using a distribution-based bias correction of regional climate model simulations. *Journal of Hydrology*, 598.
- Hosseinzadehtalaei P., Tabari H., Willems P. (2017). Uncertainty assessment for climate change impact on intense precipitation: how many model runs do we need? *International Journal of Climatology*, 37: 1105-1117.
- Hosseinzadehtalaei P., Tabari H., Willems P. (2019). Regionalization of anthropogenically forced changes in 3 hourly extreme precipitation over Europe. *Environmental Research Letters*, 14.
- Hosseinzadehtalaei P., Tabari H., Willems P. (2020). Climate change impact on short-duration extreme precipitation and intensity–duration–frequency curves over Europe. *Journal of Hydrology*, 590: 125249.
- IPCC (2021). *Climate Change 2021: The Physical Science Basis. Contribution of Working Group I to the Sixth Assessment Report of the Intergovernmental Panel on Climate Change*. Cambridge University Press, Cambridge, United Kingdom and New York, NY, USA, pp. 2391p.
- Jensen A.M., Götmark F., Löf M. (2012). Shrubs protect oak seedlings against ungulate browsing in temperate broadleaved forests of conservation interest: A field experiment. *Forest Ecology and Management*, 266: 187-193.
- Jerina K., Dajčman M., Adamič M. (2008). Red deer (*Cervus elaphus*) bark stripping on spruce with regard to spatial distribution of supplemental feeding places. *Zbornik gozdarstva in lesarstva*, 86: 33-43.
- Jonard M., André F., de Coligny F., de Wergifosse L., Beudez N., Davi H., Ligot G., Ponette Q., Vincke C. (2020). HETEROFOR 1.0: a spatially explicit model for exploring the response of structurally complex forests to uncertain future conditions – Part 1: Carbon fluxes and tree dimensional growth. *Geosci. Model Dev.*, 13: 905-935.
- Jonard M., Nicolas M., Coomes D.A., Caignet I., Saenger A., Ponette Q. (2017). Forest soils in France are sequestering substantial amounts of carbon. *Science of the Total Environment*, 574: 616-628.
- Juckles M., Taylor E.K., Durack J.P., Lawrence B., Mizielinski S.M., Pamment A., Peterschmitt J.Y., Rixen M., Senesi S. (2020). The CMIP6 Data Request (DREQ, version 01.00.31). *Geoscientific Model Development*, 13: 201-224.
- Julve P. (1998). *Baseflor. Index botanique, écologique et chorologique de la flore de France*.
- Knoke T. (2012). The Economics of Continuous Cover Forestry. In: Pukkala T, Gadow K, editors. *Continuous Cover Forestry*. 23. Springer Dordrecht, pp. 167-193.
- Kohler M., Pyttel P., Kuehne C., Modrow T., Bauhus J. (2020). On the knowns and unknowns of natural regeneration of silviculturally managed sessile oak (*Quercus petraea* (Matt.) Liebl.) forests—a literature review. *Annals of Forest Science*, 77.
- Kurz W.A., Dymond C.C., White T.M., Stinson G., Shaw C.H., Rampley G.J., Smyth C., Simpson B.N., Neilson E.T., Trofymow J.A., Metsaranta J., Apps M.J. (2009). CBM-CFS3: A model of carbon-dynamics in forestry and land-use change implementing IPCC standards. *Ecological Modelling*, 220: 480-504.
- Lafond V., Lagarrigues G., Cordonnier T., Courbaud B. (2014). Uneven-aged management options to promote forest resilience for climate change adaptation: Effects of group selection and harvesting intensity. *Annals of Forest Science*, 71: 173-186.
- Lange S. (2019). Trend-preserving bias adjustment and statistical downscaling with ISIMIP3BASD (v1.0). *Geoscientific Model Development*, 12: 3055-3070.

- Lange S. (2020). ISIMIP3b bias adjustment fact sheet. Potsdam Institute for Climate Impact Research (PIK).
- Larrieu L., Amberger C. (Unpublished). Ecological tree scoring system based on TreMs for marteloscopes, pp. 5 p.
- Larrieu L., Paillet Y., Winter S., Bütler R., Kraus D., Krumm F., Lachat T., Michel A.K., Regnery B., Vandekerckhove K. (2018). Tree related microhabitats in temperate and Mediterranean European forests: A hierarchical typology for inventory standardization. *Ecological Indicators*, 84: 194-207.
- Ligot G., Balandier P., Fayolle A., Lejeune P., Claessens H. (2013a). Height competition between *Quercus petraea* and *Fagus sylvatica* natural regeneration in mixed and uneven-aged stands. *Forest Ecology and Management*, 304: 391-398.
- Ligot G., Gheysen T., Lehaire F., Hébert J., Licoppe A., Lejeune P., Brostaux Y. (2013b). Modeling recent bark stripping by red deer (*Cervus elaphus*) in South Belgium coniferous stands. *Annals of Forest Science*, 70: 309-318.
- Ligot G., Gheysen T., Perin J., Candaele R., de Coligny F., Licoppe A., Lejeune P. (2023). From the simulation of forest plantation dynamics to the quantification of bark-stripping damage by ungulates. *European Journal of Forest Research*, 142: 899-916.
- Lloyd J., Taylor J.A. (1994). On the temperature dependence of soil respiration. *Functional Ecology*, 8: 315-323.
- Löffler H. (1975). The spreading of wound rot in Norway spruce. *Forstwissenschaftliches Centralblatt*, 94: 175-183.
- Lu Y., Qin X.S. (2014). Multisite rainfall downscaling and disaggregation in a tropical urban area. *Journal of Hydrology*, 509: 55-65.
- Maraun D. (2016). Bias Correcting Climate Change Simulations - a Critical Review. *Current Climate Change Reports*, 2: 211-220.
- Margalef R. (1958). Information theory in ecology. *General Systems*, 3: 36-71.
- Martinez del Castillo E., Zang C.S., Buras A., Hacket-Pain A., Esper J., Serrano-Notivoli R., Hartl C., Weigel R., Klesse S., Resco de Dios V., Scharnweber T., Dorado-Liñán I., van der Maaten-Theunissen M., van der Maaten E., Jump A., Mikac S., Banzragch B.E., Beck W., Cavin L., Claessens H., Čada V., Čufar K., Dulamsuren C., Gričar J., Gil-Pelegrián E., Janda P., Kazimirovic M., Kreyling J., Latte N., Leuschner C., Longares L.A., Menzel A., Merela M., Motta R., Muffler L., Nola P., Petritan A.M., Petritan I.C., Prislan P., Rubio-Cuadrado Á., Rydval M., Stajić B., Svoboda M., Toromani E., Trotsiuk V., Wilmking M., Zlatanov T., de Luis M. (2022). Climate-change-driven growth decline of European beech forests. *Communications Biology*, 5.
- Mehrotra R., Westra S., Sharma A., Srikanthan R. (2012). Continuous rainfall simulation: 2. A regionalized daily rainfall generation approach. *Water Resources Research*, 48.
- Myhre G., Samset B.H., Schulz M., Balkanski Y., Bauer S., Bernsten T.K., Bian H., Bellouin N., Chin M., Diehl T., Easter R.C., Feichter J., Ghan S.J., Hauglustaine D., Iversen T., Kinne S., Kirkevåg A., Lamarque J.F., Lin G., Liu X., Lund M.T., Luo G., Ma X., Van Noije T., Penner J.E., Rasch P.J., Ruiz A., Seland Ø., Skeie R.B., Stier P., Takemura T., Tsigaridis K., Wang P., Wang Z., Xu L., Yu H., Yu F., Yoon J.H., Zhang K., Zhang H., Zhou C. (2013). Radiative forcing of the direct aerosol effect from AeroCom Phase II simulations. *Atmospheric Chemistry and Physics*, 13: 1853-1877.
- O'Neill B.C., Tebaldi C., Van Vuuren D.P., Eyring V., Friedlingstein P., Hurtt G., Knutti R., Kriegler E., Lamarque J.F., Lowe J., Meehl G.A., Moss R., Riahi K., Sanderson B.M. (2016). The Scenario Model Intercomparison Project (ScenarioMIP) for CMIP6. *Geoscientific Model Development*, 9: 3461-3482.

- Ossó A., Craig P., Allan R.P. (2023). An assessment of CMIP6 climate signals and biases in temperature, precipitation and soil moisture over Europe. *International Journal of Climatology*, 43: 5698-5719.
- Pichancourt J.B., Manso R., Ningre F., Fortin M. (2018). A carbon accounting tool for complex and uncertain greenhouse gas emission life cycles. *Environmental Modelling and Software*, 107: 158-174.
- Rakotoarison H., Faratiana (2009). Analyse et modélisation de la gestion du grand gibier: cas de la région Aquitaine. Ph.D. thesis. Université Montesquieu - Bordeaux IV.
- RMI (2022). Gridded observational data.
- Ruosteenoja K., Jylhä K., Räisänen J., Mäkelä A. (2017). Surface air relative humidities spuriously exceeding 100% in CMIP5 model output and their impact on future projections. *Journal of Geophysical Research: Atmospheres*, 122: 9557-9568.
- Shannon C.E., Weaver W. (1949). *The Mathematical Theory of Communication*: University of Illinois Press.
- Sharma A., Srikanthan S. (2006). Continuous rainfall simulation: A nonparametric alternative. 30th Hydrology and Water Resources Symposium, HWRS.
- Sherwood S., Fu Q. (2014). A drier future? *Science*, 343: 737-739.
- Simpson E.H. (1949). Measurement of Diversity. *Nature*, 163: 688.
- Sivapalan M., Blöschl G. (1998). Transformation of point rainfall to areal rainfall: Intensity-duration-frequency curves. *Journal of Hydrology*, 204: 150-167.
- Sobolowski S., Somot S., Fernandez J., Evin G., Maraun D., Kotlarski S., Jury M., Benestad R.E., Teichmann C., Christensen O.B., Katharina B., Buonomo E., Katragkou E., Steger C., Sørland S., Nikulin G., McSweeney C., Dobler A., Palmer T., Wilke R., Boé J., Brunner L., Ribes A., Qasmi S., Nabat P., Sevault F., Oudar T., Brands S. (2023). EURO-CORDEX CMIP6 GCM Selection & Ensemble Design: Best Practices and Recommendations. Zenodo.
- Stemmelen A., Castagneyrol B., Ponette Q., Prospero S., Martin G.S., Schneider S., Jactel H. (2023). Tree diversity reduces co-infestation of Douglas fir by two exotic pests and pathogens. *NeoBiota*, 84: 397-413.
- Svennevik H., Hicks S.A., Riegler M.A., Storelvmo T., Hammer H.L. (2024). A dataset for predicting cloud cover over Europe. *Scientific Data*, 11: 245.
- Tabari H., De Troch R., Giot O., Hamdi R., Termonia P., Saeed S., Brisson E., Van Lipzig N., Willems P. (2016). Local impact analysis of climate change on precipitation extremes: Are high-resolution climate models needed for realistic simulations? *Hydrology and Earth System Sciences*, 20: 3843-3857.
- Tabari H., Hosseinzadehtalaei P., Aghakouchak A., Willems P. (2019). Latitudinal heterogeneity and hotspots of uncertainty in projected extreme precipitation. *Environmental Research Letters*, 14.
- Tabari H., Willems P. (2022). Trivariate Analysis of Changes in Drought Characteristics in the {CMIP6} Multimodel Ensemble at Global Warming Levels of 1.5°, 2°, and 3°C. *Journal of Climate*, 35: 5823-5837.
- Termonia P., Van Schaeybroeck B., De Cruz L., De Troch R., Caluwaerts S., Giot O., Hamdi R., Vannitsem S., Duchêne F., Willems P., Tabari H., Van Uytven E., Hosseinzadehtalaei P., Van Lipzig N., Wouters H., Vanden Broucke S., van Ypersele J.P., Marbaix P., Villanueva-Birriel C., Fettweis X., Wyard C., Scholzen C., Doutreloup S., De Ridder K., Gobin A., Lauwaet D., Stavrou T., Bauwens M., Müller J.F., Luyten P., Ponsar S., Van den Eynde D., Pottiaux E. (2018). The CORDEX.be initiative as a foundation for climate services in Belgium. *Climate Services*, 11: 49-61.

- Vacek Z., Cukor J., Linda R., Vacek S., Šimůnek V., Brichta J., Gallo J., Prokúpková A. (2020). Bark stripping, the crucial factor affecting stem rot development and timber production of Norway spruce forests in Central Europe. *Forest Ecology and Management*, 474.
- van Vuuren D.P., Edmonds J., Kainuma M., Riahi K., Thomson A., Hibbard K., Hurtt G.C., Kram T., Krey V., Lamarque J.F., Masui T., Meinshausen M., Nakicenovic N., Smith S.J., Rose S.K. (2011). The representative concentration pathways: An overview. *Climatic Change*, 109: 5-31.
- Vítková L., Ní Dhubháin Á. (2013). Transformation to continuous cover forestry - a review. *Irish Forestry*, 70: 119-140.
- Von Gadow K. (1993). Zur bestandesbeschreibung in der Forsteinrichtung. *Forst und Holz*, 21: 602-606.
- Vospersnik S. (2006). Probability of bark stripping damage by red deer (*Cervus elaphus*) in Austria. *Silva Fennica*, 40: 589-601.
- Walters M.B., Farinosi E.J., Willis J.L. (2020). Deer browsing and shrub competition set sapling recruitment height and interact with light to shape recruitment niches for temperate forest tree species. *Forest Ecology and Management*, 467: 118134.
- Wam H.K., Hofstad O. (2007). Taking timber browsing damage into account: A density dependant matrix model for the optimal harvest of moose in Scandinavia. *Ecological Economics*, 62: 45-55.
- Ward A.I., White P.C.L., Smith A., Critchley C.H. (2004). Modelling the cost of roe deer browsing damage to forestry. *Forest Ecology and Management*, 191: 301-310.
- Weisberg P.J., Bugmann H. (2003). Forest dynamics and ungulate herbivory: From leaf to landscape. *Forest Ecology and Management*, 181: 1-12.
- Westra S., Mehrotra R., Sharma A., Srikanthan R. (2012). Continuous rainfall simulation: 1. A regionalized subdaily disaggregation approach. *Water Resources Research*, 48.
- Wohlfrom P. (2022). Les produits bois et leur potentiel de stockage de carbone : une solution dans l'atténuation du changement climatique ? Etude des résineux issus de la filière bois wallonne. Institut de Gestion de l'Environnement et d'Aménagement du Territoire, Faculté des Sciences. Université Libre de Bruxelles, Brussels, pp. 67p.
- Yan Z., Bond-Lamberty B., Todd-Brown K.E., Bailey V.L., Li S., Liu C., Liu C. (2018). A moisture function of soil heterotrophic respiration that incorporates microscale processes. *Nature Communications*, 9.

ANNEXES

Minutes of the follow-up committee held on 19 October 2021

The project partners presented the project and the different work packages in turn. These presentations generated very rich discussions underlining the interest of the project for the various members of the committee and allowing to better specify the work to be carried out. The main points decided/suggested during this meeting are:

- to lower the priority for the implementation of a soil organic carbon module (Task 1.3 in the project proposal). Indeed, the modelling of soil organic carbon dynamics is complex, with a large number of compartments to be considered, and the availability of the data required for their initialization is quite limited which requires to make strong assumptions. Furthermore, while relevant as model output, soil organic carbon has no implication on other processes described in the model. In addition, this aspect was considered as somewhat out of scope during the project evaluation;
- to dedicate the time originally reserved for soil carbon modelling to the consideration of the effect of extreme events (i.e., storms, droughts, late frosts) in the simulations as these events are likely to play a critical role in the response of forest ecosystems to climate change. Though the increase in their frequency is a major concern for foresters, their consideration remains limited in existing modelling approaches. It is also suggested to investigate the possibility of accounting for attacks by pathogens/pests;
- add a study case representative of pine stands on sandy soil. Such a stand, located in the Bois de Lauzelle, is currently characterized in the framework of a master thesis and the corresponding data will be available for the REG+ project;
- to identify the most sensitive climate variables for the simulations through sensitivity analyses. It is also recommended to carry out simulations with a maximum of climate projections to encompass the uncertainty associated with climate scenarios;
- to draw up the management scenarios to be tested in close consultation with managers, including in particular the DNF;
- to characterize the climate scenarios by considering the warming instead of the radiative forcing, the latter being less meaningful for the manager.

Minutes of the meeting with forest stakeholders held on 13 March 2023

The main objective of this meeting was to gather insights for the definition of the silvicultural scenarios to be used for the simulation experiment.

After a round table, the objectives and the methodology of the REG+ project were first presented. A first set of questions arose regarding the values of forest productivity and economical profitability presented to illustrate two of the possible model outputs to be used to compare the simulations. We explain that the sometimes high values reported for productivity result partly from the fertilizing effect of increasing CO₂ atmospheric concentrations with time, especially for the for climate projections corresponding to the most pessimistic emission scenarios, and also from the fact that some of the considered sites were located on fertile sites. Furthermore, the relatively high values for the average yearly profit result from the fact that the simulations started with adult stands which present therefore a substantial economical value, and this initial value strongly influence economical indicators. To correct for this to avoid overestimations, it is recommended to subtract the expected value of the initial stand, instead of its current economical value as done presently, when determining the average yearly profit. In other respects, it is also emphasized that the withholding tax and taxes linked to cadastral income must be taken into account for economic calculations in private forests.

Then, so as to initiate discussion on the definition of the scenarios, the results of preliminary simulation trials starting from three contrasted case studies (i.e., old even-aged beech stand in Louvain-la-Neuve, oak and hornbeam coppice-with-standards stand in Chimay, and old Norway spruce plantation in conversion into uneven-aged stand close to Léglise) were presented. For each case, three silvicultural scenarios were considered for the simulations: (i) continuous natural regeneration under forest cover so as to maintain or evolve towards an uneven-aged stand, (ii) natural regeneration through progressive cuts to maintain or evolve towards an even-aged stand, and (iii) plantation following clear-cut generating an even-aged stand. For each of these scenarios, alternative versions considering or not the introduction of tree species for diversification were simulated.

The 13 forest stands selected as case studies for the project were then reviewed so as to propose for each of them appropriate silvicultural scenarios to be simulated. For its implementation in the model, each scenario has to be defined based on a set of parameters: characterization of the cuttings (intensity, frequency, type, canopy gap size and spatial arrangement), species in presence to favour and species to consider for diversification and the timing to introduce them, and maximum tree harvest dimensions for each species.

Based on this, some relevant general remarks were formulated:

- in some cases, such as notably the coppice-with-standards of Chimay or in mixed oak-beech forests, the natural regeneration and the development of a target species (e.g., oak) may be compromised due to its limited growth dynamics compared with other target or secondary species, which do not appear to be accounted for in these first simulations. In practice, the solution is to act in favour of slowly growing species by maintaining their regeneration areas and individuals of high quality under optimal light conditions through regular cut of faster growing trees in their surroundings;
- the detrimental effect of ground vegetation on regeneration development should also be considered, especially when intensive cuts are simulated. This effect of ground vegetation will be species-dependent (e.g., stronger for oak than for beech);

- the species to be considered for diversification have to be adapted to the site, their aptitudes should be checked based on the Fichier écologique des essences;
- the selected case studies are very contrasted, not only in terms of species composition but also, for a given species, in terms of stand development stage. Therefore, relevant silvicultural scenarios to be tested has then to be examined specifically for each case, as discussed below for most of the selected sites.

Silvicultural scenarios proposed for beech-dominated study cases

With average trunk circumference at breast height (C130) around 120 cm, the beech stands of Eupen and Baileux are still rather young and the trees have not yet reached the recommended C130 for harvest around 220 cm for the Haute Ardenne to 250 cm for richer sites. Therefore, it is advised to continue the current management as even-aged stand by performing mixed cuttings for 50 years before considering initiating the regeneration and/or the conversion into uneven-aged stand, otherwise sacrifices of exploitability would occur.

Once the harvest dimension is reached, progressive cuts are preferred to plantation for the regeneration towards a new even-aged stand. Indeed, plantations produce more random results for beech and forest managers try to avoid them. Yet, even using progressive cuts, it is important to pay attention to blockage situations that may arise due to the development of the ground vegetation (bramble, fern).

Conversion into an uneven-aged stand would be carried out through progressive reduction of the stand density to reach a target basal area of 16 m²/ha while limiting the harvest intensity to maximum 20% of the standing basal area at each cutting. For this, cuts are performed among the largest trees, by removing first the less well shaped individuals, and creating thereby canopy gaps stimulating regeneration development.

Diversification could be done either by promoting the development of the natural regeneration of other species if adult trees are present in the surroundings of the stand or by the introduction of 2-3 deciduous species in regeneration cones through monospecific plantations in cells of 3 to 5 ares located into gaps generated by the tree harvesting. However, this necessitates regular breaking or girdling of the concurrent beech individuals to maintain the species mixture. Another possibility for diversification is to introduce species at once in cells covering in total 10% of the stand area. When carried out at the occasion of progressive cuts, plantations for diversification should be carried out after the last cut to avoid damages. Potential candidate species for diversification in such stands are sessile oak, linden, maple, chestnut, wild cherry and red oak.

Silvicultural scenarios proposed for oak-dominated study cases

The management of oak dominated stands with the presence of hornbeams and a beech regeneration in the understorey towards an uneven-aged oak-beech stand would request to perform cuttings from below by harvesting much preferentially beech. A potentially successful technique to this aim comes from the 'qualification – dimensioning (QD) method' and consists in the creation of triangular openings of 2-3 ares covering 10-15% of the stand area and located each at the south of an adult oak tree which is expected to produce acorns for initiating the natural regeneration. The operations in favour of the installation and the development of the regeneration are conducted exclusively in those regeneration cones. Plantations will be carried out if natural regeneration fails. Linden, wild cherry and wild service tree are suitable species for diversification.

The management aiming at maintaining an even-aged stand appears not to be appropriate at these sites.

Silvicultural scenarios proposed for oak-beech mixture study cases

Regeneration of those stands could be initiated either through the creation of openings in the canopy or by performing cuts from below. In these situations, sacrifices of exploitability are acceptable to promote regeneration and to maintain the mixture, and it is therefore not necessary to wait for the trees to reach the harvest dimension before acting in favour of the regeneration.

Silvicultural scenarios proposed for Norway spruce-dominated study cases

For the three corresponding selected sites (i.e., Gedinne, Les Fossés and Buchholz), the current stands are too old to consider conversion to uneven-aged stands. Indeed, the creation of openings in the canopy or cuts from above are highly likely to destabilize the stands and to cause windfall damages. Similarly, progressive cuts to regenerate naturally towards even-aged stands also appear risky and, if adopted, should be made in a short period of time: two cuts spaced by six years maximum. The clear cut of the stands followed by plantation seems to be the best option here. Yet, it is recommended to seek advice from practitioners more familiar with such situations, who could not be present at this meeting.

For Gedinne, a detailed stand characterization allowing to initialize the model is also available for the year 1999. Starting the simulations from that younger stand would be an option to allow for natural regeneration of the stand.

Silvicultural scenarios proposed for Douglas fir-dominated study cases

Douglas fir trees present a greater individual resistance to windfall compared to spruce, and the creation of openings in the canopy as well as quite intensive cuts from above are possible in the selected stands even though their advanced age.

Based on this discussion with the stakeholders, the selection of the study cases needs to be revised to better consider stands at a development stage allowing for natural regeneration, which corresponds to the silvicultural phase of prime interest for this project. Indeed, some initially selected stands were either too young to initiate regeneration without generating sacrifices of exploitability or too old to allow cuttings favouring the installation of regeneration without risking to destabilize the stand, especially for Norway spruce in the latter case. Modifications of the initial selection of the study cases and their justifications are presented in Task 4.1 in this report.

Regarding the silvicultural scenarios to be tested for the selected study cases, following this meeting we propose to primarily investigate scenarios resorting to natural regeneration and to consider the evolutions towards both even-aged and uneven-aged structures in case of even-aged initial stand, and to act so as to maintain the uneven-aged structure when starting from an uneven-aged stand. In each case, scenarios will be simulated with and without consideration of species diversification, which aims at introducing at least 40% of other species than the main one. Plantations will be used only when required, namely, in case of blockage situations in which natural regeneration fails or for the introduction of new species in the stand for diversification.